

Technical Report

**TR-24-02**

December 2024



# Long term test of bentonite buffer (LOT) at the Äspö HRL

## Evaluating bentonite stability in the LOT A3 and S2 experiments after 20 years of heating

Daniel Svensson

Terese Bladström

Ann Dueck

Ulf Nilsson

Viktor Jensen

Johan Lindén

Fredrik Lindroos

Stuart M R Turner

Steven Hillier

SVENSK KÄRNBRÄNSLEHANTERING AB

SWEDISH NUCLEAR FUEL  
AND WASTE MANAGEMENT CO

Box 3091, SE-169 03 Solna  
Phone +46 8 459 84 00  
skb.se

SVENSK KÄRNBRÄNSLEHANTERING



ISSN 1404-0344

**SKB TR-24-02**

ID 2048228

December 2024

# **Long term test of bentonite buffer (LOT) at the Äspö HRL**

## **Evaluating bentonite stability in the LOT A3 and S2 experiments after 20 years of heating**

Daniel Svensson, Terese Bladström  
Svensk Kärnbränslehantering AB

Ann Dueck, Ulf Nilsson, Viktor Jensen  
Clay Technology AB

Johan Lindén, Fredrik Lindroos  
Åbo Akademi

Stuart M R Turner, Steven Hillier  
James Hutton Limited Analytical Laboratory Services

*Keywords:* Bentonite, Montmorillonite, Stability, Field experiment, LOT, Mineralogy, Chemistry, Swelling pressure, Hydraulic conductivity, Unconfined compression test, Long term stability, CEC, XRD.

This report is published on [www.skb.se](http://www.skb.se)

© 2024 Svensk Kärnbränslehantering AB



# Abstract

This report focuses on the bentonite stability in the LOT S2 and A3 experiments after 20 years of heating in the Äspö laboratory, Sweden. LOT S series are at standard conditions similar to repository conditions, while the LOT A-series are at adverse conditions with higher temperatures than repository conditions. This report has no focus on copper corrosion as this has been reported separately.

Minor changes in the chemistry and mineralogy of the bentonite were observed, particularly in the warmer sections of the LOT A3 experiment. It's important to note that most of these changes were minimal, often close to the detection limit. All observations were consistent with expectations and closely aligned with previous field experiments conducted at the Äspö laboratory using bentonite clay. No signs of montmorillonite alteration were observed.

A slight accumulation of magnesium (Mg) was detected near the heater, possibly due to the adsorption of ionic Mg onto the montmorillonite. Additionally, a very minor decrease in silicon (Si) content was noted closer to the heater, possibly resulting from the dissolution of silica phases, such as quartz, cristobalite and/or amorphous silica, which reprecipitate nearer to the cooler rock. This minor change in silica content was interpreted as a possible cause of the minor increase in montmorillonite content observed close to the heater (based on quantitative XRD and CEC measurements). The magnitude of the changes are in the vicinity of the detection limits of the methods.

A slight increase in the Fe(II)/Fe(III) ratio was also observed, most likely due to the chemical reduction of iron within the montmorillonite's octahedral sheet through reaction with pyrite.

These changes were too minor to impact the swelling pressure performance, which remained unaffected throughout the experiments. A minor increase in hydraulic conductivity was observed, along with indications of reduced maximum deviator stress in unconfined compression tests.

The minor changes observed in the unconfined compression tests and hydraulic conductivity may be linked to the dissolution and reprecipitation of silica phases, potentially altering particle sizes and causing slight cementation. However, the extent of these changes is too small to significantly affect the overall performance of the repository.

Sulfate accumulation was observed towards the heater in LOT A3/S2 and the amount was rather substantial. The results are snap shots in time and even higher accumulations cannot be excluded. An increase in sulfates close to canister will result in a decrease in montmorillonite content. The process is expected to be reversible and that the sulfates are expected to dissolve when the temperature decreases. It is however difficult to predict if this sulfate accumulation have any impact on the properties of the bentonite close to the canister. A lower sulfate content in the original bentonite material could therefore be an advantage.

## Sammanfattning

Denna rapport fokuserar på bentonitstabilitet i LOT S2- och A3-experimenten efter 20 års uppvärmning i Äspölaboratoriet. LOT S-serien genomfördes under standardförhållanden som liknar förhållandena i ett KBS-3 slutförvar, medan LOT A-serien genomförs under mer ogynnsamma förhållanden med högre temperaturer. Denna rapport behandlar inte kopparkorrosion, då detta har rapporterats tidigare.

Mindre förändringar i kemin och mineralogin hos bentoniten observerades, särskilt i de varmare delarna av LOT A3-experimentet. Det är viktigt att notera att de flesta av dessa förändringar var mycket små, ofta nära eller eventuellt under detektionsgränsen. Alla observationer var i linje med förväntningarna och stämde väl överens med tidigare fältexperiment utförda vid Äspölaboratoriet med bentonitlera. Inga tecken på montmorillonitombildning observerades.

En liten ackumulering av magnesium (Mg) upptäcktes nära värmaren, möjligen på grund av adsorption av joniskt Mg på montmorillonitens yta. Dessutom noterades en liten minskning av kisel (Si)-halten närmare värmaren, som skulle kunna vara en följd av upplösning av kiselhaltiga faser, såsom kvarts, kristobalit och amorft kisel, vilka kan ha fallit ut igen närmare det svalare berget. Denna omfördelning av kisel ledde till en liten ökning av katjonbyteskapaciteten (CEC), vilket beror på att montmorillonithalten ökade närmast värmaren vid kiselomfördelningen.

En liten ökning av Fe(II)/Fe(III)-förhållandet observerades, sannolikt på grund av kemisk reduktion av järnet i montmorillonitens oktahederskikt genom reaktion med pyrit.

Dessa förändringar var för små för att påverka svälltryckets prestanda, som förblev opåverkad under experimenten. En mindre ökning av den hydrauliska konduktiviteten observerades, tillsammans med indikationer på minskad maximal deviatorstress i tryckhållfasthetstester. Dessa mindre förändringar som observerades kan eventuellt kopplas till upplösningen och omkristallisationen av kiselhaltiga faser, vilket potentiellt kan förändra partikelstorlekar och orsaka viss cementering. Dock är omfattningen av dessa förändringar för liten för att ha någon betydande inverkan på slutförvarets prestanda.

Sulfatackumulering observerades mot värmaren i LOT A3/S2 och mängden var ganska betydande. Resultaten är ögonblicksbilder i tiden och ännu högre ackumuleringar kan inte uteslutas. En ökning av sulfater nära kapseln kommer att leda till en minskning av montmorillonitnehåll. Processen förväntas vara reversibel och sulfaterna förväntas lösas upp sig när temperaturen senare sjunker. Det är dock svårt att förutsäga om denna sulfatackumulering kommer att ha någon påverkan på egenskaperna hos bentoniten nära kapseln. En lägre sulfatnivå i det ursprungliga bentonitmaterialet skulle därför kunna vara en fördel.

# Contents

<b>1</b>	<b>Introduction</b>	7
1.1	Experimental layout and excavation	9
1.2	Temperature and density distributions	12
<b>2</b>	<b>Investigations at the Äspö laboratory</b>	13
2.1	Experimental procedures	13
2.1.1	X-ray Fluorescence (XRF) Spectroscopy	13
2.1.2	Powder X-ray Diffraction (XRD)	13
2.1.3	Specific Cation Exchange Capacity (CEC)	13
2.1.4	Swelling Pressure and Hydraulic Conductivity	14
2.2	Hydromechanical properties	15
2.2.1	Swelling pressure on grinded and recompacted samples	15
2.2.2	Hydraulic conductivity on grinded and recompacted samples	15
2.3	Chemistry and mineralogy	19
2.3.1	Chemistry and mineralogy of bulk samples	19
2.3.2	Chemistry and mineralogy of Ca-exchanged samples from SP-HC measurements	36
2.3.3	Clay fractions	40
2.3.4	Scraping samples from the heater	43
<b>3</b>	<b>Hydromechanical properties, Clay Technology</b>	45
3.1	Test plan	45
3.2	Denomination of specimens	46
3.3	Type of water	46
3.4	Determination of water content and density	46
3.5	Swelling pressure and hydraulic conductivity test	47
3.5.1	General	47
3.5.2	Test equipment	47
3.5.3	Preparation of specimen and test procedure	47
3.5.4	Results	48
3.5.5	Discussion	53
3.5.6	Comparison with LOT A2	54
3.6	Unconfined compression test	55
3.6.1	General	55
3.6.2	Test equipment	55
3.6.3	Preparation of specimen and test procedure	55
3.6.4	Results	56
3.6.5	Discussion	62
3.6.6	Comparison with LOT A2	63
<b>4</b>	<b>Mössbauer spectroscopy, Åbo Akademi</b>	65
4.1	Experimental	65
4.2	Results	66
<b>5</b>	<b>Mineralogy at James Hutton Limited Analytical Laboratory Services</b>	69
5.1	Samples	69
5.2	Method description	69
5.3	Statistics and error estimates	69
5.4	Results	69

<b>6</b>	<b>Assessment of the evolution of the bentonite in the LOT S2 and A3 parcels</b>	71
6.1	Hydromechanical properties	71
6.2	Chemistry and mineralogy	71
6.2.1	Comparison with other similar field experiments	73
6.2.2	Increase of CEC in hot sections	73
6.2.3	Accumulation of Mg towards the heater	74
6.2.4	Reduction of trivalent to divalent iron	75
<b>7</b>	<b>Summary and conclusions</b>	77
	<b>References</b>	79
<b>Appendix 1</b>	Photos from the sampling for the hydro-mechanical analyses	81
<b>Appendix 2</b>	Swelling pressure tests – time evolution	85
<b>Appendix 3</b>	Unconfined compression tests – deviator stress as a function of strain	89
<b>Appendix 4</b>	Mössbauer spectroscopy	95

# 1 Introduction

Bentonite clay is a key component of the Swedish KBS-3 design for final repositories of high-level radioactive waste. In this design, copper canisters are used as corrosion-resistant containers for the waste, which are placed at a depth of approximately 500 meters in crystalline rock. Compact bentonite blocks are installed as buffer material between the canister and the rock to minimize water flow and transport between them. The swelling pressure of the clay maintains the canister's position and reduces microbiological activity. Additionally, the clay's plasticity ensures it does not transfer forces from rock displacements to the canister. Transport through the buffer is primarily controlled by diffusion, affecting both corrosive components in the groundwater and corrosion products, as well as any escaping radionuclides in the event of canister failure.

The designed lifetime of a KBS-3 repository ranges from 0.1 to 1 million years. Therefore, it is crucial that the elevated temperatures from the spent fuel radioactive decay do not significantly impact the important properties of bentonite over time. Several buffer alteration models are discussed by Karnland and Birgersson (2006). According to these models, no significant alteration of the buffer is expected in a KBS-3 repository. Field experiments can validate these models by testing the stability of bentonite. In these experiments, the stability is assessed by comparing the original material with excavated material from the experiment in two ways: (i) by testing the primary properties of the bentonite, such as swelling pressure and hydraulic conductivity, and (ii) by investigating the mineralogical content, with a special focus on montmorillonite content and any alteration or neoformation of other clay minerals.

The LOT (Long Term Test of Buffer Material) field experiments are a number of medium-scale field experiments performed at Äspö HRL focused on the long-term performance of bentonite buffer (Figure 1-1). The complete test series includes seven different test parcels of which only one is still running (LOT S3). In the late 1990s, seven test parcels were installed at a depth of approximately 450 meters in the Äspö Hard Rock Laboratory (HRL). Each parcel consisted of bentonite rings (10 cm high and 30 cm in diameter) stacked around a long copper pipe (10.8 cm in diameter and approximately 4 meters in length) containing a heater. The LOT experiments are divided into two series: the S-series, which represents standard conditions, and the A-series, which represents adverse conditions with elevated temperatures. The focus in this report are the two test parcels S2 and A3 that were installed in 1999 and dismantled after 20 years, in September 2019.

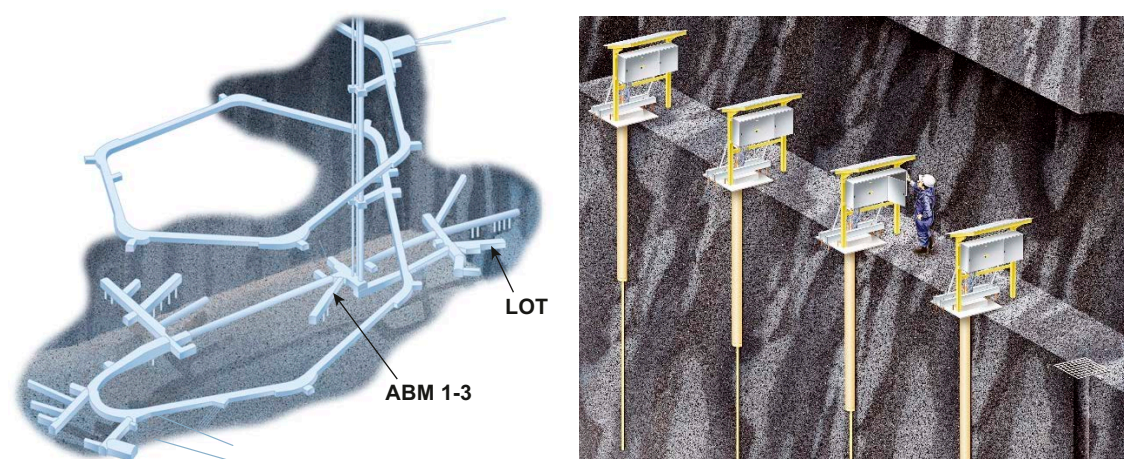


**Figure 1-1.** Left: test sites in the lower part of the Äspö HRL. Right: a schematic illustration of the LOT-experiments.

Although 20 years is a significant duration, it is relatively short compared to the 100 000-year lifespan of a KBS-3 repository. However, the LOT A3 experiment covers a substantial portion of the heating period in a KBS-3 repository with respect to kinetic reactions by utilizing adverse conditions. This approach is based on that the temperature drops rather rapidly over time in a KBS-3 deposition hole (from 90 °C to 50 °C within 1 000 years; Figure 1-2). The LOT A-series experiments are conducted at much higher temperatures compared to the KBS-3 canister target temperature, reaching up to 120–150 °C at the heater surface compared to 90 °C in the KBS-3 design.

The experiment was retrieved and the bentonite blocks were divided into smaller pieces. The clays are analysed regarding their important properties, as well as chemical and mineralogical composition. This is in order to investigate if the central properties such as swelling pressure and hydraulic conductivity are essentially unaffected by the thermal treatment, as well as the mineralogical evolution of the bentonite buffer.

Several montmorillonite alteration mechanisms are possible and one important alteration reaction is illitisation, which will be used for an example here to show the kinetic impact from temperature on alteration reactions. Illitisation has an activation energy of around 28 kcal/mole (Huang et al. 1993). Using this activation energy, the relative increase in alteration kinetics (alteration rate) can be calculated using the Arrhenius equation (Figure 1-3). The rate of illitisation increases approximately by a factor of 20 to 50 when the temperature is raised from 90 °C to 120 °C or 130 °C. Therefore, 20 years of heating in LOT A3 corresponds approximately to 400 to 1 000 years of heating at 90 °C in the warmest locations of the experiment, when it comes to illitisation or any other alteration reaction with similar activation energy. After 1 000 years, the buffer temperature at the canister interface is approximately 50 °C (Figure 1-2). At this temperature, the reaction rate is only 1 % of the rate at 90 °C (Figure 1-3), and as time progresses, the conversion rate continues to decrease.

Hence, although the length of the LOT A3 and S2 experiments, 20 years it not much compared to the designed life time of a KBS-3 repository of 100 000 years, however the kinetic impact from the thermal load in the A3 experiment is actually rather comparable to the actual thermal load in a KBS-3 deposition hole.

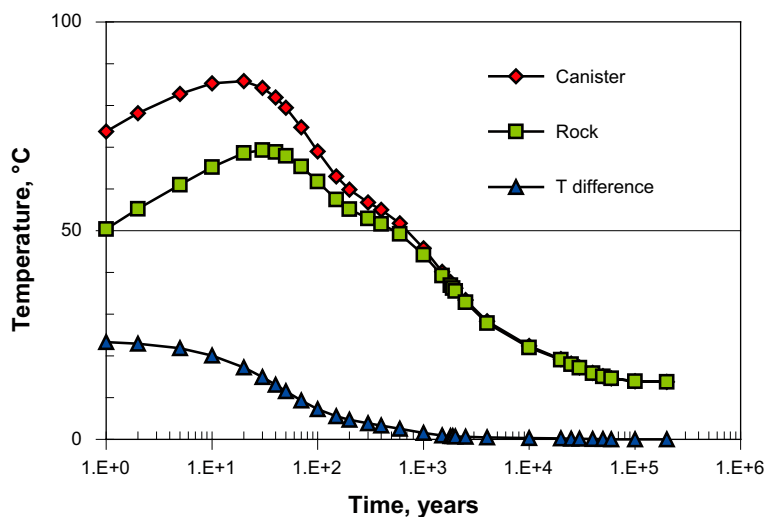


**Figure 1-2.** Calculated temperature evolution in a typical KBS-3 deposition hole showing the buffer temperatures at the interfaces to the canister and the rock, and the temperature gradient over the buffer, respectively (Karnland et al. 2009).

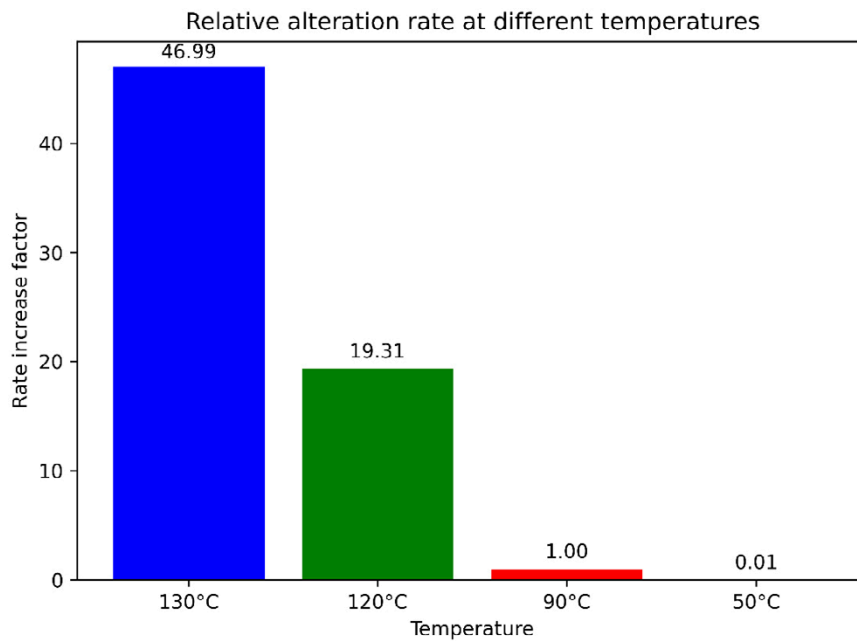


**Figure 1-3.** Example of calculated relative alteration rates at 50, 90, 120 and 130 °C using 28 kcal/mole as activation energy (illitisation of smectite) in the Arrhenius equation (calculated by D. Svensson).

## 1.1 Experimental layout and excavation

Each of the LOT test parcels consists of a central copper tube with an electrical heater inside. The electrical heater gives a maximum temperature between 90 °C and 150 °C. Prefabricated ring-shaped bentonite blocks with a height of 100 mm are placed around the copper tube in the 4-meter deep borehole.

The bentonite buffer consists of compacted Wyoming Na dominated bentonite with the commercial name MX-80 (delivered by Askania AB and manufactured by Volclay LTD). The material has been used in many projects including large field tests and laboratory studies.

The installation, test conditions, monitoring of installed sensors, dismantling and initial analyses of the material from LOT parcels S2 and A3 have been reported by Sandén and Nilsson (2020). LOT parcels dismantled after 1 to 6 years have been reported by Karnland et al. (2000, 2009, 2011).

During the excavation the clay was separated from the copper tube (Figure 1-4), and at the copper heater contact white precipitates were occasionally observed (Figure 1-5).

No microbiological work was done on the LOT A3 and S2 experiments. Plenty of work was done in the full scale experiments of the Prototype outer section (Arlinger et al. 2013), and it was concluded during the planning of the LOT analysis that microbiological work on the LOT packages were unlikely to add additional new important information on the topic.



**Figure 1-4.** Sampling of a LOT-experiment. Top: sawing and cutting of the heater. All handling was documented by continuous filming. Bottom: example of how bentonite and copper surfaces and interfaces looked.



*Figure 1-5. Sampling of a LOT-experiment. Top: gypsum was sometimes seen as a web like white precipitate in the bentonite innermost to the heater. Bottom: a cross cut of the copper tube. Photos by D. Svensson.*

## 1.2 Temperature and density distributions

Specimens were taken from LOT S2 and A3 from blocks number 9 and 11 for the hydro-mechanical analyses in this study. Based on data presented by Sandén and Nilsson (2020), maximum temperatures at relevant positions and relevant density distributions at dismantling are shown in Figure 1-6 and Figure 1-7 respectively.

In each test parcel the electrical heater was placed in the lower 2 m of the copper tube and the blocks 9 and 11 were placed in the most heated part (approximately 0.85 m and 1.05 m, respectively, from the bottom of each borehole). The outer diameter of the copper tube was 108 mm and with the nominal outer diameter of the borehole of approximately 300 mm the thickness of the bentonite ring after saturation was approximately 96 mm.

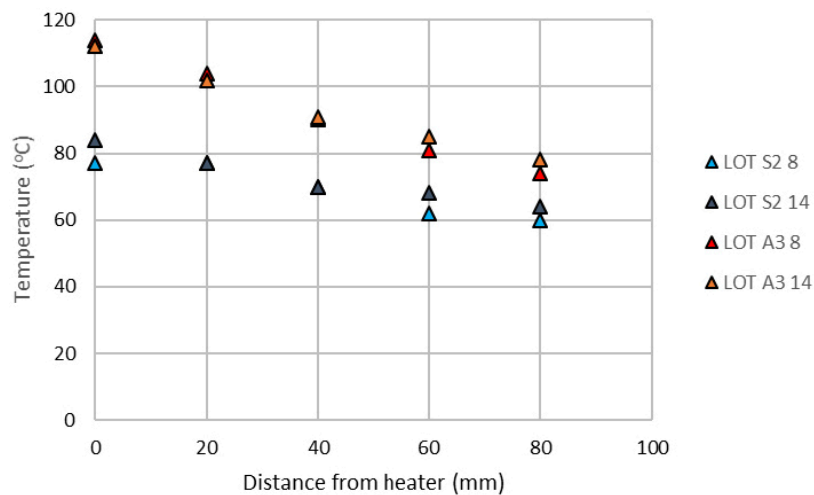


**Figure 1-6.** Maximum temperature at specific positions of blocks 8 and 14 from test parcels S2 and A3. The blocks were placed approximately 0.75 m and 1.35 m, respectively, from the bottom of each borehole. Based on data from the report by Sandén and Nilsson (2020).

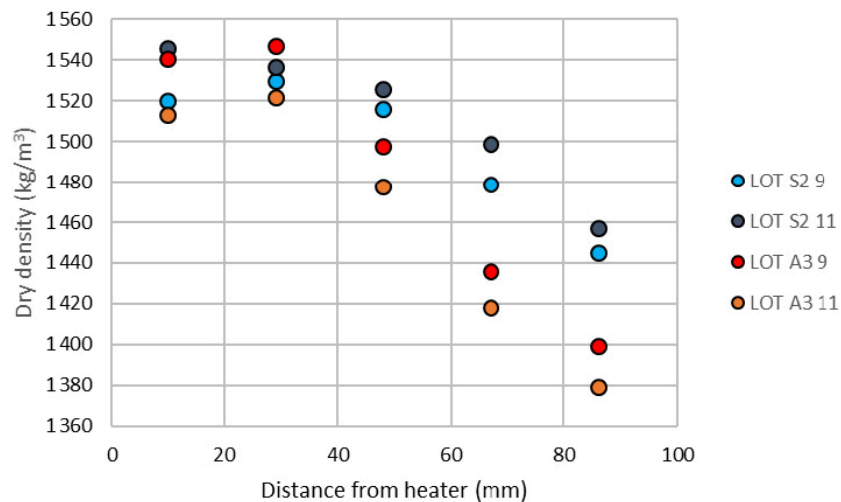


**Figure 1-7.** Dry density distribution after dismantling of blocks 9 and 11 of LOT parcels S2 and A3. Based on data from the report by Sandén and Nilsson (2020).

## 2 Investigations at the Äspö laboratory

The stability was assessed by comparing the original material with excavated material from the experiment in two ways: (i) by testing the primary hydromechanical properties of the bentonite, such as swelling pressure and hydraulic conductivity, and (ii) by investigating the mineralogical content of the bentonite, with a special focus on montmorillonite content and any alteration or neoformation of other clay minerals.

### 2.1 Experimental procedures

#### 2.1.1 X-ray Fluorescence (XRF) Spectroscopy

The XRF analysis was conducted using a Panalytical Epsilon 3 XL spectrometer equipped with a Rh X-ray tube. To minimize absorption by air, helium gas was flowed over the sample during measurement. Samples were analyzed either as compacted discs of pure clay or as milled samples placed on Mylar foil, depending on the available sample quantity. The measurement setup and evaluation followed the standard procedures provided by the manufacturer (referred to as Omnia). XRF is unable to measure elements with atomic numbers lower than sodium. The reported elements are presented as oxides, and the sum is normalized to 100 %.

#### 2.1.2 Powder X-ray Diffraction (XRD)

XRD data were collected in reflection mode (theta-theta configuration) using a Panalytical X'Pert Pro system with a Co X-ray source (broad focus;  $\lambda = 1.789 \text{ \AA}$ ). A PIXcel1D linear detector and programmable divergence and anti-scatter slits were employed. To maximize intensity, no monochromator was used; however, a thin Fe filter was implemented to suppress white and Co K-beta radiation, reducing K-beta intensity to less than 1 % of K-alpha. Samples were either back-loaded or prepared on a zero-background Si substrate, depending on the available sample quantity. Data collection typically lasted 1–3 hours per sample at 40 kV and 40 mA. Quantification of XRD patterns was done using Siroquant version 5.

#### 2.1.3 Specific Cation Exchange Capacity (CEC)

The specific cation exchange capacity (CEC) was measured using a  $\text{Cu}^{2+}$ -triethylenetetramine complex, following methods established by Meier and Kahr (1999) and Ammann et al. (2005). Due to the strong blue color of the Cu-tri complex, the exchange was quantified via spectrophotometry. The measured CEC of pure montmorillonite (or other smectites) closely aligns with the calculated layer charge of Wyoming montmorillonite based on chemical composition (Karlund et al. 2006), confirming that the  $\text{Cu}^{2+}$  complex is adsorbed as a divalent cation in amounts corresponding to the permanent charge of the smectite. Milled bentonite ( $400 \text{ mg} \pm 10 \text{ mg}$ ) was dispersed in deionized water (33 ml) on a vibrating table for 30 minutes, followed by ultrasonic treatment for 15 minutes. The bentonite was then equilibrated with Cu(II)-triethylenetetramine solution (7 ml; 45 mM) and left on the vibrating table for 30 minutes. After 5 minutes of centrifugation at 3 000 RCF (relative centrifugal force), spectrophotometric measurement of the supernatant at 583 nm was performed against a calibration curve. The CEC was calculated by the difference in copper concentration before and after ion exchange with the clay and is expressed as  $\text{cmol}(+)/\text{kg}$  dry weight. Since the CEC is reported relative to the dry weight of the bentonite sample, the water content of the material was determined by weighing a separate bentonite sample before and after drying at  $105 \text{ }^\circ\text{C}$  for 24 hours.

### 2.1.4 Swelling Pressure and Hydraulic Conductivity

The following procedure, based on Karnland et al. (2006) and Svensson et al. (2019), outlines the tests for swelling pressure and hydraulic conductivity (Figure 2-1). The entire process typically takes approximately six weeks:

1. A compacted clay disc, with a diameter of 35 mm and an approximate height of 5 mm, is placed into the swelling pressure cell or compacted in situ within the cell. The clay is prepared to a specific target density of choice.
2. The clay is then saturated with deionized water, and the swelling pressure is continuously measured using an external force cell over a period of about one week. The swelling pressure is calculated as the force divided by the cross-sectional area of the specimen and is recorded once the pressure (force) stabilizes.
3. The hydraulic conductivity of the specimen is measured using deionized water. This is done by applying a constant pore pressure gradient across the specimen while continuously measuring the water flow rate over time. The gradient is defined as the applied pressure (in meters of water column) divided by the height of the sample. The evaluation follows Darcy's law, and the measurement continues for about one week, with results interpreted when the outflow stabilizes.
4. Step 2 is repeated using a 1 M CaCl<sub>2</sub> solution instead of deionized water to exchange the bentonite to its Ca-form.
5. Step 3 is then repeated with the 1 M CaCl<sub>2</sub> solution.
6. Step 2 is repeated once more using deionized water to remove the salt from the bentonite.
7. Finally, the specimen is removed from the swelling pressure cell, and its bulk density and water content are determined. Bulk density is measured by weighing the sample in air and then submerged in paraffin oil of known density. Water content is determined by drying the sample in an oven at 105 °C for 24 hours. The dry density is then calculated using the known density and water content.

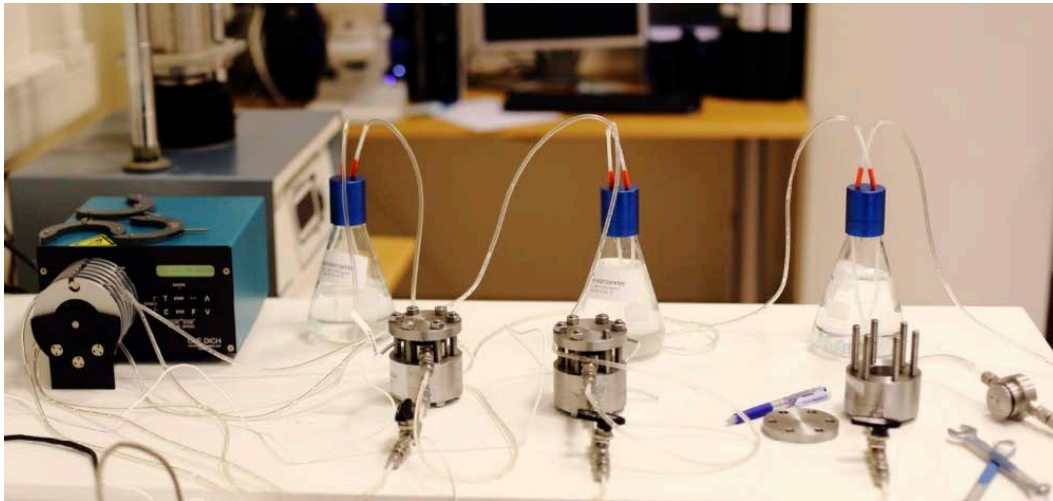


*Figure 2-1. Equipment for measuring swelling pressure and hydraulic conductivity.*

## 2.2 Hydromechanical properties

Overview of the swelling pressure and hydraulic conductivity sequential procedure:

1. Swelling pressure (SP) of original clay sample with deionised water (DI) for approximately 1 week.
2. Hydraulic conductivity using DI water for approximately 1 week.
3. Swelling pressure (SP) using 1 M CaCl<sub>2</sub> solution for approximately 1 week.
4. Hydraulic conductivity using 1 M CaCl<sub>2</sub> solution for approximately 1 week.
5. Swelling pressure (SP) of Ca-exchanged sample with deionised water (DI) for approximately 1 week.

This procedure gives several datasets showing the swelling pressure and hydraulic conductivity during several different conditions (Table 2-1a-d).

In order to remove effects from the type of interlayer cation and any salts in the sample, the Ca-exchanged samples with deionised water were selected to study details in the swelling pressure in LOT A3 and S2, while hydraulic conductivity was studied in detail using the 1 M CaCl<sub>2</sub> solution case, as it is the most demanding on the bentonite. As differences arising from cation exchange reactions otherwise easily can overshadow any differences in performance due to any potential mineralogical alterations.

### 2.2.1 Swelling pressure on grinded and recompacted samples

Swelling pressure data of samples taken from LOT A3 and LOT S2 are indistinguishable from the reference data (Figure 2-2a-b). Hence, the swelling pressure performance was unaffected by the long term heating in the experiments.

### 2.2.2 Hydraulic conductivity on grinded and recompacted samples

Hydraulic conductivity in 1 M CaCl<sub>2</sub> solution, show a very small, but still significant increase in the field samples compared to the reference samples (Figure 2-2c-d), especially at the lower densities it seems.

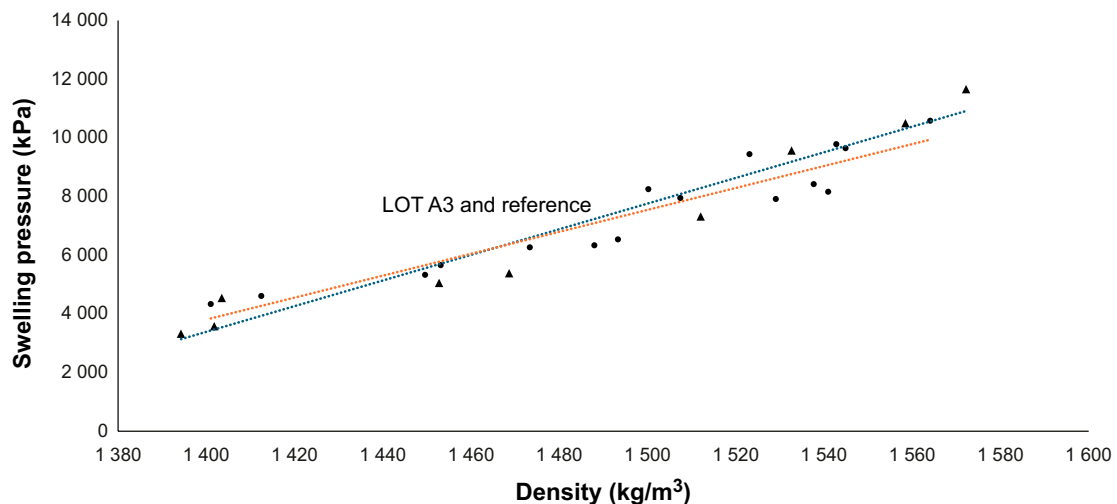


**Figure 2-2a.** LOT A3 swelling pressure of Ca-exchanged samples after washing with deionised water: Circles = field experiment samples. Triangles = reference samples. Fittings are present as guides for the eyes.

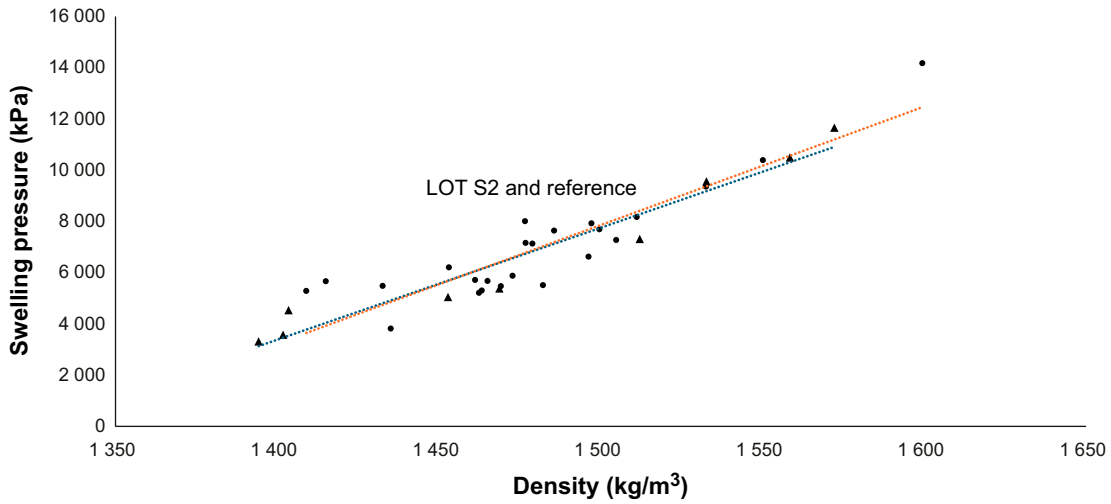


**Figure 2-2b.** LOT S2 swelling pressure of Ca-exchanged samples after washing with deionised water. Circles = field experiment samples. Triangles = reference samples. Fittings are present as guides for the eyes.

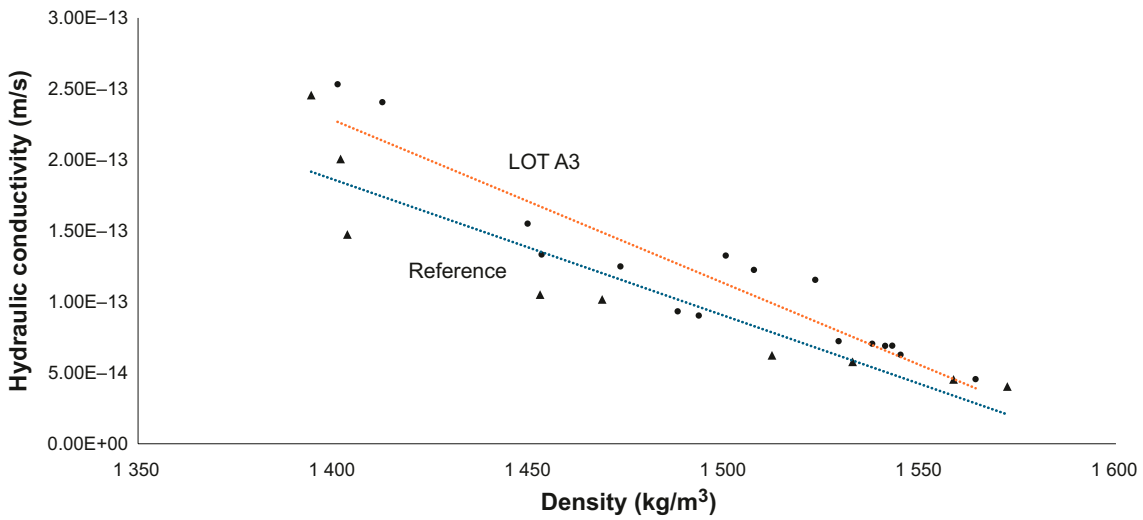


**Figure 2-2c.** LOT A3 hydraulic conductivity in 1 M CaCl<sub>2</sub> solution. Circles = field experiment samples. Triangles = reference samples. Fittings are present as guides for the eyes.

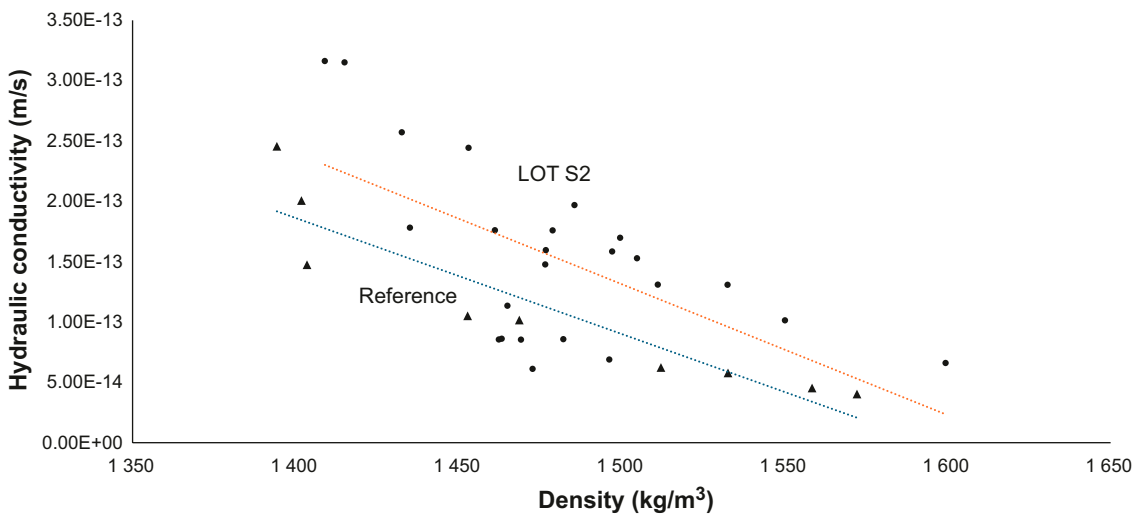


**Figure 2-2d.** LOT S2 hydraulic conductivity in 1 M CaCl<sub>2</sub> solution. Circles = field experiment samples. Triangles = reference samples. Fittings are present as guides for the eyes.

**Table 2-1a. LOT A3 and reference swelling pressure data.**

Test No	Dry density (kg/m <sup>3</sup> )	SP DI (kPa)	SP 1 M CaCl <sub>2</sub> (kPa)	SP DI Ca-exchanged (kPa)
LOT A3 #15 Ref. 1	1404	4435.5	2790.2	4540.1
LOT A3 #15 Ref. 2	1453	4828.7	3063.0	5051.1
LOT A3 #15 Ref. 3	1512	6841.3	5091.2	7316.7
LOT A3 #15 Ref. 4	1394	3378.4	1908.9	3320.2
LOT A3 #15 Ref. 5	1469	4994.4	3312.9	5382.2
LOT A3 #15 Ref. 6	1572	10353.8	9259.6	11657.6
LOT A3 #15 Ref. 7	1402	3565.9	1931.5	3579.7
LOT A3 #15 Ref. 8	1533	8643.1	6917.8	9564.2
LOT A3 #15 Ref. 9	1558	9387.3	7803.6	10497.9
LOT A3 #9E 0–10 mm 1	1538	7565.5	6625.9	8419.2
LOT A3 #9E 0–10 mm 2	1493	6005.6	4513.4	6538.2
LOT A3 #9E 10–20 mm 1	1543	8807.6	7691.0	9783.5
LOT A3 #9E 10–20 mm 2	1564	9343.8	8517.4	10582.7
LOT A3 #9E 20–50 mm 1	1401	4181.2	2547.2	4333.9
LOT A3 #9E 20–50 mm 2	1412	4412.6	2829.2	4608.9
LOT A3 #9E 50–100 mm 1	1453	5302.9	3575.6	5660.7
LOT A3 #9E 50–100 mm 2	1507	7130.2	5450.7	7946.7
LOT A3 #11N 0–10 mm 1	1488	5701.7	4255.7	6336.9
LOT A3 #11N 0–10 mm 2	1545	8555.6	7528.4	9646.2
LOT A3 #11N 10–20 mm 1	1529	7011.7	5673.5	7915.5
LOT A3 #11N 10–20 mm 2	1541	7190.7	5969.9	8158.2
LOT A3 #11N 20–50 mm 1	1473	5756.0	4182.6	6268.2
LOT A3 #11N 20–50 mm 2	1450	4983.4	3391.4	5329.2
LOT A3 #11N 50–100 mm 1	1500	7422.2	5966.0	8250.1
LOT A3 #11N 50–100 mm 2	1523	8215.5	7064.3	9441.5

**Table 2-1b. LOT A3 and reference hydraulic conductivity data.**

Test No	Dry density (kg/m <sup>3</sup> )	HC DI (m/s)	HC 1 M CaCl <sub>2</sub> (m/s)
LOT A3 #15 Ref. 1	1404	1.74E-13	1.47E-13
LOT A3 #15 Ref. 2	1453	1.54E-13	1.05E-13
LOT A3 #15 Ref. 3	1512	1.22E-13	6.23E-14
LOT A3 #15 Ref. 4	1394	1.83E-13	2.46E-13
LOT A3 #15 Ref. 5	1469	1.16E-13	1.02E-13
LOT A3 #15 Ref. 6	1572	6.71E-14	4.03E-14
LOT A3 #15 Ref. 7	1402	1.82E-13	2.01E-13
LOT A3 #15 Ref. 8	1533	7.74E-14	5.78E-14
LOT A3 #15 Ref. 9	1558	8.35E-14	4.53E-14
LOT A3 #9E 0–10 mm 1	1538	1.49E-13	7.05E-14
LOT A3 #9E 0–10 mm 2	1493	1.58E-13	9.03E-14
LOT A3 #9E 10–20 mm 1	1543	1.39E-13	6.91E-14
LOT A3 #9E 10–20 mm 2	1564	1.04E-13	4.56E-14
LOT A3 #9E 20–50 mm 1	1401	2.80E-13	2.53E-13
LOT A3 #9E 20–50 mm 2	1412	2.81E-13	2.41E-13
LOT A3 #9E 50–100 mm 1	1453	2.08E-13	1.33E-13
LOT A3 #9E 50–100 mm 2	1507	1.55E-13	1.22E-13
LOT A3 #11N 0–10 mm 1	1488	1.52E-13	9.33E-14
LOT A3 #11N 0–10 mm 2	1545	1.25E-13	6.28E-14
LOT A3 #11N 10–20 mm 1	1529	1.19E-13	7.22E-14
LOT A3 #11N 10–20 mm 2	1541	1.28E-13	6.90E-14
LOT A3 #11N 20–50 mm 1	1473	1.58E-13	1.25E-13
LOT A3 #11N 20–50 mm 2	1450	1.93E-13	1.55E-13
LOT A3 #11N 50–100 mm 1	1500	1.63E-13	1.33E-13
LOT A3 #11N 50–100 mm 2	1523	1.57E-13	1.16E-13

**Table 2-1c. LOT S2 swelling pressure data.**

Test No	Dry density (kg/m <sup>3</sup> )	SP DI (kPa)	SP 1 M CaCl <sub>2</sub> (kPa)	SP DI Ca-exchanged (kPa)
LOT S2 #9E 0–10 mm 1	1482	5202.8	3733.4	5513.3
LOT S2 #9E 0–10 mm 2	1465	5247.0	3452.7	5678.8
LOT S2 #9E 10–20 mm 1	1479	6338.7	4953.5	7133.4
LOT S2 #9E 10–20 mm 2	1533	8129.0	7104.8	9359.8
LOT S2 #9 20–50 mm 1	1433	4839.4	3515.3	5484.4
LOT S2 #9 20–50 mm 2	1500	6755.8	5674.3	7697.1
LOT S2 #9 50–100 mm 1	1550	8904.2	8018.1	10395.5
LOT S2 #9 50–100 mm 2	1599	12165.4	11697.2	14180.7
LOT S2 #11 0–10 mm 1	1435	3744.2	2203.5	3822.1
LOT S2 #11 0–10 mm 2	1469	5057.0	3269.2	5473.5
LOT S2 #11 10–20 mm 1	1453	5577.2	4079.1	6211.0
LOT S2 #11 10–20 mm 2	1486	6720.9	5305.1	7646.4
LOT S2 #11 20–50 mm 1	1461	5140.3	3766.9	5718.9
LOT S2 #11 20–50 mm 2	1511	7201.6	6081.9	8173.6
LOT S2 #11 50–100 mm 1	1477	6526.0	4945.6	7161.0
LOT S2 #11 50–100 mm 2	1477	7021.7	5709.1	8011.8
LOT S2 #33 0–10 mm 1	1463	5049.8	3032.0	5306.5
LOT S2 #33 0–10 mm 2	1462	4956.7	3104.7	5217.8
LOT S2 #33 10–20 mm 1	1473	5568.2	3656.6	5882.1
LOT S2 #33 10–20 mm 2	1496	6146.8	4144.1	6628.5
LOT S2 #33 20–50 mm 1	1415	4954.9	3612.0	5664.9
LOT S2 #33 20–50 mm 2	1409	4756.5	3373.2	5287.3
LOT S2 #33 50–100 mm 1	1505	6557.6	4887.2	7277.8
LOT S2 #33 50–100 mm 2	1497	7050.9	5231.1	7927.9

**Table 2-1d. LOT S2 hydraulic conductivity data.**

Test No	Dry density (kg/m <sup>3</sup> )	HC DI (m/s)	HC 1 M CaCl <sub>2</sub> (m/s)
LOT S2 #9E 0–10 mm 1	1482	1.87E–13	8.58E–14
LOT S2 #9E 0–10 mm 2	1465	1.96E–13	1.13E–13
LOT S2 #9E 10–20 mm 1	1479	2.89E–13	1.76E–13
LOT S2 #9E 10–20 mm 2	1533	2.18E–13	1.31E–13
LOT S2 #9 20–50 mm 1	1433	3.14E–13	2.57E–13
LOT S2 #9 20–50 mm 2	1500	2.47E–13	1.70E–13
LOT S2 #9 50–100 mm 1	1550	1.54E–13	1.01E–13
LOT S2 #9 50–100 mm 2	1599	1.23E–13	6.61E–14
LOT S2 #11 0–10 mm 1	1435	2.11E–13	1.78E–13
LOT S2 #11 0–10 mm 2	1469	1.49E–13	8.54E–14
LOT S2 #11 10–20 mm 1	1453	3.41E–13	2.44E–13
LOT S2 #11 10–20 mm 2	1486	2.82E–13	1.97E–13
LOT S2 #11 20–50 mm 1	1461	2.49E–13	1.76E–13
LOT S2 #11 20–50 mm 2	1511	2.16E–13	1.31E–13
LOT S2 #11 50–100 mm 1	1477	2.10E–13	1.60E–13
LOT S2 #11 50–100 mm 2	1477	1.96E–13	1.48E–13
LOT S2 #33 0–10 mm 1	1463	1.60E–13	8.62E–14
LOT S2 #33 0–10 mm 2	1462	1.73E–13	8.55E–14
LOT S2 #33 10–20 mm 1	1473	1.56E–13	6.12E–14
LOT S2 #33 10–20 mm 2	1496	1.15E–13	6.89E–14
LOT S2 #33 20–50 mm 1	1415	3.36E–13	3.15E–13
LOT S2 #33 20–50 mm 2	1409	3.29E–13	3.16E–13
LOT S2 #33 50–100 mm 1	1505	1.74E–13	1.53E–13
LOT S2 #33 50–100 mm 2	1497	1.96E–13	1.58E–13

## 2.3 Chemistry and mineralogy

### 2.3.1 Chemistry and mineralogy of bulk samples

#### *Mineralogy of bulk samples (Powder XRD)*

Powder XRD of some of the A3 bulk samples closest to the heater show a new reflection around 30 degree two theta (Figure 2-3a and Figure 2-4a). This is anhydrite (Figure 2-3d), formed by accumulation and dehydration of gypsum in the bentonite. The most common accessory minerals in the bentonite are marked and shown in detail in Figure 2-3d and Figure 2-3e.

In most samples no changes can be seen in the low angle region where the basal reflections are. Changes here are typically correlating to the hydration of the montmorillonite and is mainly affected by cation exchange reactions e.g. from  $\text{Na}^+$  to  $\text{Ca}^{2+}$ . The lack of change in this region indicate that most of the montmorillonite exchanged very little of its interlayer cations in the experiment. One exception is seen in LOT A3 block #35 (Figure 2-5) where the basal reflections are broader and has a shoulder towards lower angles, indicating the presence of more  $\text{Ca}^{2+}$  in the interlayer, that was hydrating stronger at the relative humidity in the laboratory.

In the 060 region, the dioctahedral, or trioctahedral nature of the smectite can be seen. No change could be observed (Figure 2-3c and Figure 2-4c), indicating that the dioctahedral nature of the montmorillonite was unchanged.

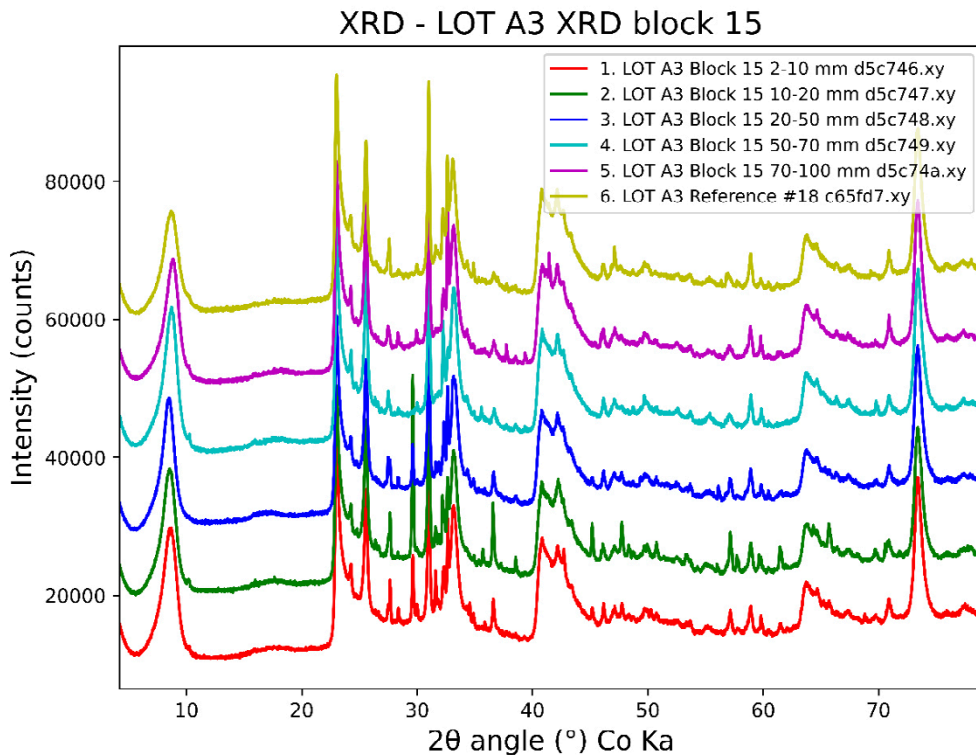


*Figure 2-3a. XRD of LOT A3 block #15 full pattern.*

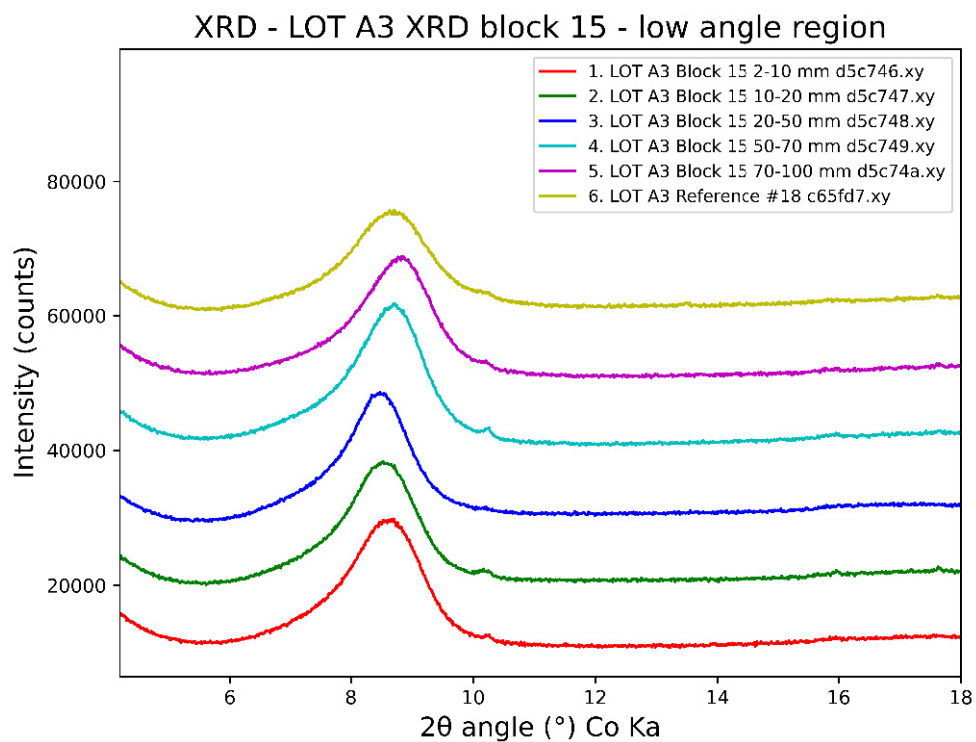


*Figure 2-3b. XRD of LOT A3 block #15 closeup of low angle 001 region.*

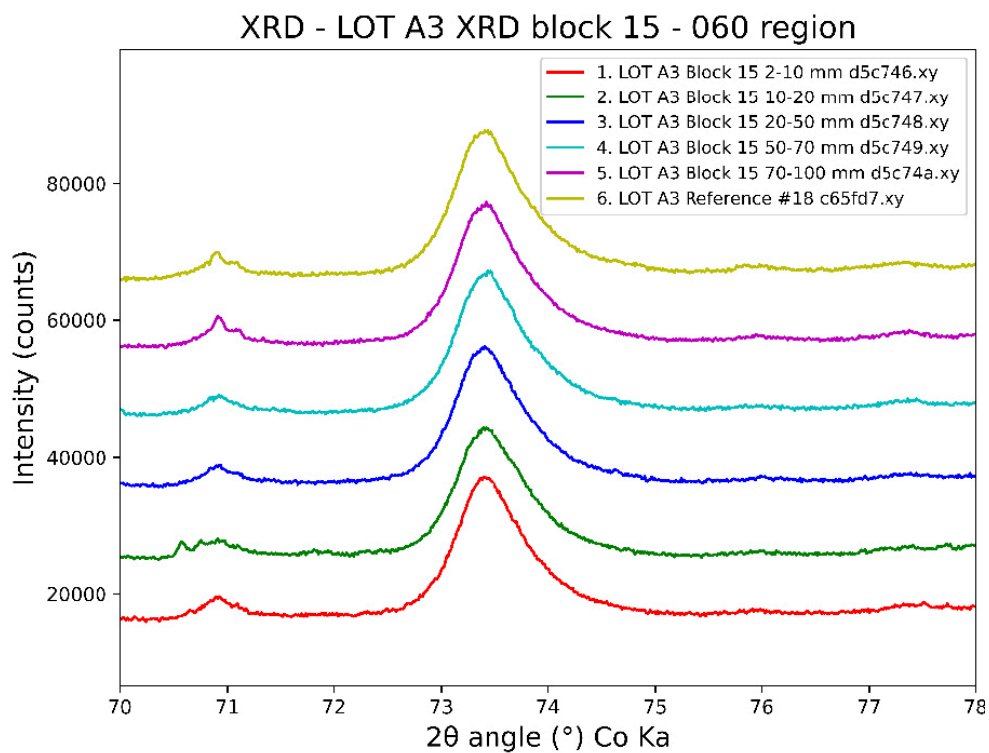


*Figure 2-3c. XRD of LOT A3 block #15 closeup of 060 reflections.*

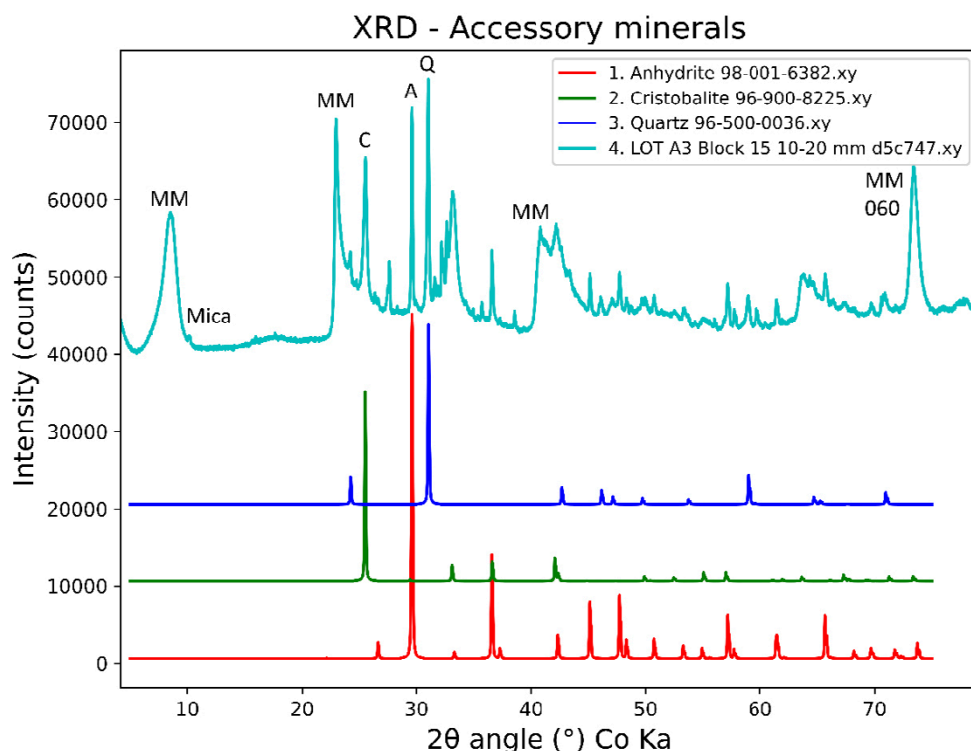


**Figure 2-3d.** XRD of LOT A3 block #15, 10–20 mm sample with simulated accessory minerals. Montmorillonite (MM), cristobalite (C), quartz (Q), Mica.

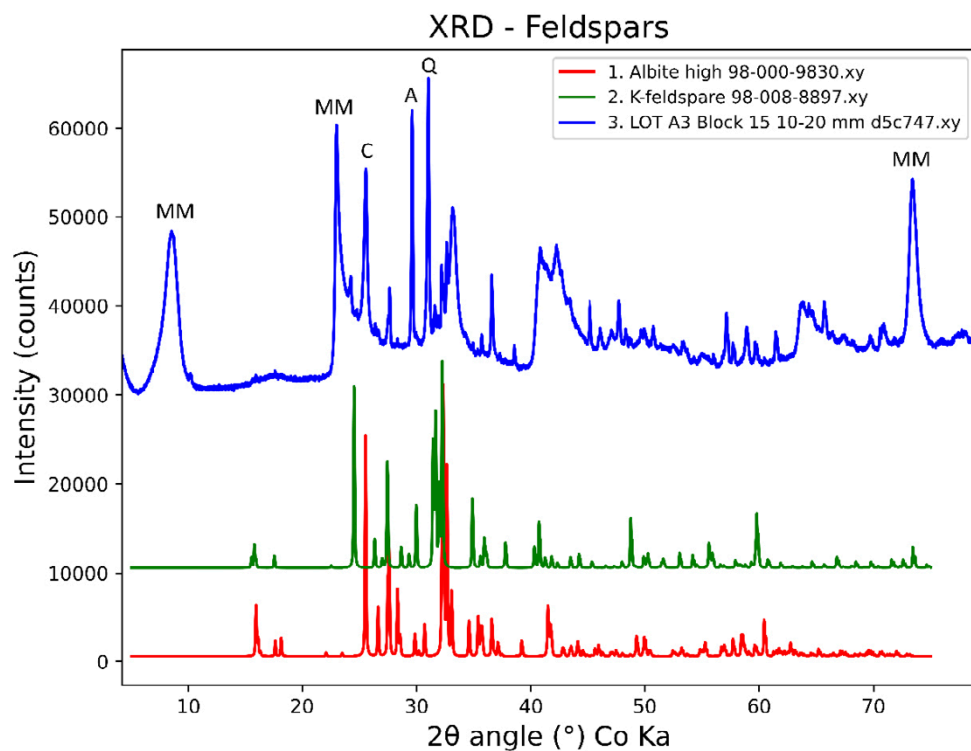


**Figure 2-3e.** XRD of LOT A3 block #15, 10–20 mm sample compared to simulated feldspare phases. Montmorillonite (MM), cristobalite (C), quartz (Q), Mica.

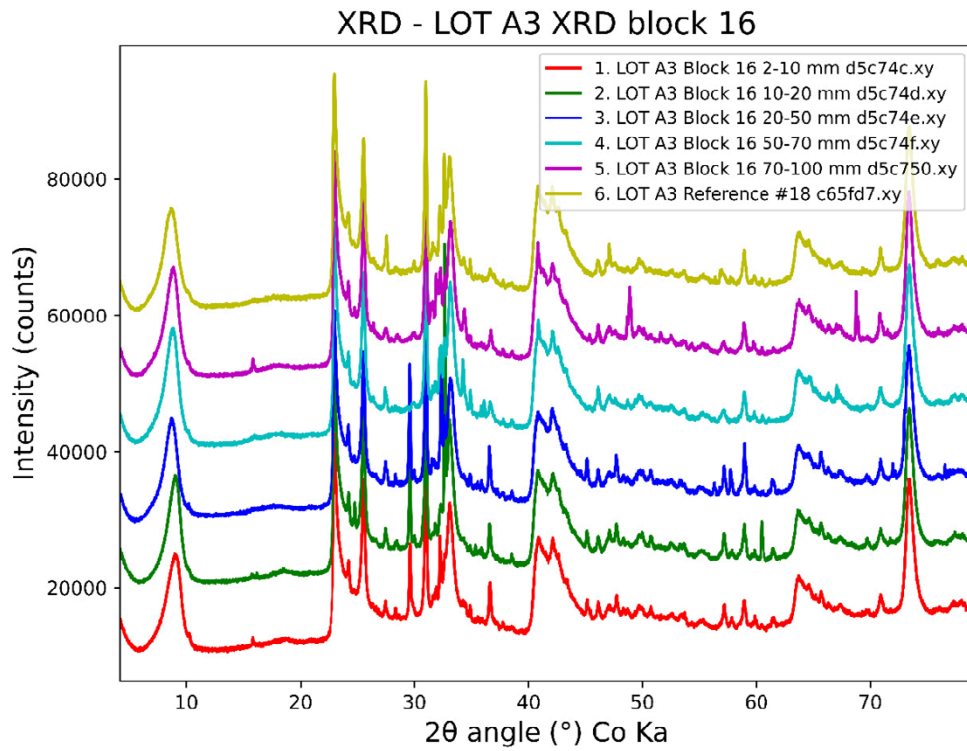


**Figure 2-4a.** XRD of LOT A3 block #16 full pattern.

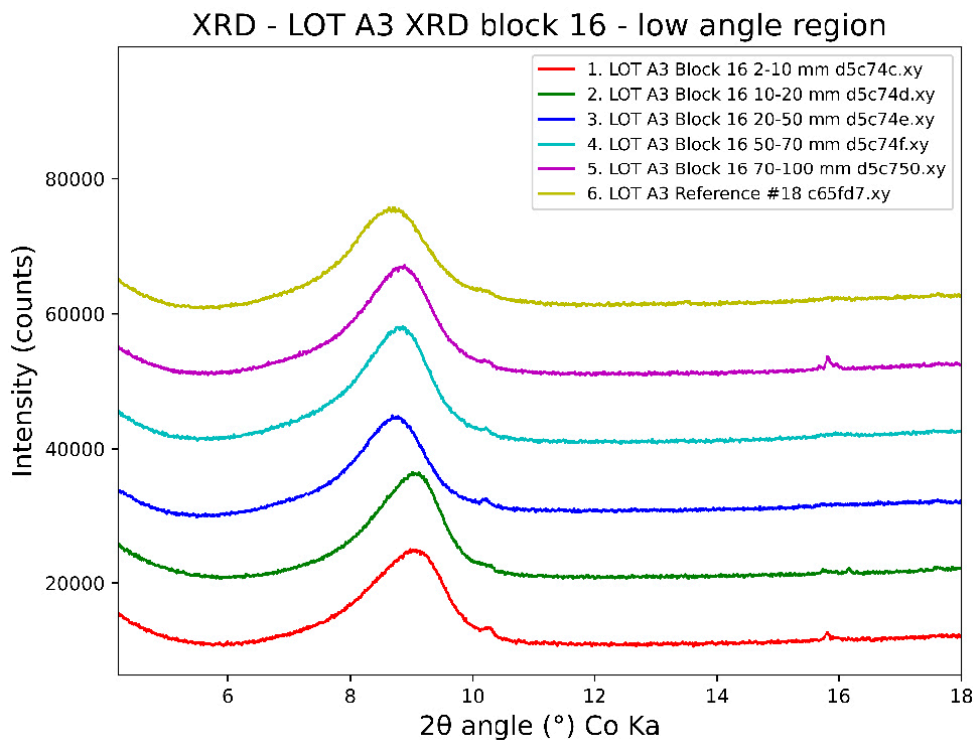


**Figure 2-4b.** XRD of LOT A3 block #16 closeup of low angle 001 region.

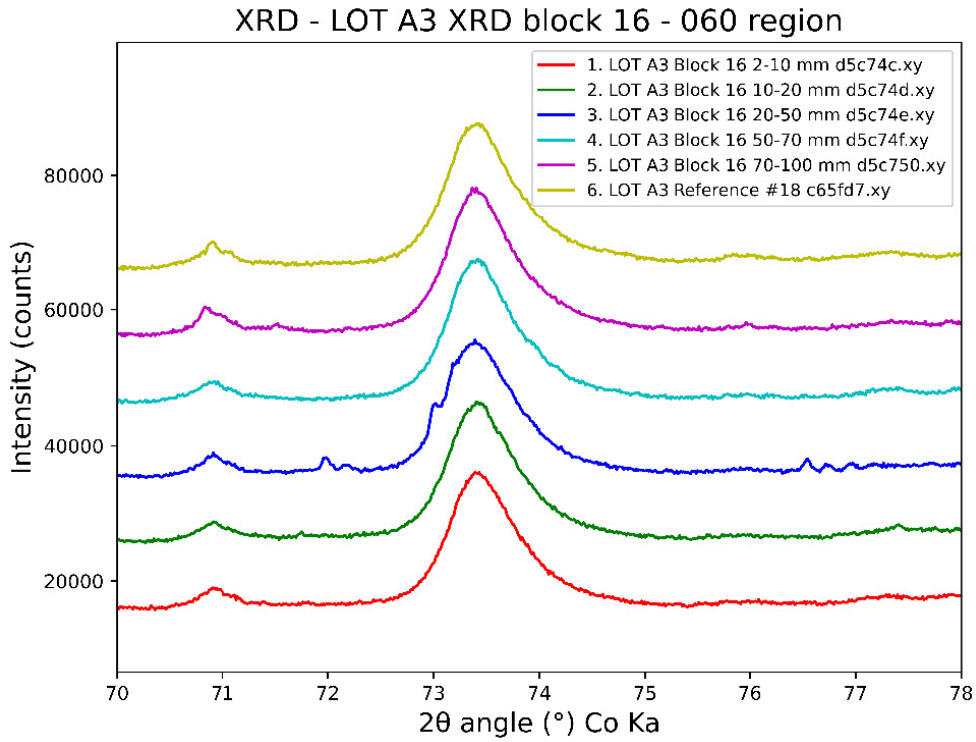


**Figure 2-4c.** XRD of LOT A3 block #16 full pattern closeup of 060 reflections.

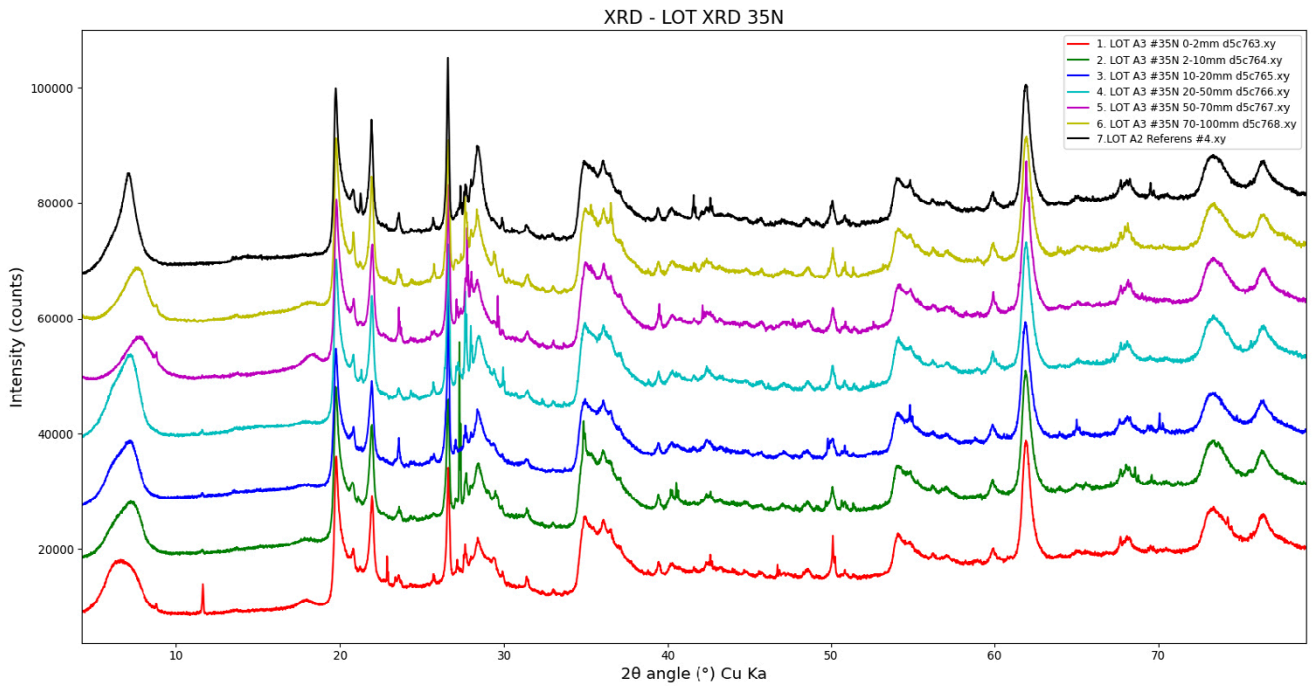


**Figure 2-5.** XRD of LOT A3 block #35 full pattern.

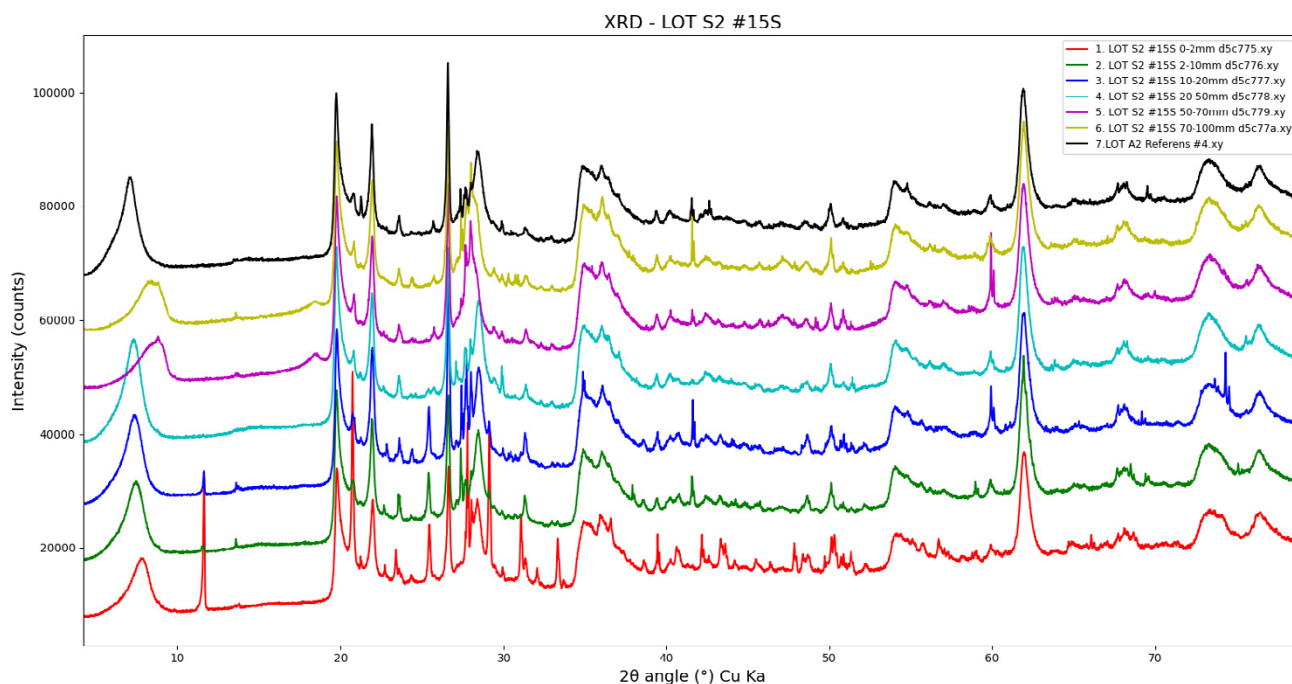


**Figure 2-6.** XRD of LOT S2 block #15 full pattern.

### **Chemical composition of bulk samples (XRF)**

Due to corrosion the amount of Cu increased in the vicinity of the heater (Figure 2-7 and Figure 2-8). The copper corrosion in the experiment has been handled separately in detail in Johansson et al. 2020 and will not be further mentioned in this report.

Sulfur and calcium are associated with each other as they predominantly exist together as calcium sulfate in the form of gypsum or anhydrite depending on the temperature in the bentonite. In field experiments the calcium sulfate is typically observed to accumulate towards the central heater. This is observed also here both in the LOT A3 and S2 experiments (Figure 2-7; Figure 2-8; Table 2-2). The accumulation is heterogeneous and looks different in the different blocks.

The average CaO content of the reference material is 1.72 wt% (Table 2-2). While in the samples closest to the rock the values are generally lower, except for LOT A3 block 33 and 35. This is compatible with the conclusions from the powder XRD data above, that most samples had very limited cation exchange from  $\text{Na}^+$  to  $\text{Ca}^{2+}$ , however with the exception of some areas such as the LOT A3 block 33 and 35 that did have some cation exchange with the Äspö ground water.

Increase in MgO was observed in LOT A3 block 9, 11, 15, and 16, but not in the rest of the samples (Table 2-2). No significant change in the potassium content ( $\text{K}_2\text{O}$ ) could be identified. Chloride (Cl) was 0.02 wt% in the reference material and roughly 0.1–0.3 wt% in the samples from the experiments, due to the uptake of Äspö ground water, being very homogeneously distributed.

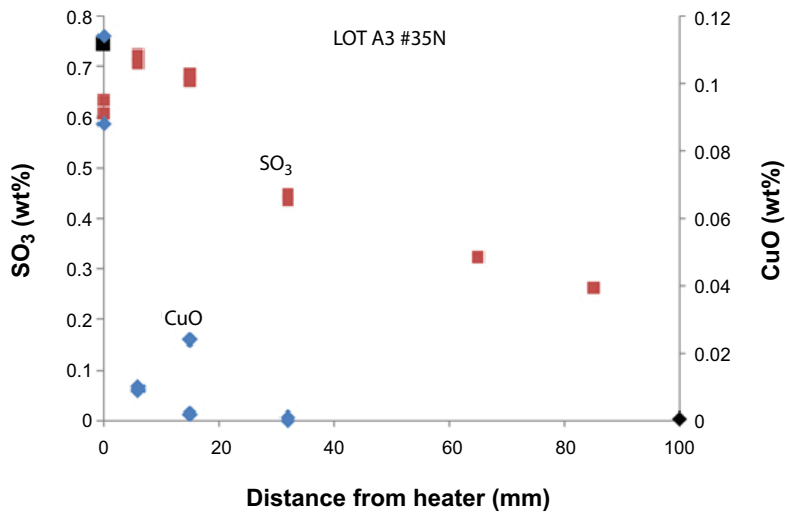
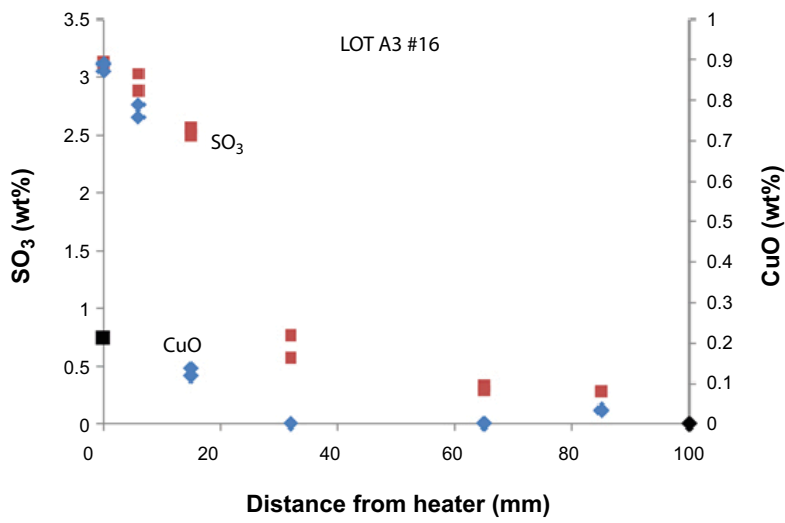
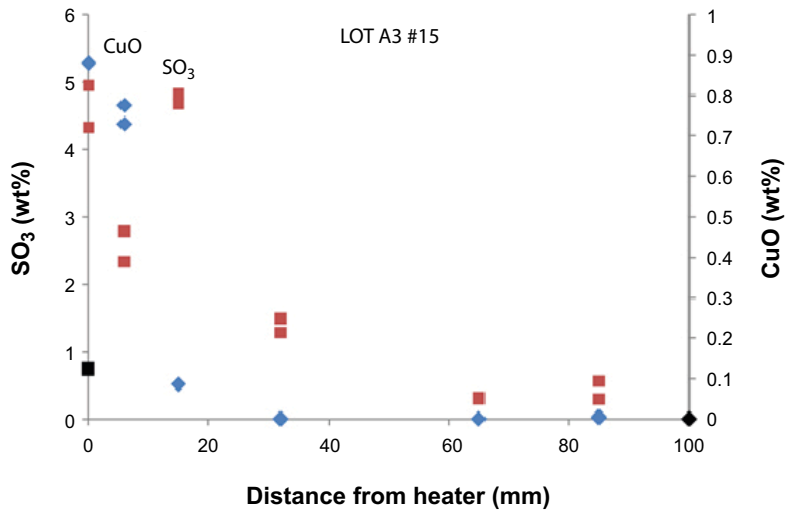


Figure 2-7. Copper and sulfur levels in some LOT A3 profiles as a function of the distance from the heater (XRF data).

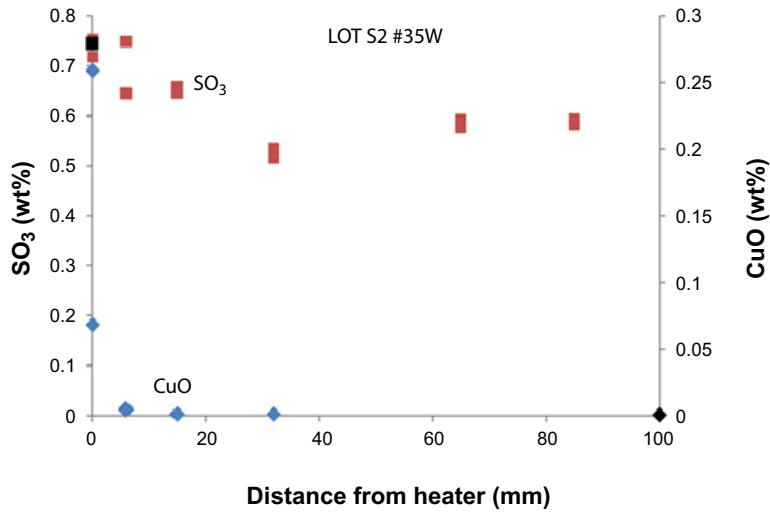
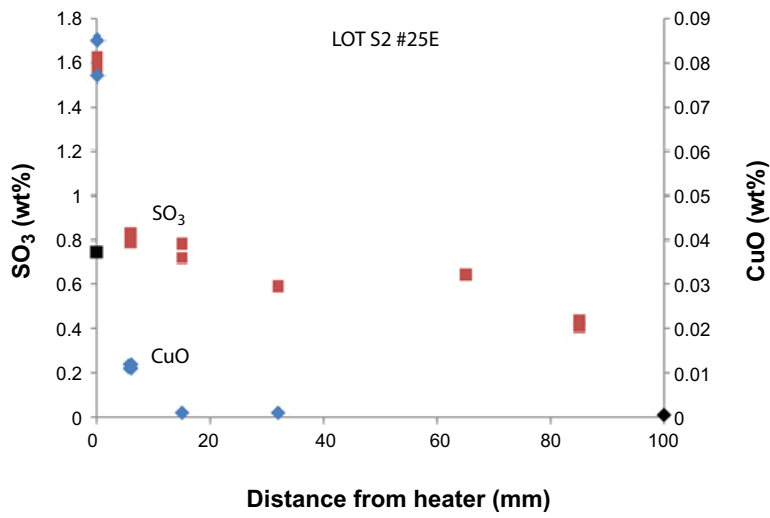
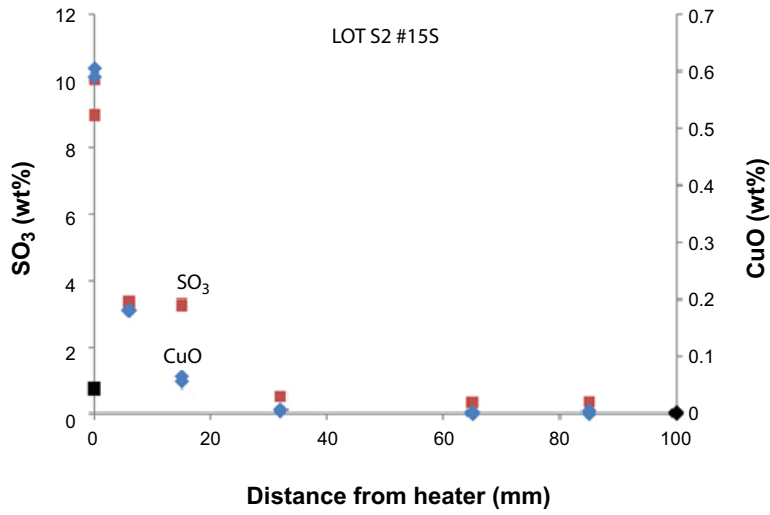


Figure 2-8. Copper and sulfur levels in some LOT S2 profiles as a function of the distance from the heater (XRF data).

**Table 2-2a. LOT A2 MX80 Reference material. XRF data.**

Sample	Na <sub>2</sub> O	MgO	Al <sub>2</sub> O <sub>3</sub>	SiO <sub>2</sub>	SO <sub>3</sub>	Cl	K <sub>2</sub> O	CaO	TiO <sub>2</sub>	MnO	Fe <sub>2</sub> O <sub>3</sub>	CuO
LOT A2 MX80 Referens block 4	1.68	2.33	20.51	67.54	0.67	0.01	0.71	1.73	0.18	0.02	4.61	0.00
LOT A2 MX80 Referens block 4	1.60	2.39	20.61	67.83	0.71	0.01	0.52	1.55	0.18	0.01	4.60	0.00
LOT A2 MX80 Referens block 29	1.66	2.35	20.52	67.59	0.67	0.01	0.67	1.72	0.18	0.02	4.62	0.00
LOT A2 MX80 Referens block 29	1.68	2.33	20.54	67.71	0.66	0.01	0.67	1.65	0.18	0.02	4.55	0.00
LOT A2 MX80 Referens block 24	1.67	2.34	20.52	67.65	0.74	0.01	0.64	1.69	0.18	0.01	4.54	0.00
LOT A2 MX80 Referens block 24	1.68	2.35	20.41	67.63	0.76	0.01	0.66	1.74	0.18	0.02	4.57	0.00
LOT A2 MX80 Referens block 29	1.56	2.42	20.79	67.35	0.92	0.01	0.51	1.70	0.17	0.01	4.55	0.00
LOT A2 MX80 Referens block 29	1.61	2.42	20.75	67.33	0.69	0.02	0.51	1.80	0.18	0.01	4.69	0.00
LOT A2 MX80 Referens block 24	1.58	2.44	20.83	67.46	0.75	0.01	0.50	1.66	0.18	0.01	4.58	0.00
LOT A2 MX80 Referens block 24	1.63	2.45	21.05	66.73	0.90	0.01	0.51	1.91	0.18	0.01	4.63	0.00
LOT A2 MX80 Referens Block 4	1.55	2.41	20.62	67.50	0.80	0.02	0.52	1.80	0.18	0.01	4.61	0.00
LOT A2 MX80 Referens Block 4	1.68	2.35	20.59	67.43	0.68	0.07	0.68	1.72	0.19	0.02	4.58	0.00
<b>Average</b>	<b>1.63</b>	<b>2.38</b>	<b>20.64</b>	<b>67.48</b>	<b>0.75</b>	<b>0.02</b>	<b>0.59</b>	<b>1.72</b>	<b>0.18</b>	<b>0.01</b>	<b>4.59</b>	<b>0.00</b>
SD	0.05	0.04	0.18	0.28	0.09	0.02	0.09	0.09	0.00	0.00	0.04	0.00

**Table 2-2b. LOT S2 samples. XRF data.**

Sample	Na <sub>2</sub> O	MgO	Al <sub>2</sub> O <sub>3</sub>	SiO <sub>2</sub>	SO <sub>3</sub>	Cl	K <sub>2</sub> O	CaO	TiO <sub>2</sub>	MnO	Fe <sub>2</sub> O <sub>3</sub>	CuO
LOT S2 #15S 0–2 mm	1.45	2.14	17.43	57.15	10.03	0.12	0.55	5.86	0.17	0.01	4.45	0.60
LOT S2 #15S 2–10 mm	1.64	2.35	19.42	65.23	3.24	0.15	0.56	2.50	0.17	0.01	4.53	0.18
LOT S2 #15S 10–20 mm	1.65	2.32	19.46	65.38	3.23	0.16	0.56	2.51	0.17	0.01	4.48	0.07
LOT S2 #15S 20–50 mm	1.76	2.38	20.71	67.94	0.52	0.18	0.56	1.26	0.18	0.02	4.51	0.01
LOT S2 #15S 50–70 mm	1.73	2.31	20.66	68.15	0.34	0.17	0.56	1.26	0.18	0.01	4.63	0.00
LOT S2 #15S 70–100 mm	1.69	2.30	20.55	68.16	0.35	0.18	0.57	1.30	0.18	0.02	4.70	0.00
LOT S2 #25E 0–2 mm	1.71	2.27	19.98	67.02	1.62	0.12	0.61	1.89	0.18	0.01	4.48	0.09
LOT S2 #25E 2–10 mm	1.77	2.31	20.25	68.01	0.79	0.19	0.57	1.41	0.18	0.01	4.50	0.01
LOT S2 #25E 10–20 mm	1.73	2.32	20.13	68.28	0.72	0.21	0.57	1.43	0.17	0.01	4.41	0.00
LOT S2 #25E 20–50 mm	1.71	2.36	20.70	67.82	0.59	0.16	0.55	1.38	0.18	0.01	4.53	0.00
LOT S2 #25E 50–70 mm	1.69	2.33	20.65	67.74	0.64	0.14	0.56	1.46	0.18	0.01	4.61	0.00
LOT S2 #25E 70–100 mm	1.72	2.35	20.69	67.94	0.44	0.16	0.55	1.33	0.18	0.01	4.62	0.00
LOT S2 #35w 0–2 mm	1.66	2.29	20.26	67.69	0.75	0.07	0.64	1.63	0.18	0.01	4.55	0.26
LOT S2 #35w 2–10 mm	1.61	2.30	20.25	68.23	0.65	0.09	0.59	1.46	0.17	0.02	4.63	0.01
LOT S2 #35w 10–20 mm	1.68	2.28	20.21	68.32	0.65	0.12	0.63	1.45	0.18	0.01	4.47	0.00
LOT S2 #35w 20–50 mm	1.71	2.34	20.79	67.87	0.52	0.10	0.57	1.41	0.17	0.01	4.50	0.00
LOT S2 #15S 50–70 mm	1.73	2.32	20.66	68.11	0.32	0.16	0.58	1.30	0.18	0.02	4.61	0.00
LOT S2 #35W 70–100 mm	1.66	2.33	20.62	67.91	0.59	0.08	0.58	1.45	0.17	0.01	4.59	0.00

**Table 2-2c. LOT A3 samples. XRF data.**

Sample	Na <sub>2</sub> O	MgO	Al <sub>2</sub> O <sub>3</sub>	SiO <sub>2</sub>	SO <sub>3</sub>	Cl	K <sub>2</sub> O	CaO	TiO <sub>2</sub>	MnO	Fe <sub>2</sub> O <sub>3</sub>	CuO
LOT A3 #15 0–2 mm d5c745	1.39	3.19	18.58	62.07	4.95	0.14	0.53	3.34	0.18	0.02	4.73	0.88
LOT A3 #15 2–10 mm d5c746	1.50	2.57	19.28	65.55	2.34	0.15	0.59	2.16	0.18	0.01	4.89	0.78
LOT A3 #15 10–20 mm d5c747	1.52	2.25	18.84	63.82	4.67	0.16	0.60	3.06	0.18	0.01	4.79	0.09
LOT A3 #15 20–50 mm d5c748	1.59	2.24	19.69	67.73	1.28	0.18	0.60	1.70	0.20	0.01	4.77	0.00
LOT A3 #15 50–70 mm d5c749	1.60	2.23	20.05	68.68	0.30	0.24	0.55	1.34	0.18	0.01	4.82	0.00
LOT A3 #15 70–100 mm d5c750	1.62	2.22	19.99	68.65	0.30	0.28	0.58	1.28	0.19	0.01	4.88	0.00
LOT A3 #16 0–2 mm d5c74b	1.46	2.96	19.16	64.10	3.13	0.14	0.52	2.48	0.19	0.02	4.95	0.89
LOT A3 #16 2–10 mm d5c74c	1.49	2.39	19.02	65.19	3.03	0.14	0.59	2.48	0.18	0.01	4.69	0.79
LOT A3 #16 10–20 mm d5c74d	1.55	2.33	19.39	66.07	2.49	0.15	0.58	2.11	0.19	0.01	4.98	0.14
LOT A3 #16 20–50 mm d5c74e	1.59	2.23	19.75	68.32	0.77	0.23	0.62	1.57	0.20	0.02	4.70	0.00
LOT A3 #16 50–70 mm d5c74f	1.62	2.23	19.96	68.65	0.33	0.25	0.55	1.35	0.18	0.02	4.86	0.00
LOT A3 block 16 70–100 mm c5c750	1.66	2.23	20.29	68.83	0.30	0.15	0.56	1.17	0.18	0.01	4.62	0.00
LOT A3 #35N 0–2 mm	1.11	2.31	20.36	67.64	0.63	0.09	0.65	2.44	0.18	0.01	4.48	0.11
LOT A3 #35N 2–10 mm	1.10	2.26	20.32	67.85	0.71	0.09	0.65	2.25	0.18	0.01	4.57	0.01
LOT A3 #35N 10–20 mm	1.11	2.25	20.18	67.90	0.69	0.11	0.63	2.35	0.18	0.01	4.59	0.00
LOT A3 #35N 20–50 mm	1.13	2.31	20.85	67.74	0.43	0.13	0.58	2.11	0.18	0.01	4.52	0.00
LOT A3 #35N 50–70 mm	1.15	2.29	20.70	67.98	0.32	0.10	0.60	2.03	0.18	0.01	4.65	0.00
LOT A3 #35N 70–100 mm	1.14	2.30	20.73	68.11	0.26	0.11	0.59	2.00	0.18	0.01	4.58	0.00
LOT A3 #11N 0–2 mm d5c757	1.58	3.24	20.08	65.90	1.25	0.15	0.54	1.63	0.17	0.02	4.63	0.83
LOT A3 #11N 2–10 mm d5c758	1.59	2.65	19.99	66.68	1.30	0.15	0.57	1.61	0.18	0.01	4.74	0.52
LOT A3 #11N 10–20 mm d5c759	1.63	2.50	19.84	66.37	2.11	0.14	0.53	1.86	0.17	0.01	4.79	0.04
LOT A3 #11N 20–50 mm d5c75a	1.67	2.38	20.45	66.98	1.26	0.17	0.54	1.77	0.19	0.02	4.57	0.00
LOT A3 #11N 50–70 mm d5c75b	1.7	2.3	20.8	67.8	0.3	0.2	0.6	1.5	0.2	0	4.6	0
LOT A3 #11N 70–100 mm d5c75c	1.69	2.29	20.70	68.21	0.29	0.22	0.58	1.12	0.18	0.01	4.70	0.02
LOT A3 #9E 0–2 mm d5c751	1.51	3.38	19.64	65.06	1.97	0.13	0.52	2.08	0.17	0.02	4.69	0.81
LOT A3 #9E 2–10 mm d5c752	1.57	2.50	19.65	66.68	1.52	0.14	0.64	1.80	0.18	0.01	4.68	0.63
LOT A3 #9E 10–20 mm d5c753	1.64	2.39	19.97	67.22	1.51	0.14	0.61	1.63	0.18	0.01	4.66	0.03
LOT A3 #9E 20–50 mm d5c754	1.67	2.33	20.23	66.52	1.82	0.13	0.56	1.99	0.18	0.02	4.55	0.00
LOT A3 #9E 50–70 mm d5c755	1.68	2.29	20.59	67.81	0.31	0.16	0.59	1.72	0.20	0.02	4.64	0.00
LOT A3 #9E 70–100 mm d5c756	1.7	2.3	20.8	68.2	0.3	0.2	0.6	1.2	0.2	0	4.6	0
LOT A3 #33E 0–2 mm d5c75d	0.83	2.24	20.43	67.86	0.51	0.07	0.59	2.61	0.18	0.01	4.62	0.04
LOT A3 #33E 2–10 mm d5c75e	0.82	2.22	20.32	68.07	0.58	0.07	0.56	2.57	0.18	0.01	4.59	0.00
LOT A3 #33E 10–20 mm d5c75f	0.83	2.25	20.31	68.07	0.64	0.07	0.56	2.50	0.18	0.01	4.59	0.00
LOT A3 #33E 20–50 mm d5c760	0.83	2.27	20.71	67.75	0.51	0.07	0.53	2.55	0.18	0.02	4.58	0.00
LOT A3 #33E 50–70 mm d5c761	0.86	2.26	20.85	67.82	0.31	0.08	0.54	2.46	0.18	0.02	4.62	0.00
LOT A3 #33E 70–100 mm d5c762	0.85	2.25	20.85	67.91	0.25	0.08	0.54	2.44	0.18	0.02	4.61	0.00

**Cation exchange capacity of bulk samples (CEC)**

The samples were measured in eight different batches (Table 2-3). In every batch, an MX80 sample (not the LOT MX80 reference) was included to capture variations in the CEC absolute values (bias error) between the different batches as it is known that the repeatability of the method is much better than reproducibility (Svensson et al. 2019).

The variation in the MX80 reference was rather high (Table 2-3), and it was decided to evaluate the CEC data both as raw values, and as normalised data. The MX80 reference ranged from 78.98 to 85.17 cmol(+)/kg. Normalisation factors were calculated as the CEC value of the reference divided by the maximum observed value of the reference (85.17). Hence, normalisation factors of 0.93 to 1.0 were obtained (Table 2-3). Normalised CEC was calculated as the raw CEC divided by the normalisation factor of the batch. Hence if the reference was 5 % lower than the maximum, each CEC values were increased with a corresponding amount. This is not a standard procedure and will be used here as an alternative interpretation of the data.

In the CEC raw data (Figure 2-9a and Figure 2-10a), some samples decreased in CEC, while others increased. That is most likely due to calcium sulfate accumulation towards the heater.

In the normalised CEC data, it looks a bit different (Figure 2-9b and 2-10b). The profile A3 #33 changes appearance a bit since it has data from two different batches with different normalisation factors. Taking into account the variability of the method itself, there is probably no significant change between the S2, LOT A3 block #33 and the reference.

However, in the warmer mid section of the LOT A3 there seems to be small but significant increase in the CEC (block 9 and 11; Figure 2-9b).

Looking on the clay fractions, the interpretation is the same in both the raw data and in the normalised data. The CEC of the clay fractions in LOT S2 are very close to the LOT clay fraction reference value. Supporting the interpretation above of the normalised data of the S2 profile that the CEC was unaffected by the S2 experiment.

And the clay fractions of the LOT A3 mid section (block 9 and 11) show a small but significant increase in the CEC, supporting the interpretation of a very minor increase in the bulk samples. The average of the 3 innermost samples in A3 block 9 was 83.2 cmol(+)/kg and the reference was 80.5, making the average value 3.3 % higher than the reference value (83.2/80.5). This is a very small change and would have been discarded as scatter, if it was not for the more significant change in the CEC of the clay fractions that supports a small change in the bulk as well. However, measurements of clay fractions are more difficult than bulk samples (more difficult to disperse, smaller samples sizes etc), and the results should be interpreted with some caution.

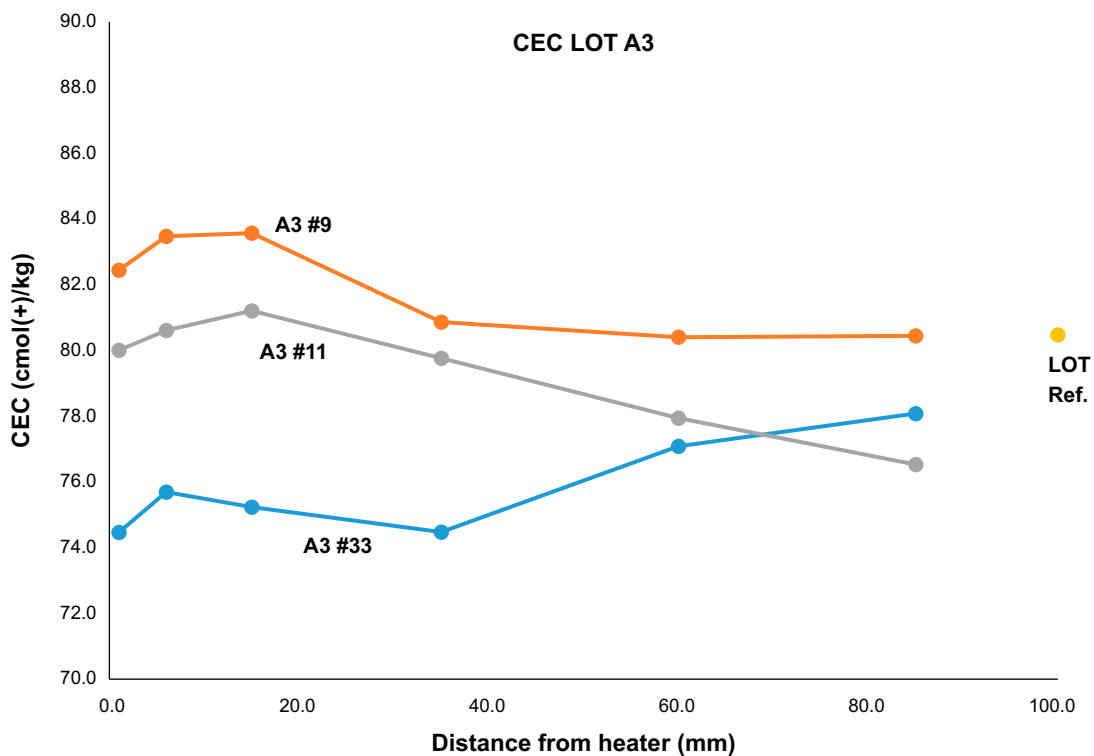


Figure 2-9a. LOT A3 CEC (cmol(+)/kg).

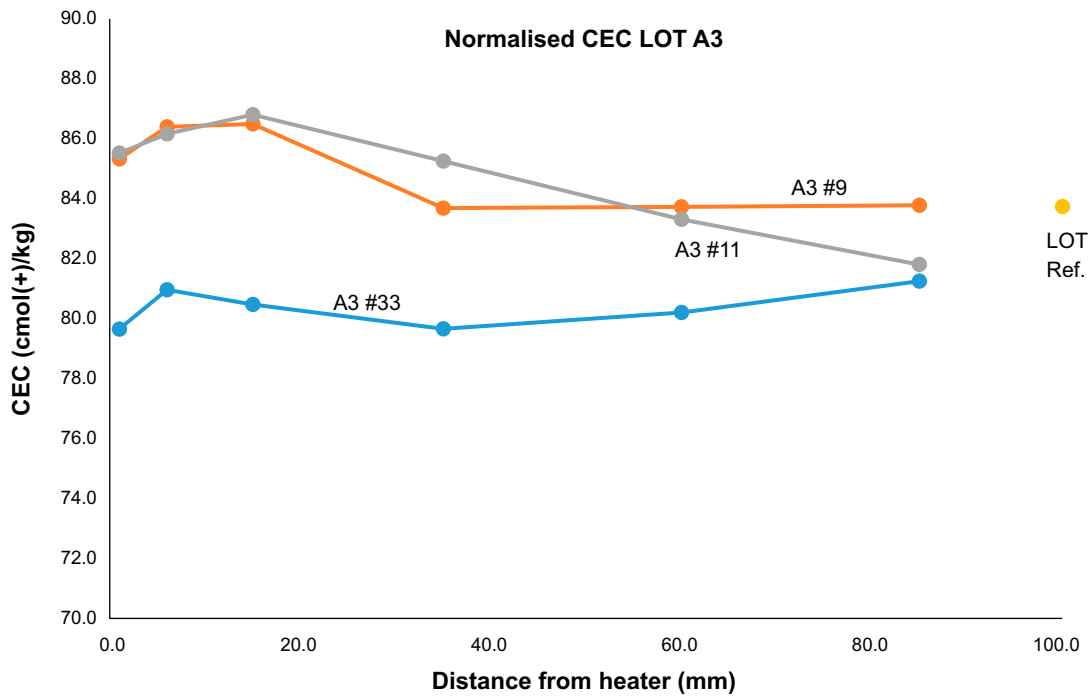


Figure 2-9b. LOT A3 Normalised CEC (cmol(+)/kg).

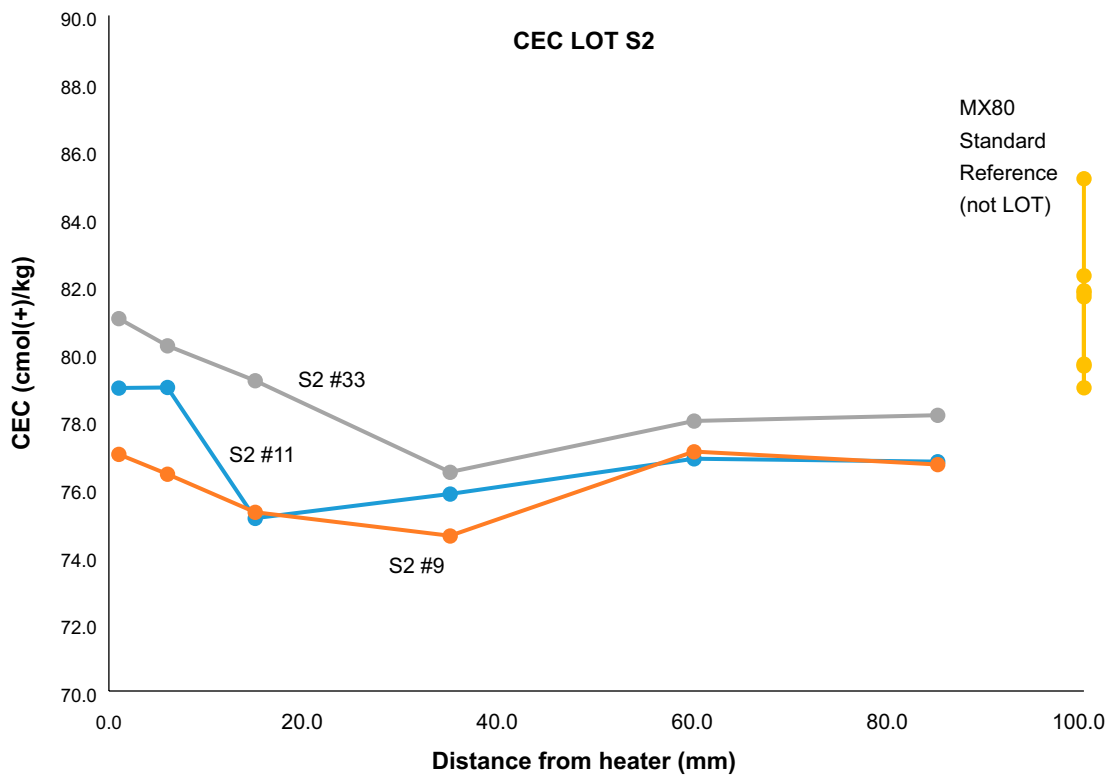


Figure 2-10a. LOT S2 CEC (cmol(+)/kg).

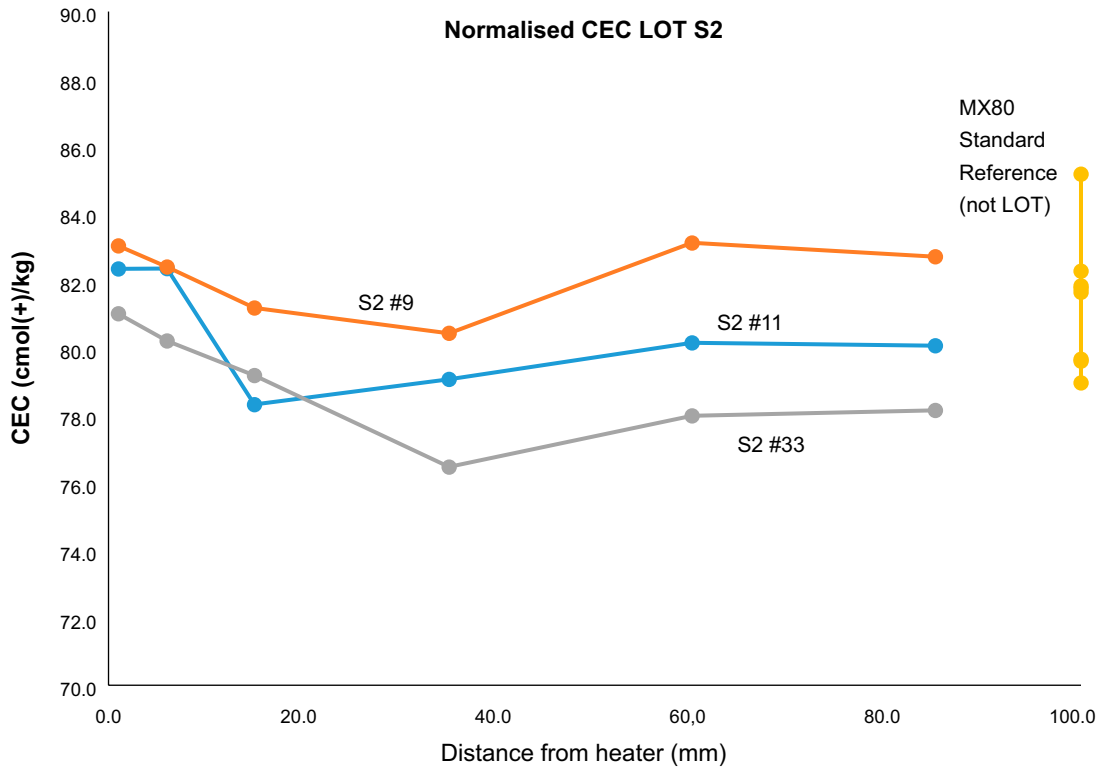


Figure 2-10b. LOT S2 Normalised CEC (cmol(+)/kg).

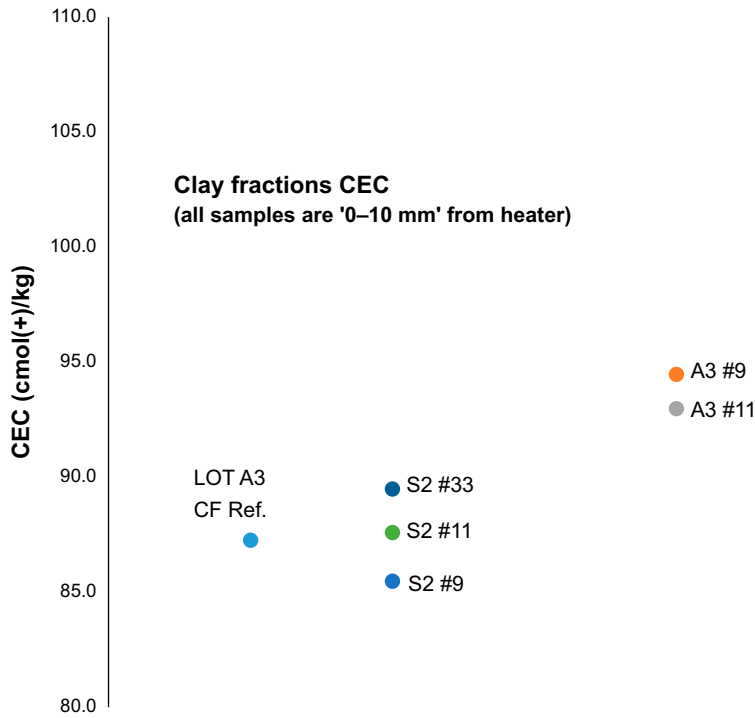


Figure 2-11a. LOT Clay fractions CEC (cmol(+)/kg).

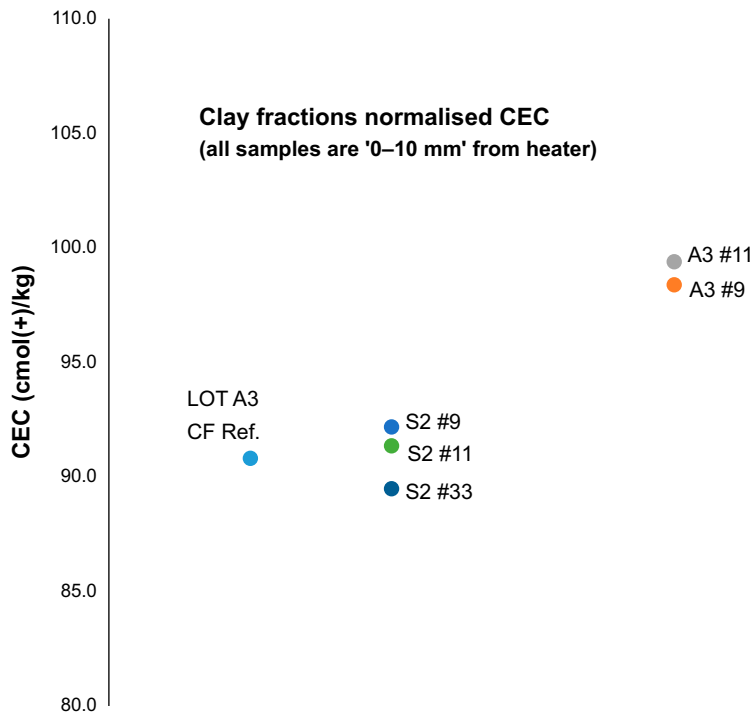


Figure 2-11b. LOT Clay fractions normalised CEC (cmol(+)/kg).

Table 2-3a. LOT A3 CEC (cmol(+)/kg) data.

Sample	CEC	Batch	Batch info		Norm. CEC
<b>LOT A3 #33</b>					
LOT A3 #33 0–2 mm	74.5	Batch #1	MX80 reference:	79.62	79.7
LOT A3 #33 2–10 mm	75.7	Batch #1	Normalisation factor:	0.93	81.0
LOT A3 #33 10–20 mm	75.2	Batch #1			80.5
LOT A3 #33 20–50 mm	74.5	Batch #1			79.7
LOT A3 #33 50–70 mm	77.1	Batch #2	MX80 reference:	81.85	80.2
LOT A3 #33 70–100 mm	78.1	Batch #2	Normalisation factor:	0.96	81.2
LOT Referens	80.5	Batch #2			83.7
LOT Referens Clayfr.	87.3	Batch #2			90.8
<b>LOT A3 #9</b>					
LOT A3 #9 0–2 mm	82.4	Batch #4	MX80 reference:	82.30	85.3
LOT A3 #9 2–10 mm	83.5	Batch #4	Normalisation factor:	0.97	86.4
LOT A3 #9 10–20 mm	83.6	Batch #4			86.5
LOT A3 #9 20–50 mm	80.9	Batch #4			83.7
LOT A3 #9 50–70 mm	80.4	Batch #3	MX80 reference:	81.78	83.7
LOT A3 #9 70–100 mm	80.4	Batch #3	Normalisation factor:	0.96	83.8
LOT A3 #9 0–10 mm Clayfr.	94.5	Batch #3			98.4
<b>LOT A3 #11</b>					
LOT A3 #11 0–2 mm	80.0	Batch #5	MX80 reference:	79.68	85.5
LOT A3 #11 2–10 mm	80.6	Batch #5	Normalisation factor:	0.94	86.2
LOT A3 #11 10–20 mm	81.2	Batch #5			86.8
LOT A3 #11 20–50 mm	79.8	Batch #5			85.3
LOT A3 #11 50–70 mm	77.9	Batch #5			83.3
LOT A3 #11 70–100 mm	76.5	Batch #5			81.8
LOT A3 #11 0–10 mm Clayfr.	93.0	Batch #5			99.4

**Table 2-3b. LOT S2 CEC (cmol(+)/kg) data.**

Sample	CEC	Batch	Batch info		Norm. CEC
<b>LOT S2 #9</b>					
LOT S2 #9 0–2 mm	77.0	Batch #6	MX80 reference:	78.98	83.0
LOT S2 #9 2–10 mm	76.4	Batch #6	Normalisation factor:	0.93	82.4
LOT S2 #9 10–20 mm	75.3	Batch #6			81.2
LOT S2 #9 20–50 mm	74.6	Batch #6			80.4
LOT S2 #9 50–70 mm	77.1	Batch #6			83.1
LOT S2 #9 70–100 mm	76.7	Batch #6			82.7
LOT S2 #9 0–10 mm Clayfr.	85.5	Batch #6			92.2
<b>LOT S2 #11</b>					
LOT S2 #11 0–2 mm	79.0	Batch #7	MX80 reference:	81.67	82.4
LOT S2 #11 2–10 mm	79.0	Batch #7	Normalisation factor:	0.96	82.4
LOT S2 #11 10–20 mm	75.1	Batch #7			78.3
LOT S2 #11 20–50 mm	75.8	Batch #7			79.1
LOT S2 #11 50–70 mm	76.9	Batch #7			80.2
LOT S2 #11 70–100 mm	76.8	Batch #7			80.1
LOT S2 #11 0–10 mm Clayfr.	87.6	Batch #7			91.4
<b>LOT S2 #33</b>					
LOT S2 #33 0–2 mm	81.0	Batch #8	MX80 reference:	85.17	81.0
LOT S2 #33 2–10 mm	80.2	Batch #8	Normalisation factor	1.00	80.2
LOT S2 #33 10–20 mm	79.2	Batch #8			79.2
LOT S2 #33 20–50 mm	76.5	Batch #8			76.5
LOT S2 #33 50–70 mm	78.0	Batch #8			78.0
LOT S2 #33 70–100 mm	78.2	Batch #8			78.2
LOT S2 #33 0–10 mm Clayfr.	89.5	Batch #8			89.5

### Correlation matrices

A correlation matrix is a valuable tool to identify relationships between chemical components in a material such as bentonite.

Various available key components were included (e.g. Na<sub>2</sub>O, MgO, Al<sub>2</sub>O<sub>3</sub>, SiO<sub>2</sub>, CEC). The data were preprocessed to ensure accuracy, including steps such as normalization (if required), handling missing data through imputation or removal, and detecting/removing outliers.

The Pearson correlation coefficient was used to quantify the linear relationship between each pair of components. The coefficient, ranging from –1 to 1, was calculated using Pearson correlation coefficient formula, using the python library Pandas.

The Pearson coefficients for all component pairs were compiled into a correlation matrix. Each cell in the matrix shows the correlation between two components:

- **Strong Positive Correlation ( $r > 0.7$ ):** Both components increase together.
- **Strong Negative Correlation ( $r < -0.7$ ):** One component increases as the other decreases.
- **Weak Correlation ( $|r| < 0.3$ ):** Little to no linear relationship.

By analyzing the matrix, key relationships between components can be identified, such as clusters of components that behave similarly under experimental conditions. Comparing matrices across different experiments highlights consistent patterns or significant differences, revealing the impact of experimental variables.

## Comparison between LOT S2 and A3 based on correlations matrices (Figure 2-12a-b)

### Similarities

Cu, Ca and S shows strong negative correlation with distance. This is compatible with the copper corrosion and the accumulation of anhydrite and/or gypsum towards the heater.

Cl show positive correlation with distance. This is compatible with the inflow of chloride rich Äspö water at the rock interface.

Positive correlation with Si and distance from heater. In both experiments the relative amount of Si is lower at the heater.

### Differences

In LOT A3 Mg show a strong negative correlation with distance (-0.48), while in S2 there is a positive correlation (0.38).

### Correlation matrix LOT A3 block 11N (Figure 2-12c)

In the LOT A3 block 11N profile (Figure 2-12c) there is a strong positive correlation between Na and the distance from the heater, this comes from the fact that Na<sub>2</sub>O steadily increases from 1.58 wt% close to the heater, to 1.69 wt% close to the rock, a small but significant increase. And there is a rather strong negative correlation between the distance from the heater and MgO (-0.71), due to the fact that the MgO content increases from 2.29 wt% close to the rock to 3.24 wt% close to the heater. CEC has a strong negative correlation with the distance from the heater (-0.92) as the CEC is around 80 cmol(+)/kg at the heater, and 76,5 close to the rock. CuO has a strong negative correlation with the distance from the heater, as it naturally is higher close to the heater due to the corrosion. SiO<sub>2</sub> strongly positively correlates with the distance from the heater (0.96), while SO<sub>3</sub> has a strong negative correlation (-0.76), as well as CaO (-0.78). The strong correlation between Ca and S is illustrated in Figure 2-12d.

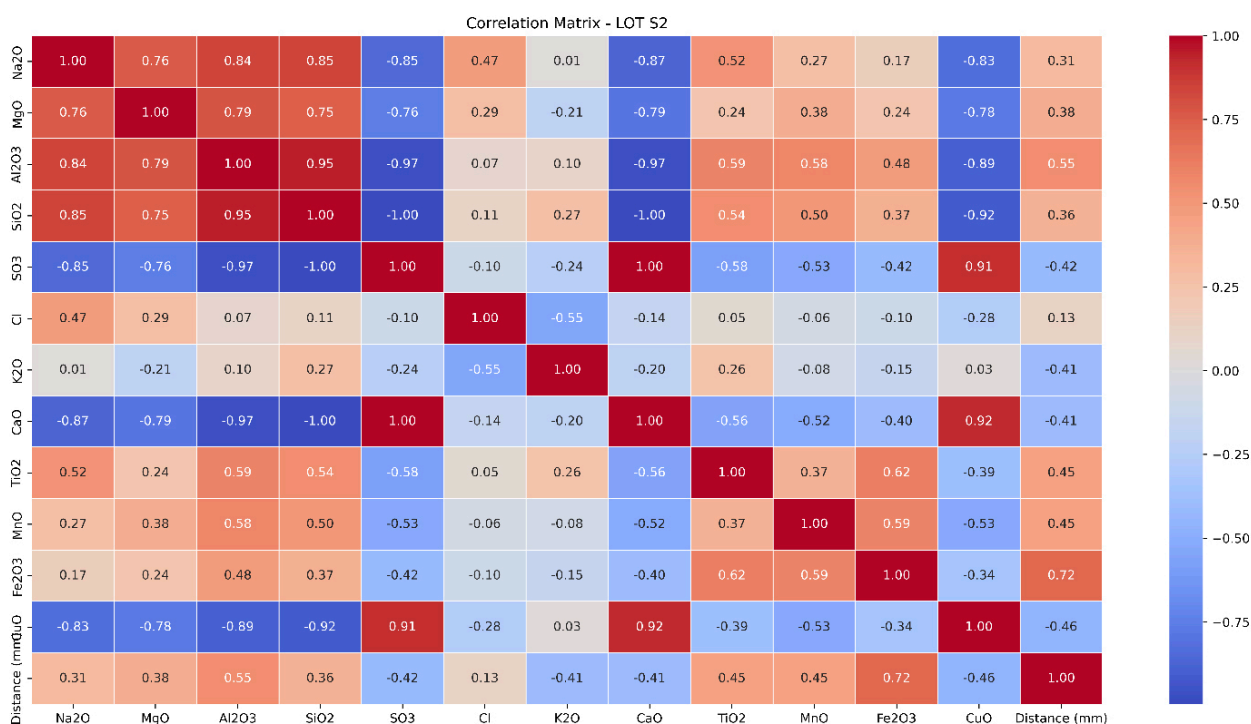


Figure 2-12a. Correlation matrix of the LOT S2 samples (n=18).

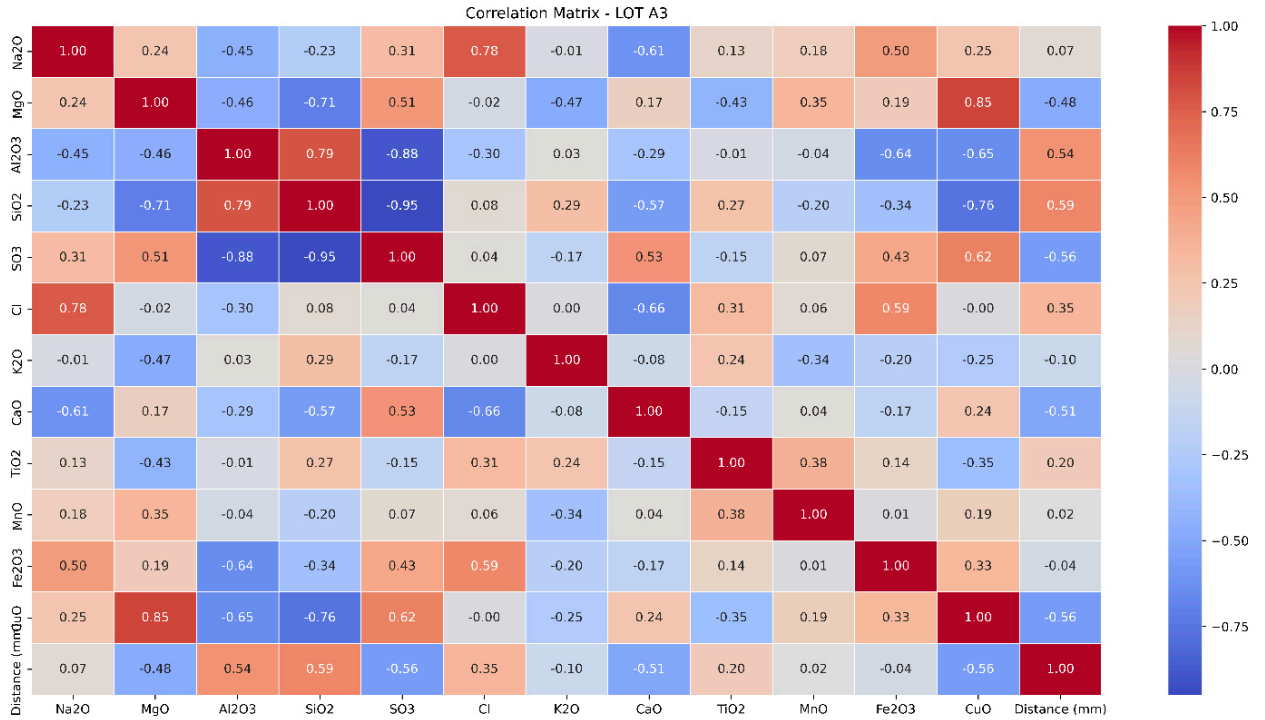


Figure 2-12b. Correlation matrix of the LOT A3 samples (n=34).

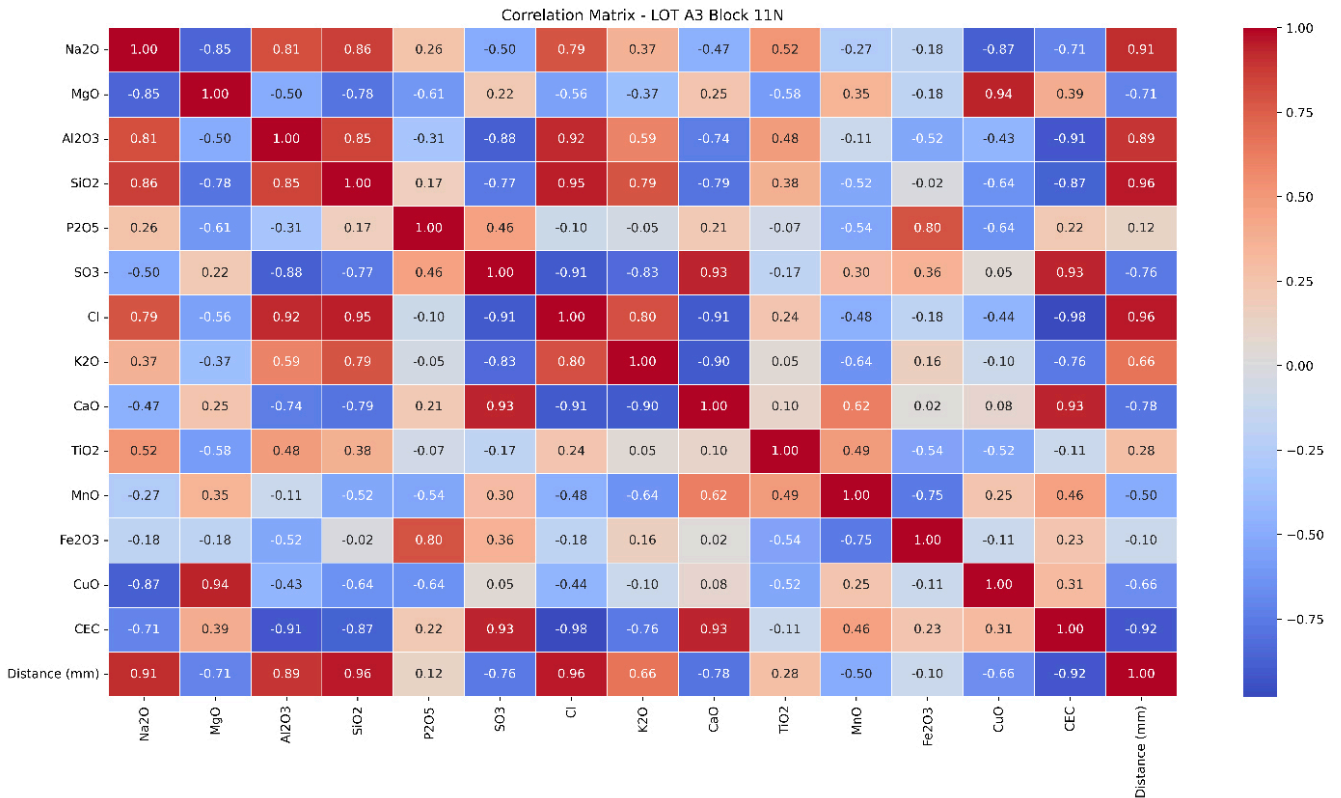
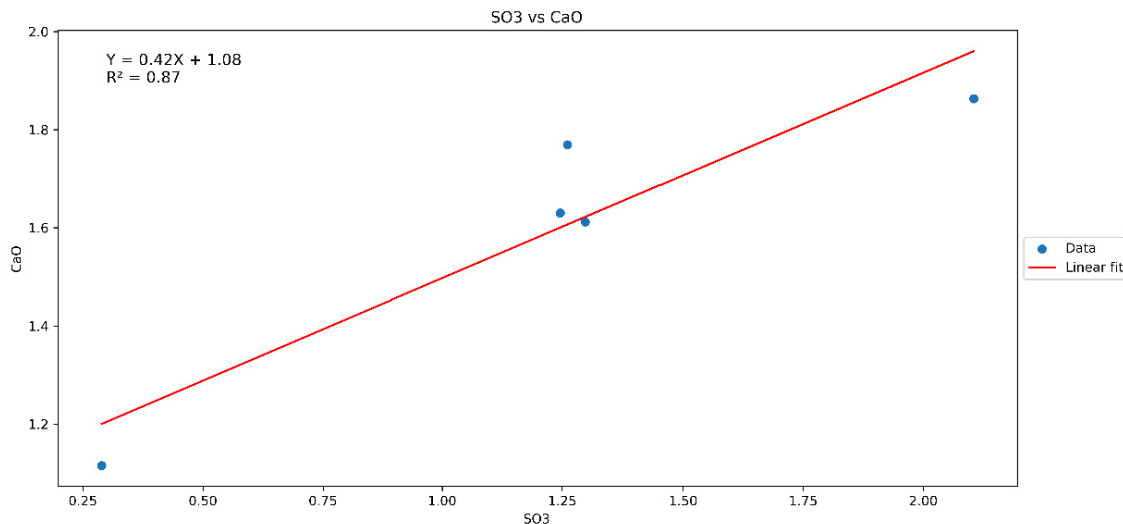


Figure 2-12c. Correlation matrix of the LOT A3 block 11N.



**Figure 2-12d.** Calcium content (CaO; wt%) as a function of sulfur content (SO<sub>3</sub>; wt%) in LOT A3 block 11N samples, illustrating the very strong correlation between the two elements.

### 2.3.2 Chemistry and mineralogy of Ca-exchanged samples from SP-HC measurements

In this section focus is on samples coming from the swelling pressure and hydraulic conductivity measurements. Hence, they are Ca-exchanged and more or less salt free. This makes it possible to investigate the bentonite samples for mineralogical changes with a higher level of detail, neglecting the water soluble phases.

#### **Powder XRD**

The XRD data of the A3 and S2 samples are indistinguishable from the reference samples (Figure 2-13). Notice how almost every single little reflection looks the same, both in the full pattern, the low angle and 060 reflection closeup.

Some samples were saturated with ethylene glycol (EG) to investigate differences in swelling behaviour (Figure 2-14). Since the sample is a little bit wet, it is difficult to make the sample perfectly smooth and at the correct sample height. This probably explains the small difference in absolute values of the basal reflections. In Olsson et al. 2013 larger variations are observed when investigating samples from the outer part of the Prototype repository.

The datasets were quantified using Siroquant version 5 (Table 2-4). The average of the reference samples was 83.1 wt% montmorillonite (6 measurements) and the average of the LOT A3 samples was 85.3 wt% montmorillonite (6 measurements). Hence, the average of the A3 samples was 2.6 % higher than the reference in montmorillonite (85.3/83.1). It is uncertain, if this small increase is significant, but it is interesting that it is on the same level as the increase in the CEC in some bulk samples of the mid LOT A3.

The relative increase in MgO content was 3 %. The (Mg+Al)/Si ratio was calculated for the samples (Table 2-6) and for the LOT reference it was 0.331 and for the LOT samples it was 0.340. This is an indirect evaluation, however for MX80 it has been shown to typically correlate to the montmorillonite content (Svensson et al. 2019).

The Mg/Al ratio was almost constant when comparing the LOT A3 #11 sample with the reference (Table 2-6), indicating that there was almost no increase in Mg in relation to Al.

Enstatite was found to possibly be present in one sample, the identification of this one is not certain, and the presence may possibly be due to coincidence as it only was present in one of the three measurements.

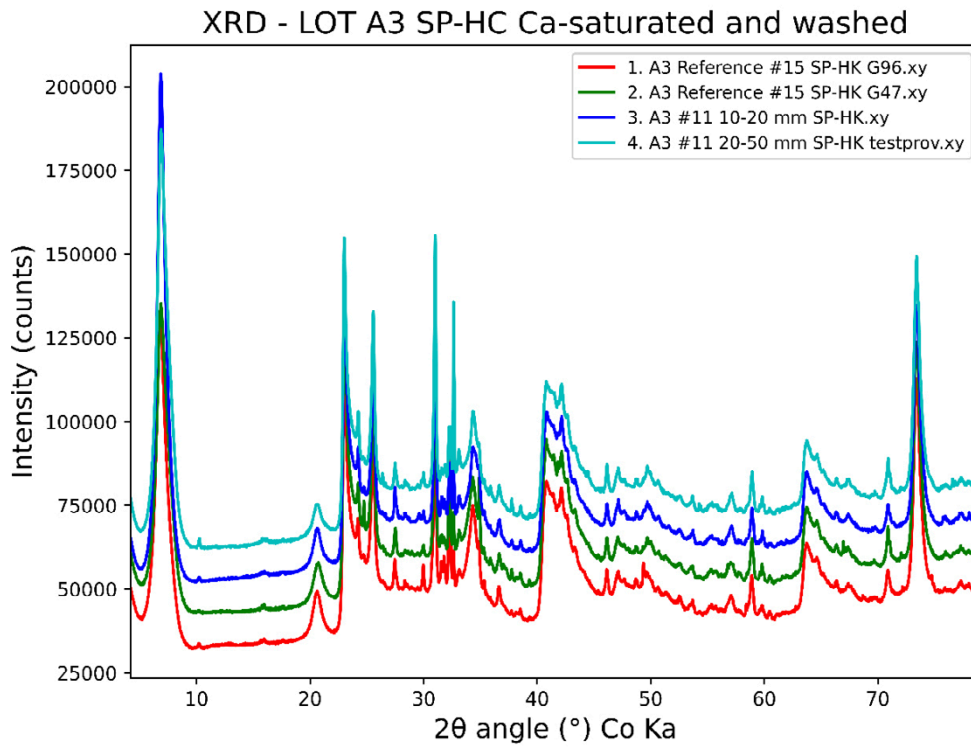


**Figure 2-13a.** Powder XRD data of samples from swelling pressure – hydraulic conductivity experiment. Ca-exchanged and salt free. Two samples from A3 field experiment (block 11 at 10–20 mm from heater and 20–50 mm from heater) and two reference samples. Each pattern is a combination of three individual patterns.

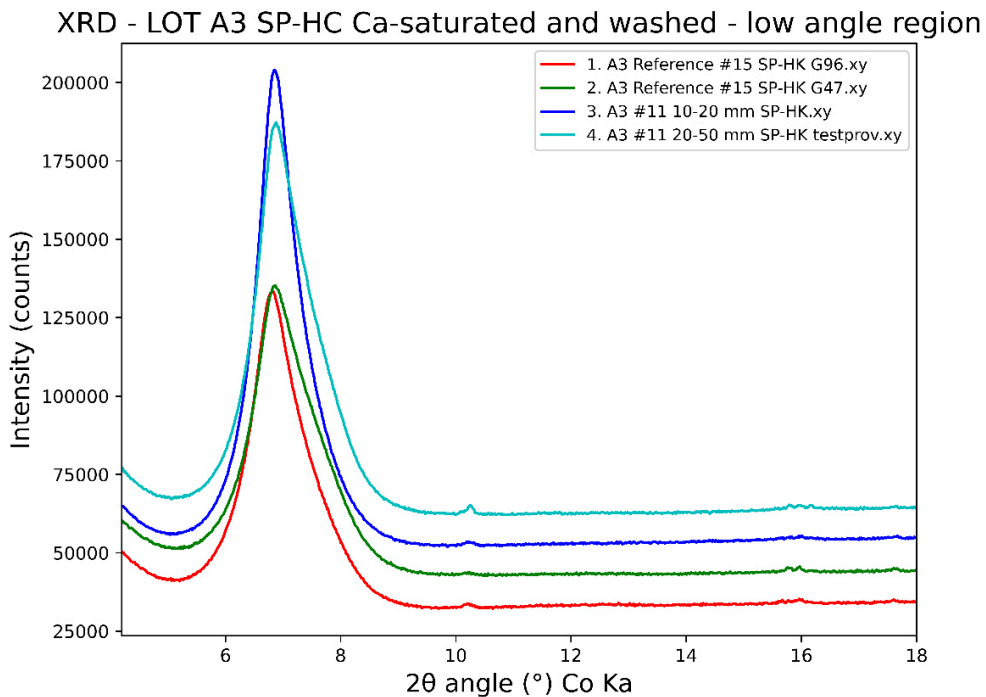


**Figure 2-13b.** Same as Figure 2-9a, but closeup on the low angle region with the 001 basal reflections.

### XRD - LOT A3 SP-HC Ca-saturated and washed - 060 region

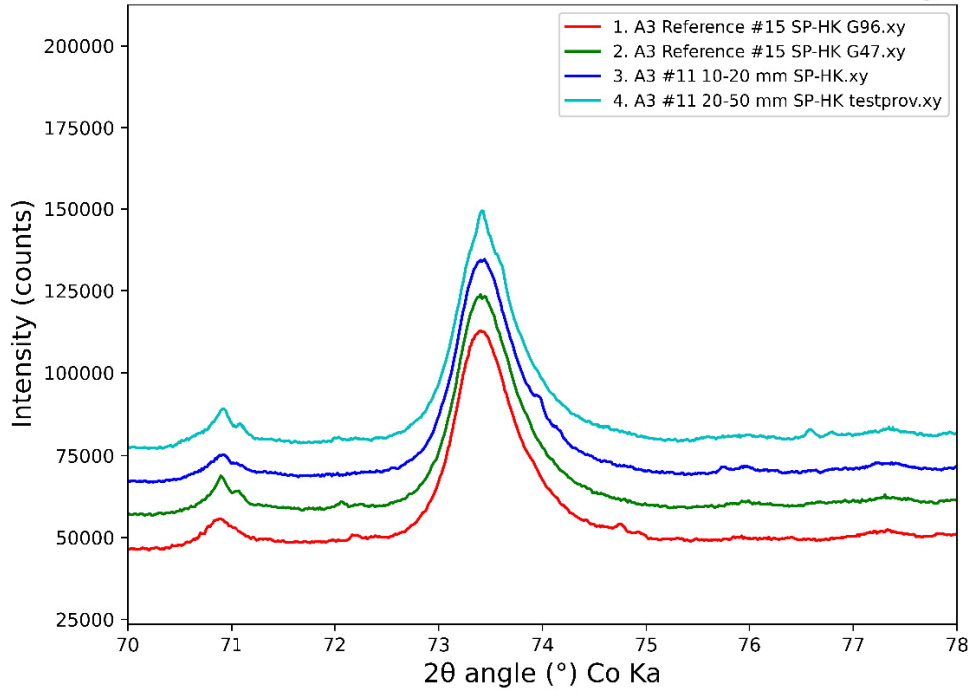


Figure 2-13c. Same as Figure 2-9a, but closeup on the 060 reflections.

### XRD - LOT A3 S2 SPHC Additional samples

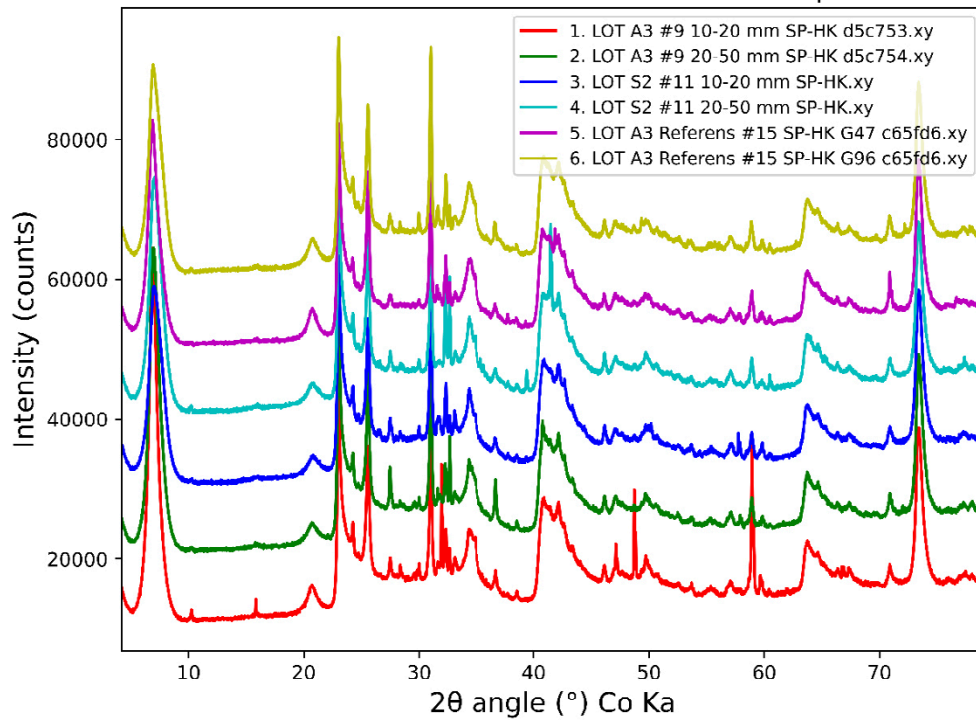


Figure 2-14. Powder XRD data of samples from swelling pressure – hydraulic conductivity experiment. Ca-exchanged and salt free.

**Table 2-4. Mineralogy (XRD) of selected Ca-exchanged SP-HC samples (n=3).**

Sample	Montmorillonite	Quartz	Calcite	Gypsum	Cristobalite	Feldspare	Mica	Enstatite
<b>Reference samples</b>								
LOT A3 Referens #15 SP-HC G96 c65fd6	83.8	5.2	2	0	3.3	1.6	4.2	0
	84	5.4	1.9	0	3.2	1.4	4.2	0
	79.9	5.8	1.9	0	4.3	4.2	3.8	0
LOT A3 Referens #15 SP-HC G47 c65fd6	83.6	5.1	1.9	0	3.7	1.4	4.4	0
	84.6	5.4	2	0.1	3	1.9	3.1	0
	82.6	5.1	2.2	0	3.4	1.9	4.7	0
<b>Average</b>	<b>83.1</b>	<b>5.3</b>	<b>2.0</b>	<b>0.0</b>	<b>3.5</b>	<b>2.1</b>	<b>4.1</b>	<b>0.0</b>
SD	1.7	0.3	0.1	0.0	0.5	1.1	0.6	0.0
Ur	<b>4.3</b>	<b>0.7</b>	<b>0.3</b>	<b>0.1</b>	<b>1.2</b>	<b>2.7</b>	<b>1.4</b>	<b>0.0</b>
<b>Samples from LOT A3 field experiment</b>								
LOT A3 #11 20–50 mm SP-HC d5c75a	83.1	4.7	1.4	0	3.2	0.7	4.2	2.7
	87.6	5.3	0.8	0	3	0	3.2	0
	85.4	4.9	2.1	0	3	0.6	4	0
LOT A3 #11 10–20 mm SP-HC d5c759	84.8	4.1	1.5	0	3	1.2	5.4	0
	85.4	4.6	1.6	0	3	1.4	4	0
	85.2	4.8	1.8	0	2.9	0.6	4.7	0
<b>Average</b>	<b>85.3</b>	<b>4.7</b>	<b>1.5</b>	<b>0.0</b>	<b>3.0</b>	<b>0.8</b>	<b>4.3</b>	<b>0.5</b>
SD	1.4	0.4	0.4	0.0	0.1	0.5	0.7	1.1
Ur	<b>3.7</b>	<b>1.0</b>	<b>1.1</b>	<b>0.0</b>	<b>0.3</b>	<b>1.3</b>	<b>1.9</b>	<b>2.8</b>
<b>Average all LOT A3 samples (references and field samples):</b>	84.2							
<b>Reference value in literature MX80 c65dae average of 10 samples (Svensson et al. 2019):</b>	84.1							

**Table 2-5. Chemical composition (XRF; Wt%) of selected Ca-exchanged SP-HC samples (n=2).**

Sample	Na <sub>2</sub> O	MgO	Al <sub>2</sub> O <sub>3</sub>	SiO <sub>2</sub>	SO <sub>3</sub>	Cl	K <sub>2</sub> O	CaO	TiO <sub>2</sub>	MnO	Fe <sub>2</sub> O <sub>3</sub>	CuO
LOT A3 Reference #15 c65fd6 G96	0.00	2.00	19.70	65.40	0.51	0.01	0.64	4.63	0.24	0.02	6.53	0.00
LOT A3 Reference #15 c65fd6 G47	0.00	1.97	19.56	65.19	0.55	0.01	0.73	4.73	0.24	0.02	6.65	0.00
<b>Average</b>	<b>0.00</b>	<b>1.98</b>	<b>19.63</b>	<b>65.29</b>	<b>0.53</b>	<b>0.01</b>	<b>0.68</b>	<b>4.68</b>	<b>0.24</b>	<b>0.02</b>	<b>6.59</b>	<b>0.00</b>
SD	0.00	0.02	0.10	0.14	0.03	0.00	0.06	0.08	0.00	0.00	0.08	0.00
LOT A3 #11 10–20 mm d5c759 SP-HK	0.00	2.09	19.68	64.84	0.72	0.00	0.62	4.62	0.23	0.02	6.74	0.10
LOT A3 #11 20–50 mm d5c75a SP-HK	0.00	1.99	19.78	64.84	0.50	0.01	0.68	4.78	0.26	0.02	6.79	0.01
<b>Average</b>	<b>0.00</b>	<b>2.04</b>	<b>19.73</b>	<b>64.84</b>	<b>0.61</b>	<b>0.01</b>	<b>0.65</b>	<b>4.70</b>	<b>0.25</b>	<b>0.02</b>	<b>6.76</b>	<b>0.05</b>
SD	0.00	0.07	0.07	0.00	0.16	0.00	0.04	0.11	0.02	0.00	0.04	0.07

**Table 2-6. Calculated chemical quotas of selected Ca-exchanged SP-HC samples.**

Sample	(Mg+Al)/Si	Mg/Al
LOT A3 Reference #15 c65fd6 gron 96	0.332	0.101
LOT A3 Reference #15 c65fd6 gron 47	0.330	0.100
Average	<b>0.33</b>	<b>0.10</b>
SD	0.00	0.00
LOT A3 #11 10–20 mm d5c759 SP-HK	0.336	0.106
LOT A3 #11 20–50 mm d5c75a SP-HK	0.336	0.100
Average	<b>0.34</b>	<b>0.10</b>
SD	0.00	0.00

### 2.3.3 Clay fractions

Powder XRD data of the clay fractions (Figure 2-17) show that they are dominated by montmorillonite, but with considerable amounts of cristobalite and quartz. The LOT S2 clay fraction looks identical to the reference samples, while the A3 sample has considerably less quartz, and probably also somewhat less cristobalite.

Chemical compositions of the LOT A3 clay fractions show increased levels of Cu, Na, Mg, Al, Fe, and decreased levels of Si and K (Table 2-7). The LOT S2 clay fraction was more like the reference clay fraction.

When the CEC of the clay fractions is plotted against the calculated chemical ratio of  $(MgO+Al_2O_3)/SiO_2$  contents a linear correlation can be seen (Figure 2-16). Most likely, the minor loss of quartz and cristobalite in LOT A3 (Figure 2-15) increased the montmorillonite content, which increased the CEC and the  $(Mg+Al)/Si$  ratio. Both Al and Mg increased, however Al only had a relative increase of 2.2 %, while Mg had a relative increase of 17 %. Hence, the increase in Mg cannot only be explained by a small increase in montmorillonite content.

The relative increase in Al/Si ratio is  $0.35/0.33=6.1$  % (Table 2-8a), which is very close to the increase in CEC of 6.5 % (see Norm CEC; Table 2-8b). Hence, the increase in CEC seems to be in the same range as the small decrease in silica phases and increase in montmorillonite.

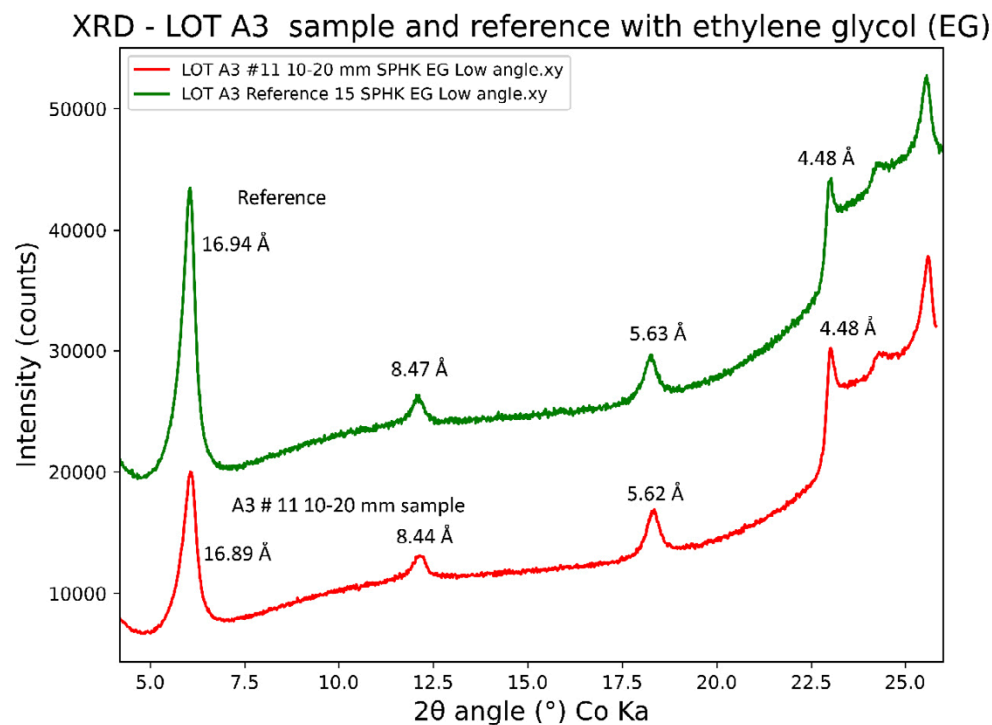


**Figure 2-15. Ca-exchanged samples with ethylene glycol (EG) from the SP HC measurements.**

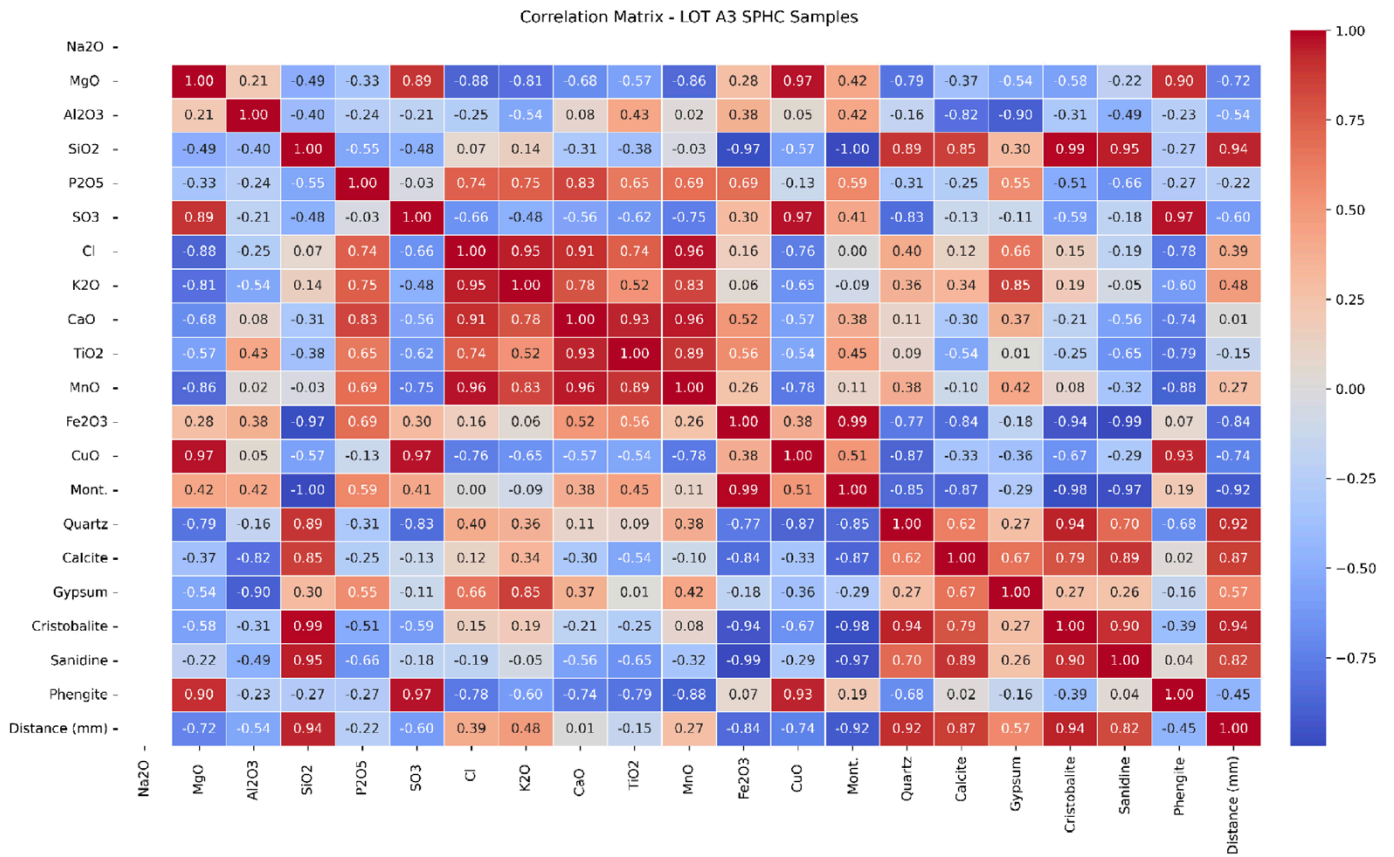


Figure 2-16. Correlation matrix of the LOT A3 SPHC samples.

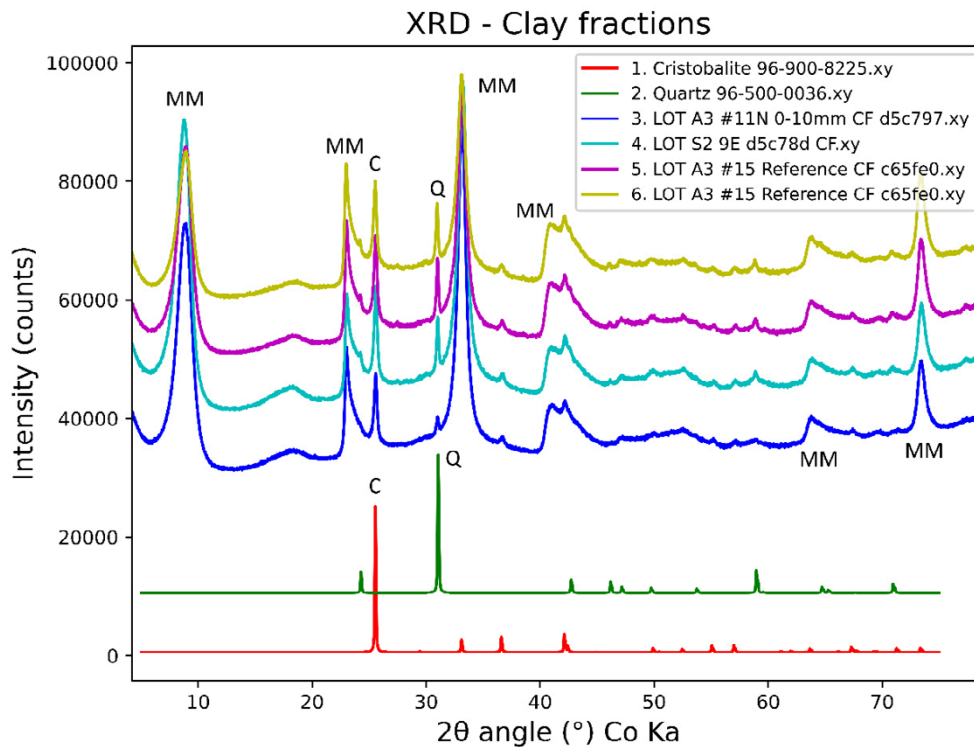


Figure 2-17. Powder XRD data of LOT A3 and S2 clay fractions and reference phases. Montmorillonite (MM), cristobalite (C), quartz (Q).

**Table 2-7. Chemical content of the clay fractions (XRF; Wt%).**

Sample	Na <sub>2</sub> O	MgO	Al <sub>2</sub> O <sub>3</sub>	SiO <sub>2</sub>	SO <sub>3</sub>	Cl	K <sub>2</sub> O	CaO	TiO <sub>2</sub>	Fe <sub>2</sub> O <sub>3</sub>	CuO
LOT A3 CF Reference block 15 c65fe0	1.94	2.5	22.47	67.5	0.115	0.003	0.17	0.32	0.17	4.8	0
LOT S2 CF block 33 0–10 mm d5c793	1.92	2.57	22.87	66.99	0.059	0.005	0.11	0.32	0.16	4.97	0.02
LOT A3 CF block 9 0–10 mm d5c791	2.14	2.93	22.87	66.05	0.033	0.001	0.06	0.19	0.15	5.22	0.35
LOT A3 CF block 11 0–10 mm d5c797	2.53	2.92	22.97	65.72	0.062	0.004	0.06	0.17	0.15	5.14	0.24

**Table 2-8a. Comparison of chemical composition and normalised values. MX80 diluted with quartz (1, 5, and 10 wt%) is also included (Svensson et al. 2019).**

Sample	MgO	Al <sub>2</sub> O <sub>3</sub>	SiO <sub>2</sub>	Norm Mg	Norm Al	Mg/Al	Norm Si	Al/Si
LOT A3 CF Reference block 15 c65fe0	2.5	22.47	67.5	1.000	1.000	0.111	1.000	0.333
LOT S2 CF block 33 0–10 mm d5c793	2.57	22.87	66.99	1.028	1.018	0.112	0.992	0.341
LOT A3 CF block 9 0–10 mm d5c791	2.93	22.87	66.05	1.172	1.018	0.128	0.979	0.346
LOT A3 CF block 11 0–10 mm d5c797	2.92	22.97	65.72	1.168	1.022	0.127	0.974	0.350
MX80	2.422	22.22	65.887	0.9688	0.989	0.109	0.976	0.337
MX80 + 1 % Quartz	2.397	22.086	65.953	0.9588	0.983	0.109	0.977	0.335
MX80 + 5 % Quartz	2.323	21.733	66.107	0.9292	0.967	0.107	0.979	0.329
MX80 + 10 % Quartz	2.235	21.348	66.724	0.894	0.950	0.105	0.989	0.320

**Table 2-8b. Comparison of chemical ratios with CEC. Some additional data from MX80 diluted with quartz (1, 5, and 10 wt%) is also included (Svensson et al. 2019).**

Sample	(MgO+Al <sub>2</sub> O <sub>3</sub> )/SiO <sub>2</sub>	Norm Mg+Al/Si	CEC (cmol(+)/kg)	Norm CEC
LOT A3 CF Reference block 15 c65fe0	0.370	1.000	87.3	1.000
LOT S2 CF block 33 0–10 mm d5c793	0.380	1.027	89.5	1.025
LOT A3 CF block 9 0–10 mm d5c791	0.391	1.057	94.5	1.082
LOT A3 CF block 11 0–10 mm d5c797	0.394	1.065	93	1.065
MX80	0.374	1.011		
MX80 + 1 % Quartz	0.372	1.005		
MX80 + 5 % Quartz	0.362	0.978		
MX80 + 10 % Quartz	0.352	0.951		

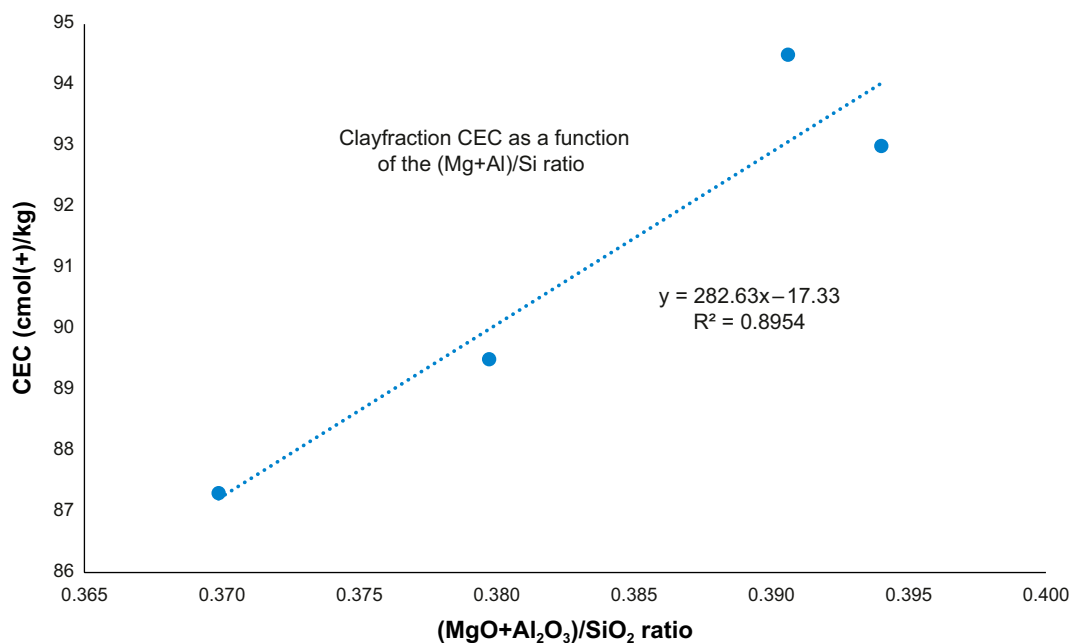


**Figure 2-18. CEC of clay fraction samples as a function of the (MgO + Al<sub>2</sub>O<sub>3</sub>)/SiO<sub>2</sub> ratio.**

### 2.3.4 Scraping samples from the heater

Some minor amounts of solids were sampled from two parts from the canister surface using a plastic tool in the A3 experiment at block positions 25–26 and 27. XRF analysis showed that the samples were rich in Cu, S, and Ca (Table 2-9). As the amount of sample was rather small, they were measured on a mylar foil (3.6  $\mu\text{m}$  thickness). The small amount of sample increases the uncertainty of the measurements somewhat, so interpretation should be done with some caution. Powder XRD was done on silicon zero background substrates due to the small amount of sample. As the sample volume was very small, the distance from the sample to the detector was not perfect due to non perfect sample height, this can be seen as small shifts in the positions of the reflection of e.g. quartz and cristobalite, as well as the montmorillonite hk-reflection around 4.48  $\text{\AA}$  (Figure 2-17). The scraping samples were very similar to the reference sample. No phase corresponding to the copper content was identified.

**Table 2-9. Chemical composition (XRF) of scraping samples from LOT A3.**

Sample	Na <sub>2</sub> O	MgO	Al <sub>2</sub> O <sub>3</sub>	SiO <sub>2</sub>	P <sub>2</sub> O <sub>5</sub>	SO <sub>3</sub>	Cl	K <sub>2</sub> O	CaO	TiO <sub>2</sub>	MnO	Fe <sub>2</sub> O <sub>3</sub>	CuO
LOT A3 Skrapprov #27	0.74	2.25	19.02	60.61	0.68	3.13	0.21	0.67	3.58	0.22	0.02	4.97	3.90
LOT A3 Skrapprov #25–26	0.31	2.30	20.05	63.62	0.51	1.38	0.17	0.60	2.63	0.21	0.02	5.11	3.09

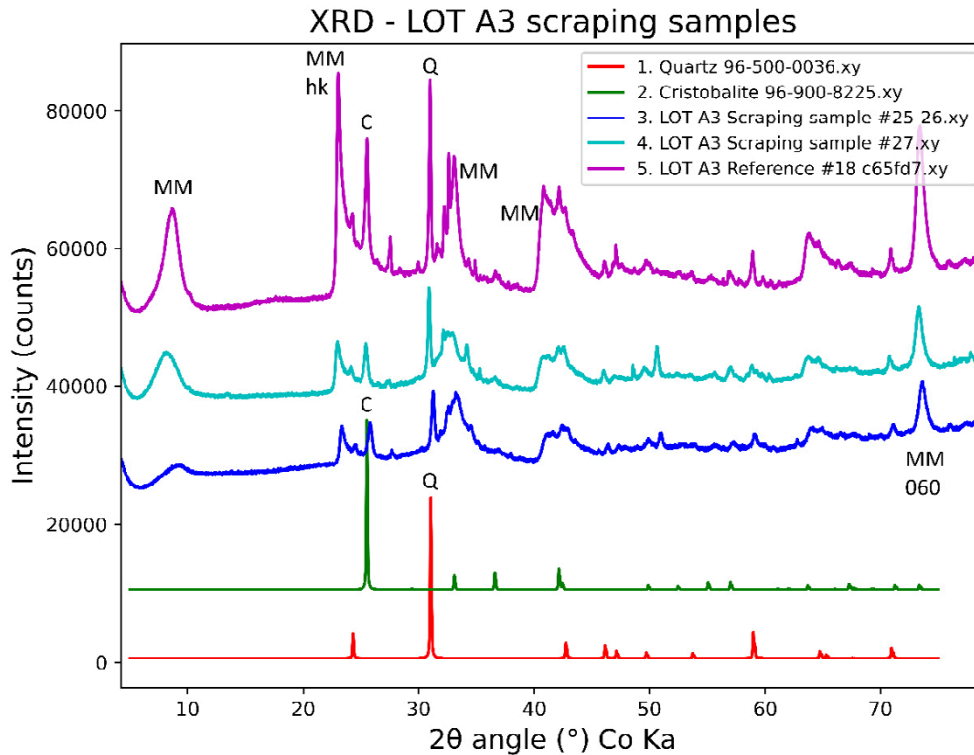


**Figure 2-19.** XRD data LOT A3 scraping samples, as compared to MX80 reference and quartz, and cristobalite calculated patterns.



### 3 Hydromechanical properties, Clay Technology

The test types were chosen to follow the program previously used after dismantling of large-scale field tests at Äspö HRL in Sweden including LOT A2. The program of analyses was performed at Clay Technology on material delivered from SKB 2019-10-07.

#### 3.1 Test plan

In this study, samples from two blocks from each of the LOT parcels S2 and A3 were analysed together with samples from the reference material. The reference material was taken from Clay Technology LOT reference material which was saved from the manufacturing of blocks 1999. Samples were taken for determinations of swelling pressure and hydraulic conductivity and for determinations of unconfined compressive strength. Drilled specimens were taken to study properties of the undisturbed profile and in addition, crushed and re-compacted specimens were tested. The testing programme and the dimensions of the specimens were decided together with SKB. The number of tests and the type of preparation for the different test types are summarized in Table 3-1 and Table 3-2.

**Table 3-1. The number of tests for swelling pressure and hydraulic conductivity measurements given with positions and type of preparation. The height of the specimens was 10 mm and the diameter 20 mm. The positions were measured from the inner mantle surface.**

LOT parcel	Bentonite block	Position cm	Preparation		
			Drilled/ trimmed	Crushed/ re-compacted	Compacted
S2	9	4, 8	2		
S2	11	4, 8	2		
S2	9	4		1	
S2	11	4		1	
A3	9	4, 8	2		
A3	11	4, 8	2		
A3	9	4		1	
A3	11	4		1	
A3, S2	LOT ref				4
<b>Total</b>			<b>8</b>	<b>4</b>	<b>4</b>

**Table 3-2. The number of unconfined compression tests given with positions and type of preparation. The height of the specimens was 20 mm and the diameter 20 mm. The positions were measured from the inner mantle surface.**

LOT parcel	Bentonite block	Position cm	Preparation		
			Drilled/ trimmed	Crushed/ re-compacted	Compacted
S2	9	2, 4, 8	6		
S2	11	2, 4, 8	6		
S2	9	2, 4		4	
S2	11	2, 4		4	
A3	9	2, 4, 8	6		
A3	11	2, 4, 8	6		
A3	9	2, 4		4	
A3	11	2, 4		4	
S2, A3	Ref				18
<b>Total</b>			<b>24</b>	<b>16</b>	<b>18</b>

From each of the parcels S2 and A3 parts from blocks 9 and 11 were delivered for the hydro-mechanical analyses. Photos from the sampling are shown in Appendix 1.

### 3.2 Denomination of specimens

The denomination or sample ID of samples from the field experiment consists of the parcel and block numbers followed by the radial distance in mm from the inner mantle surface. For example, the sample ID S2-09-40 refers to the LOT parcel S2, block 09 where the sample was taken 40 cm from the inner mantle surface. Material sampled from the field experiment and crushed and re-compacted are marked cr, e.g. S2-09-09-40cr. The reference material was denominated as LOT Ref.

### 3.3 Type of water

The LOT-water used in the tests was based on the composition measured in the supply bore hole HG0038B01 at Äspö HRL (Sandén and Nilsson, 2020). The solution used had a concentration of 0.10M Na and 0.06M Ca. The solution was based on the composition measured 2006-10-02 which differed slightly from the more recent composition measured 2018-11-05 with 0.13M Na and 0.08M Ca.

### 3.4 Determination of water content and density

The base variables water content  $w$  (%), void ratio  $e$ , and degree of saturation  $S_r$  (%) were determined according to Equations 2-1 to 2-3.

$$w = 100 \cdot \frac{m_{tot} - m_s}{m_s} \quad (\text{Equation 3-1})$$

$$e = \frac{\rho_s}{\rho} (1 + w/100) - 1 \quad (\text{Equation 3-2})$$

$$S_r = \frac{\rho_s \cdot w}{\rho_w \cdot e} \quad (\text{Equation 3-3})$$

where

$m_{tot}$  = total mass of the specimen (kg)

$m_s$  = dry mass of the specimen (kg)

$r_s$  = particle density (kg/m<sup>3</sup>)

$r_w$  = density of water (kg/m<sup>3</sup>)

$r$  = bulk density of the specimen (kg/m<sup>3</sup>)

The dry mass of the specimen was obtained from drying the wet specimen at 105 °C for 24h. The bulk density was calculated from the total mass of the specimen and the volume determined by weighing the specimen above and submerged into paraffin oil. For determination of void ratio and degree of saturation the particle density  $r_s = 2750 \text{ kg/m}^3$  and water density  $r_w = 1000 \text{ kg/m}^3$  were used (Karland et al. 2006, 2009).

## 3.5 Swelling pressure and hydraulic conductivity test

### 3.5.1 General

The swelling pressure and hydraulic conductivity were determined in a combined test in a swelling pressure device.

### 3.5.2 Test equipment

The swelling pressure and hydraulic conductivity were determined by use of the test equipment shown in Figure 3-1, made of acid proof stainless steel. The specimens were confined by a cylinder ring with a diameter of 20 mm. The specimen height was approximately 11 mm. The test volume was sealed by o-rings placed between the bottom plate and the cylinder ring and between the piston and the cylinder ring. A movable piston was placed above the specimen and stainless-steel filters were used at the top and bottom.

The swelling pressure from the samples was determined by the load cell placed between the piston and the upper lid. The displacement of the piston due to transducer deformation is 25 mm at maximum force, which is considered insignificant. The load cell was calibrated before each series and checked afterwards.

### 3.5.3 Preparation of specimen and test procedure

Tests were made on material both from the field experiment and from the LOT reference material. The specimens were prepared in three different ways:

- trimmed to fit the sample holder,
- ground to a grain size less than 1.5 mm and then re-compacted,
- compacted from powder samples.

The material from the field experiment was prepared by the two first methods. The target dry density of the re-compacted specimens was 1 540 kg/m<sup>3</sup>. The reference material was prepared by the third method aiming at different dry densities between 1 350 and 1 600 kg/m<sup>3</sup>. The specimens from parcels S2 and A3 were taken from equal positions.

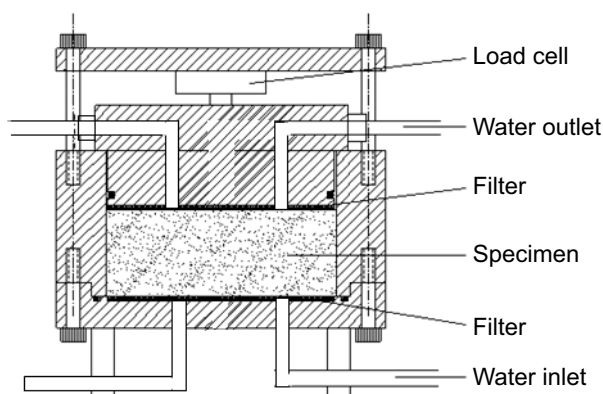


*Figure 3-1. A schematic drawing of the swelling pressure device.*

After installing the specimens into the swelling pressure device, Figure 3-1, LOT-water (see Section 3.3) was let into the filter below the specimens and 24h later also above the specimens. Saturation, ion-exchange and measurement of hydraulic conductivity of the specimens were done in the following steps:

1. Saturation by stagnant LOT-water until stable swelling pressure. Only shorter periods of circulation to remove air trapped in the filters.
2. Measurement of hydraulic conductivity of LOT-water by introducing a pore pressure gradient over the specimen.
3. Circulation of LOT-water, more or less continuously, to get full ion-equilibrium between the specimens and the LOT-water.
4. Ion-exchange to Ca-dominated specimens by continuous circulation of 1M CaCl<sub>2</sub> until stable swelling pressure.
5. Measurement of hydraulic conductivity of 1M CaCl<sub>2</sub> by introducing a pore pressure gradient over the specimen.
6. Removing excess salt by continuous circulating of DI-water (de-ionized water) through the filters.
7. End of test and dismantling.

The swelling pressure was measured during the entire test period and at stable swelling pressure the next step was taken, see above. At the measurements of hydraulic conductivity, a water pressure gradient was applied across the specimens and the volume of the outflowing water was measured as mm outflow in a tube with 2 mm diameter until the outflow rate was stable. The water pressure was thereafter reduced to zero and the test was continued when the recorded axial force was stable. The hydraulic conductivity was calculated according to Darcy's law.

At the measurements of hydraulic conductivity, the applied pore pressure was 10–50 % of the swelling pressure. The hydraulic gradients were between 4 600 m/m and 13 900 m/m which corresponded to water pressure differences between 500 kPa and 1 500 kPa over the specimens. The measurements of the outflow were made during several days, between 8 and 12 days, in order to get stable values of the evaluated hydraulic conductivity.

Four specimens were run at a time and the total time for one series with four specimens was 3–4 months. When the tests were completed water content and density of the specimens were determined after dismantling, see Section 3.4.

### **3.5.4 Results**

Below the results are presented for specimens from the parcels S2 and A3 separately. Additional results can be found in Appendix 2. The Sample ID is given according to Section 3.2.

#### ***Specimens from test parcel S2***

The results from the measurements of swelling pressure and hydraulic conductivity of specimens from test parcel S2 are given in Table 3-3, Table 3-4 and Figure 3-2 to Figure 3-4.

The results in Table 3-3 were derived using LOT-water (Section 3.3). Additional results of swelling pressure and hydraulic conductivity after ion-exchange and circulation of DI-water are given in Table 3-4. The final dry density was calculated from water content and bulk density after dismantling, i.e. after removal of excess salt.

**Table 3-3. Results from measurements of swelling pressure and hydraulic conductivity at equilibrium with LOT-water. Test ID is given together with the dry density and degree of saturation determined after dismantling. The positions of the specimens from the field experiment are given with block number and radial distance.**

Test ID	Material	Block	Radial distance mm	Preparation	Test solution <sup>1</sup>	Dry density kg/m <sup>3</sup>	Degree of saturation %	Swelling pressure kPa	Hydraulic conductivity m/s
PC1a	LS2-09-40	9	40	drilled	LOT water	1474	101	4706	1.2E-13
PC1b	LS2-09-80	9	80	drilled	LOT water	1395	101	2856	1.6E-13
PC1c	LS2-11-40	11	40	drilled	LOT water	1437	100	3557	1.3E-13
PC1d	LS2-11-80	11	80	drilled	LOT water	1360	100	1976	2.3E-13
PC3a	LS2-09-40cr	9	40	crushed + comp	LOT water	1530	100	6238	7.2E-14
PC3b	LS2-11-40cr	11	40	crushed + comp	LOT water	1537	99	7474	5.5E-14
PC4a	LOT Ref			compacted	LOT water	1346	101	2029	3.0E-13
PC4b	LOT Ref			compacted	LOT water	1428	101	3717	1.9E-13
PC4c	LOT Ref			compacted	LOT water	1508	100	5813	8.3E-14
PC4d	LOT Ref			compacted	LOT water	1579	99	9391	6.4E-14

<sup>1</sup> LOT water is defined in Section 3.3.

**Table 3-4. Results from measurements of swelling pressure and hydraulic conductivity at equilibrium with 1) LOT-water, 2) 1M CaCl<sub>2</sub> and 3) DI-water. Swelling pressure in equilibrium with LOT water is given both at stagnant (s) and circulating (c) conditions. The hydraulic conductivity is given with the gradient used. Base parameters of the specimens are shown in Table 3-3.**

Test ID	Dry density kg/m <sup>3</sup>	Ps1 (LOTs) kPa	Ps1 (LOTc) kPa	Ps2 (1M CaCl <sub>2</sub> ) kPa	Ps3 (DI) kPa	Gradient 1 m/m	kw1 (LOT) m/s	Gradient 2 m/m	kw2 (1M CaCl <sub>2</sub> ) m/s
PC1a	1474	4706	4741	2740	5135	6923	1.2E-13	6923	1.1E-13
PC1b	1395	2856	2862	1422	2970	6923	1.6E-13	6923	1.5E-13
PC1c	1437	3557	3576	1857	3986	6923	1.3E-13	6923	1.4E-13
PC1d	1360	1976	1953	971	2053	6923	2.3E-13	4606	2.3E-13
PC3a	1530	2029	1925	4508	7153	11093	7.2E-14	13873	6.3E-14
PC3b	1537	3717	3654	5783	8516	11093	5.5E-14	13873	4.9E-14
PC4a	1346	2029	1925	1050	2098	6932	3.0E-13	4606	3.6E-13
PC4b	1428	3717	3654	2104	4177	6932	1.9E-13	4606	1.7E-13
PC4c	1508	5813	5773	4027	6589	13882	8.3E-14	13873	8.9E-14
PC4d	1579	9391	9374	8058	10785	13882	6.4E-14	13873	5.3E-14

In Figure 3-2 and Figure 3-3 the resulting swelling pressure and hydraulic conductivity at equilibrium with LOT-water and 1M CaCl<sub>2</sub> are shown. The results from the drilled specimens and the crushed and re-compacted specimens are shown with triangles and diamonds, respectively. The colours (light and dark blue) show the positions from the heater (40 mm and 80 mm) and references are shown with black markers.

In Figure 3-4 the measured swelling pressure in equilibrium with the different solutions (LOT-water, 1M CaCl<sub>2</sub>, DI-water) are shown. The results of specimens from the field experiment are shown together with reference lines. The reference lines are best fit lines of the results at equilibrium with LOT-water (dashed line), after ion-exchange and equilibrium with 1M CaCl<sub>2</sub> (dotted line) and after circulation with de-ionized water removing excess salt (solid line). Equilibrium with LOT-water was done both at stagnant and circulating conditions, but only small differences between the swelling pressure at these conditions were seen, see also Table 3-4.

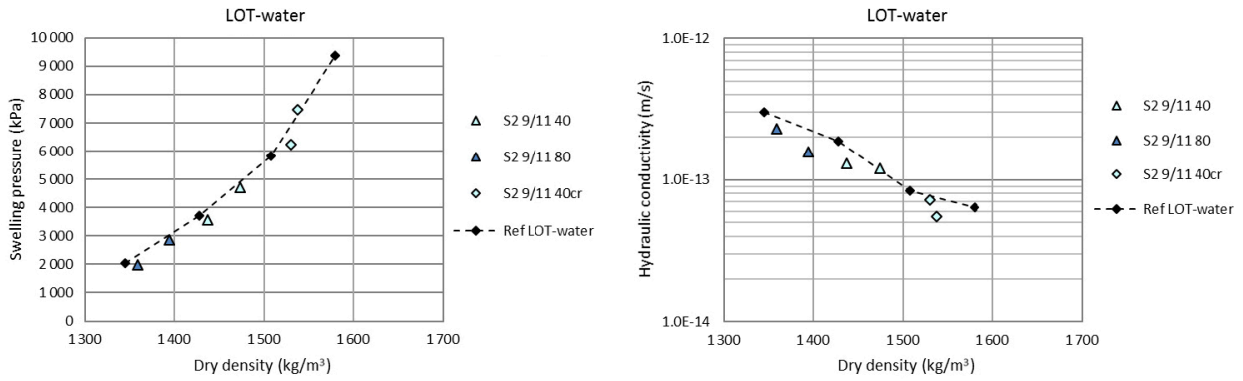


**Figure 3-2.** Measured swelling pressure (left) and hydraulic conductivity (right) of specimens taken from S2 after equilibrium with LOT-water. Results of drilled specimens (triangles) and crushed/compacted specimens (diamonds) are shown with reference results (black markers). The labels contain information about test parcel, block and distance in mm (e.g. S2 9/11 40) and cr means crushed/compacted specimen.

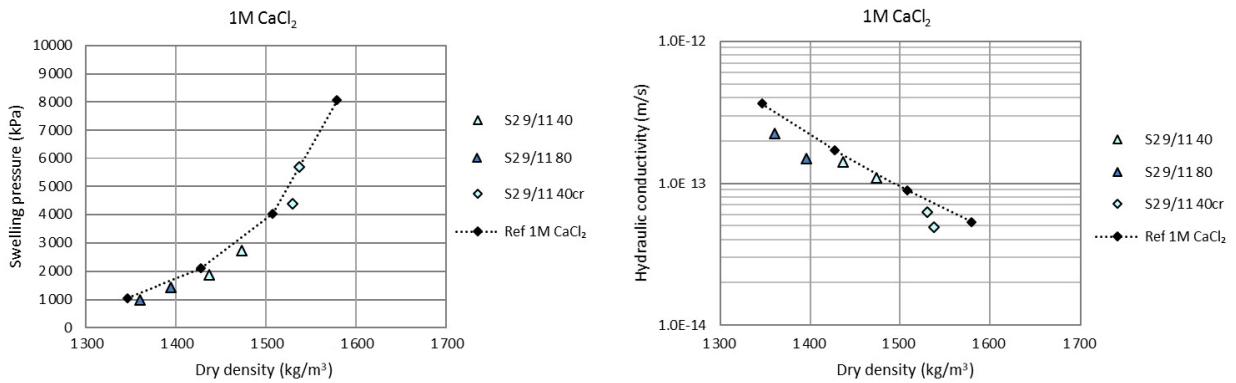


**Figure 3-3.** Measured swelling pressure (left) and hydraulic conductivity (right) of specimens taken from S2 after equilibrium with 1M CaCl<sub>2</sub>. Markers and labels are the same as in Figure 3-2.

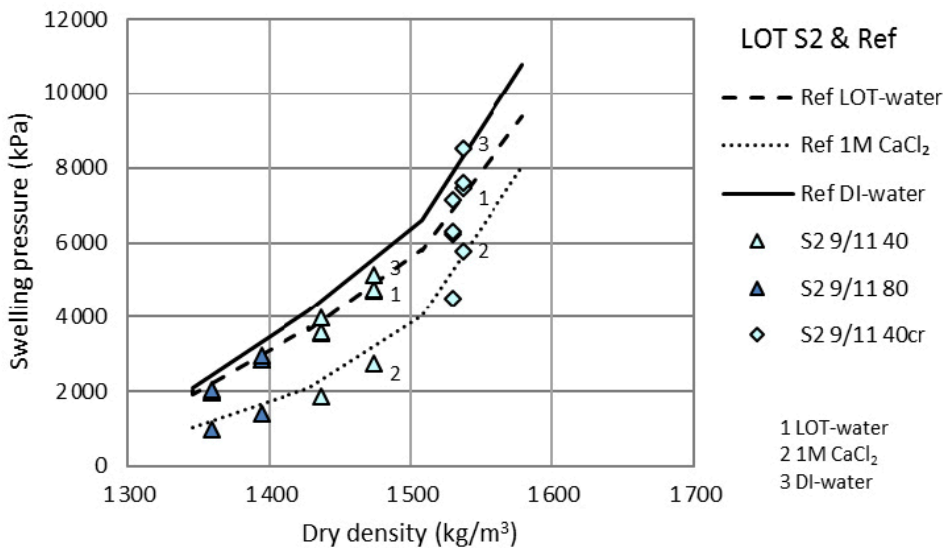


**Figure 3-4.** Measured swelling pressure of specimens sampled from LOT S2. Results from different conditions (1–3), in equilibrium with 1) LOT-water, 2) 1M CaCl<sub>2</sub>, and 3) de-ionized water. Markers and labels are the same as in Figure 3-2. Results from reference tests at the different conditions are shown with lines (dashed, dotted, solid).

No large deviations in swelling pressure and hydraulic conductivity of the four specimens drilled from S2 are seen. Compared to references, the swelling pressure and hydraulic conductivity of the specimens from the field experiment were equal or lower at all positions and conditions tested.

Crushed and re-compacted specimens were also tested, and the swelling pressure and hydraulic conductivity of these specimens coincided or were slightly lower compared to the references.

### Specimens from Test Parcel A3

The results from the measurements of swelling pressure and hydraulic conductivity are given in Table 3-5, Table 3-6 and Figure 3-5 to Figure 3-7. The results in Table 3-5 were derived using LOT-water. Additional results of swelling pressure and hydraulic conductivity after ion-exchange and washing are given in Table 3-6. The final dry density was calculated from water content and bulk density after dismantling, i.e. after removal of excess salt.

**Table 3-5. Results from measurements of swelling pressure and hydraulic conductivity at equilibrium with LOT-water. Test ID is given together with the dry density and degree of saturation determined after dismantling. The positions of the specimens from the field experiment are given with block number and radial distance.**

Test ID	Material	Block	Radial distance mm	Preparation	Test solution <sup>1</sup>	Dry density kg/m <sup>3</sup>	Degree of saturation %	Swelling pressure kPa	Hydraulic conductivity m/s
PC2a	LA3-09-40	9	40	drilled	LOT water	1482	99	4203	1.0E-13
PC2b	LA3-09-80	9	80	drilled	LOT water	1417	98	3628	1.1E-13
PC2c	LA3-11-40	11	40	drilled	LOT water	1450	99	3595	1.5E-13
PC2d	LA3-11-80	11	80	drilled	LOT water	1396	98	3012	1.5E-13
PC3c	LA3-09-40cr	9	40	crushed + comp	LOT water	1514	99	5660	1.1E-13
PC3d	LA3-11-40cr	11	40	crushed + comp	LOT water	1576	98	9522	7.0E-14

<sup>1</sup> LOT water is defined in Section 3.3.

**Table 3-6. Results from measurements of swelling pressure and hydraulic conductivity at equilibrium with 1) LOT-water, 2) 1M CaCl<sub>2</sub> and 3) DI-water. Swelling pressure in equilibrium with LOT water is given both at stagnant (s) and circulating (c) conditions. The hydraulic conductivity is given with the gradient used.**

Test ID	Dry density kg/m <sup>3</sup>	Ps1 (LOTs) kPa	Ps1 (LOTc) kPa	Ps2 (1M CaCl <sub>2</sub> ) kPa	Ps3 (DI) kPa	Gradient 1 m/m	kw1 (LOT) m/s	Gradient 2 m/m	kw2 (1M CaCl <sub>2</sub> ) m/s
PC2a	1482	4203	4363	2507	4918	6932	1.0E-13	6923	1.2E-13
PC2b	1417	3628	3625	2019	3803	6932	1.1E-13	6923	1.1E-13
PC2c	1450	3595	3675	1951	4150	6932	1.5E-13	6923	1.5E-13
PC2d	1396	3012	2949	1564	2992	6932	1.5E-13	6923	1.5E-13
PC3c	1514	5813	5773	3964	6518	11093	1.1E-13	13873	9.4E-14
PC3d	1576	9391	9374	8559	11220	11093	7.0E-14	13873	4.9E-14

In Figure 3-5 and Figure 3-6 the resulting swelling pressure and hydraulic conductivity at equilibrium with LOT-water and 1M CaCl<sub>2</sub> are shown. The results from the drilled specimens and the crushed and re-compacted specimens are shown with circles and diamonds, respectively. The colours (red and yellow) show the positions from the heater (40 mm and 80 mm) and references are shown with black markers.

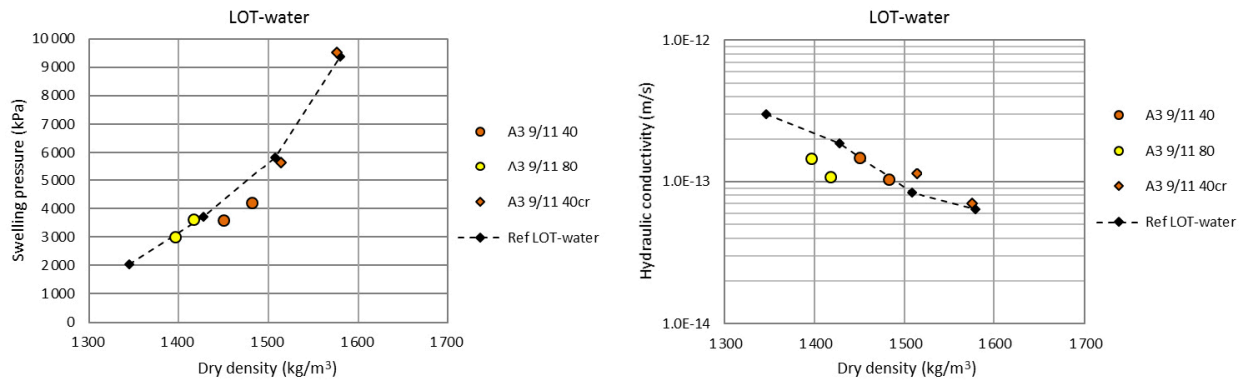


**Figure 3-5.** Measured swelling pressure (left) and hydraulic conductivity (right) of specimens from A3 after equilibrium with LOT-water. Results of drilled specimens (circles) and crushed/compacted specimens (diamonds) are shown with reference results (black markers). The labels contain information about test parcel, block and distance in mm (e.g. A3 9/11 40) and cr means crushed/compacted specimen.

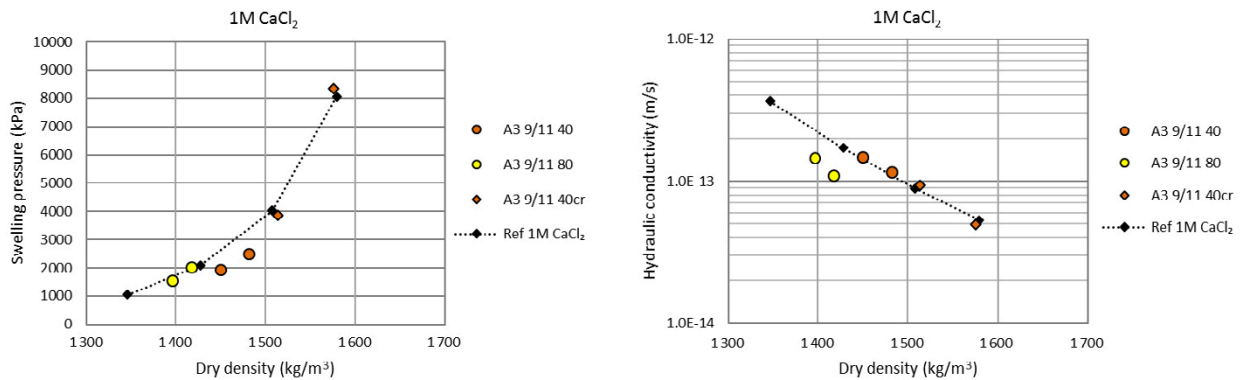


**Figure 3-6.** Measured swelling pressure (left) and hydraulic conductivity (right) of specimens from A3 after equilibrium with 1M CaCl<sub>2</sub>. Markers and labels are the same as in Figure 3-5.

In Figure 3-7 the measured swelling pressure in equilibrium with the different solutions (LOT-water, 1M CaCl<sub>2</sub>, DI-water) are shown. The results of specimens from the field experiment are shown together with reference lines. The reference lines are best fit lines of the results at equilibrium with LOT-water (dashed line), after ion-exchange and equilibrium with 1M CaCl<sub>2</sub> (dotted line) and after circulation with de-ionized water removing excess salt (solid line). Equilibrium with LOT-water was done both at stagnant and circulating conditions, but only small differences between the swelling pressure at these conditions were seen, see also Table 3-6.

No large deviations in the swelling pressure and hydraulic conductivity of the four specimens drilled from A3 are seen. Compared to references the swelling pressure and hydraulic conductivity of the specimens from the field experiment were equal or lower at all positions and conditions tested. The largest deviation from references are seen in the two specimens 40 mm from the heater and the deviation is seen at all conditions tested. However, for these specimens no deviations from the references were seen on hydraulic conductivity.

Crushed and re-compacted specimens were also tested, and the swelling pressure and hydraulic conductivity of these specimens were approximately equal to or higher than the references.

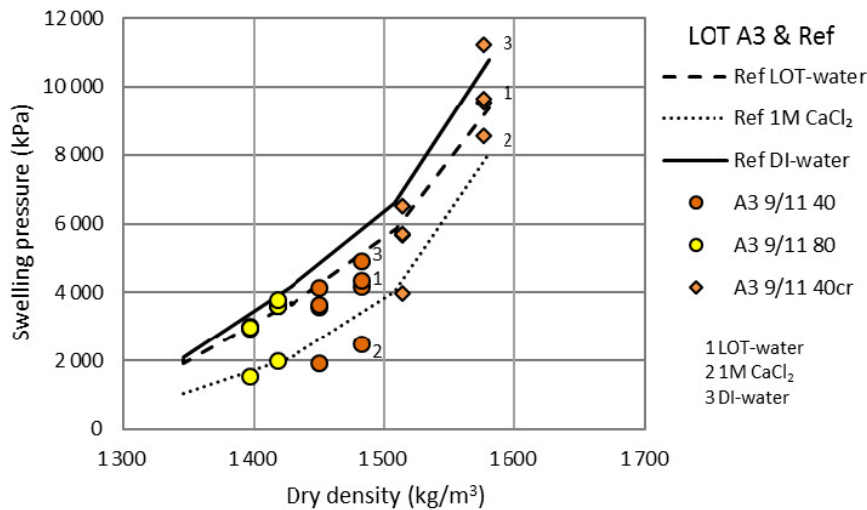


**Figure 3-7.** Measured swelling pressure of specimens sampled from LOT A3. Results from different conditions (1–3), in equilibrium with 1) LOT-water, 2) 1M CaCl<sub>2</sub>, and 3) de-ionized water. Markers and labels are the same as in Figure 3-5. Results from reference tests at the different conditions are shown with lines (dashed, dotted, solid).

### 3.5.5 Discussion

Figure 3-8 shows swelling pressure and hydraulic conductivity measured after equilibrium with LOT water of specimens from S2 and A3. The results were shown in Figure 3-2 and Figure 3-5. The results of drilled specimens from the test parcels S2 (triangles) and A3 (circles) are shown together with results from crushed and re-compacted specimens (diamonds). The results from reference tests are also shown (black dashed lines).

The specimens from different positions of S2 and A3 have been exposed to different temperatures. Specimens sampled 40 mm and 80 mm from the heater in A3 were exposed to 90 °C and 80 °C, respectively, while the specimens sampled from S2 at corresponding positions were exposed to 70 °C and 60 °C, respectively, see Section 1.2. This means that the colours used (orange, yellow, light blue, dark blue) represent different temperatures (90 °C, 80 °C, 70 °C, 60 °C). According to Figure 3-8, no influence of position or temperature can be observed.

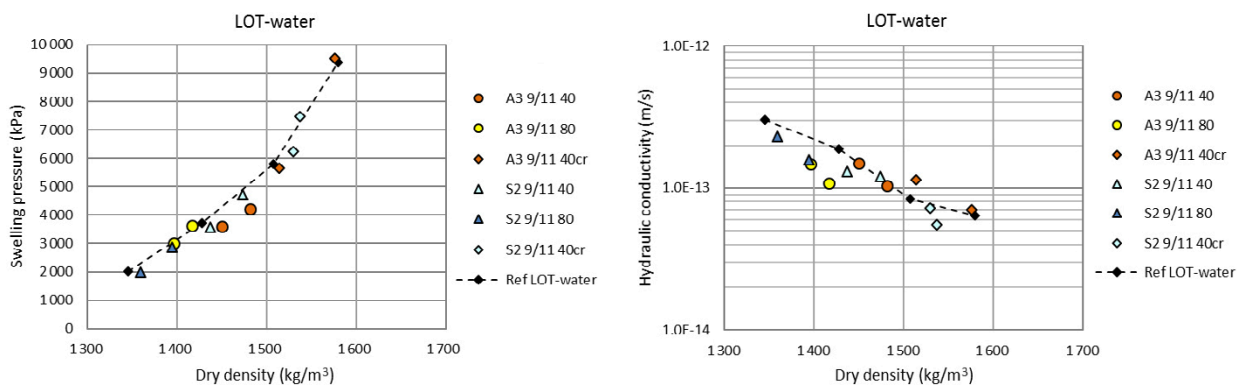


**Figure 3-8.** Measured swelling pressure (left) and hydraulic conductivity (right) of specimens from S2 and A3 after equilibrium with LOT-water. Results of drilled specimens (triangles, circles) and crushed/compacted specimens (diamonds) are shown with reference results (black markers and dashed line). The labels contain information about test parcel, block and distance in mm (e.g. A3 9/11 40) and cr means crushed/compacted specimen.

The swelling pressure  $P_{sf}$  shown in Table 3-3 to Table 3-6 were measured after lowering the water pressure, necessary for the evaluation of hydraulic conductivity. In each test the swelling pressure was also determined directly after saturation but before adding the water pressure  $P_{si}$ . The difference between these measurements  $(P_{si}-P_{sf})/P_{sf}$  was less than  $\pm 0.08$  in all tests.

The hydraulic conductivity shown in Table 3-3 to Table 3-6 were evaluated from the volume of the outflowing water  $k_w$  with evaporation from the tube taken into account (estimated from a reference tube at ambient conditions at the same time as the actual test). In Figure 3-9 the results with evaporation taken into account are shown together with results without evaporation taken into account (plus signs). In addition, the main part of the tests started with a leakage check, i.e. a check that no or negligible decreased water level was present in the outgoing tube before adding water pressure and starting the measurement.

In an attempt to estimate the maximum possible error the hydraulic conductivity  $k_w$  was evaluated by use of the inflowing water,  $k_{w,corr}$ . In each series, of four devices, the inflowing water volume  $V_{in}$  and the sum of the outflowing volume  $V_{out}$  can be compared. In all tests the relation  $V_{in}/V_{out}$  was between 1.6 and 2.2 corresponding to  $(k_{w,corr} - k_w)/k_w$  between 0.6 and 1.2. This was probably caused by leakage at the inlet, where the water is pressurized.

### 3.5.6 Comparison with LOT A2

In previous tests on material from LOT parcel A2 (Karlund et al. 2009) the swelling pressure measured was found to agree well with expected values while a minor but significant shift in hydraulic conductivity was seen between drilled specimens and crushed and re-compacted specimens. In the actual tests on specimens from S2 and A3 a scatter in hydraulic conductivity was seen but no significant difference between results from the drilled specimens and the crushed and re-compacted specimens.

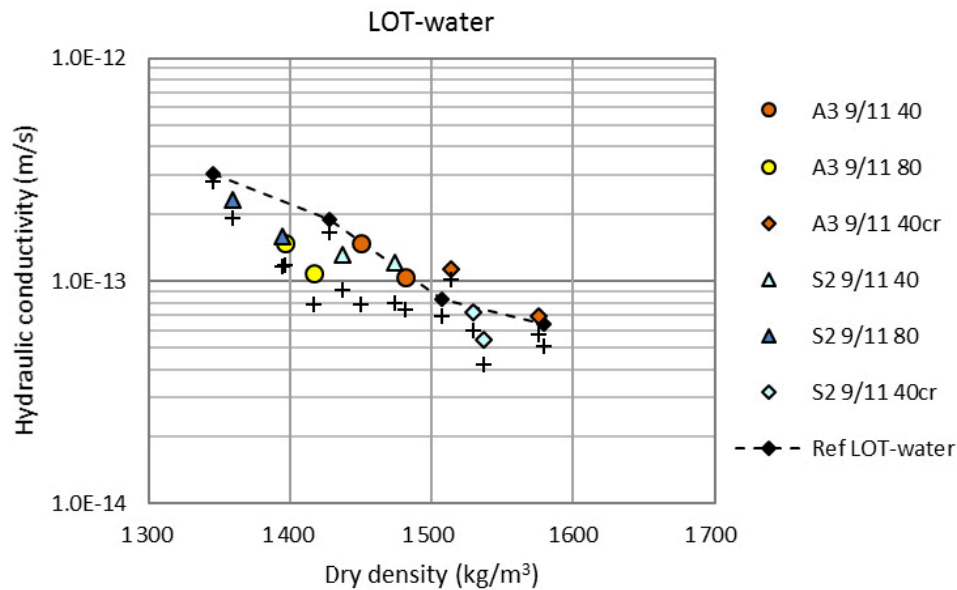


**Figure 3-9.** Hydraulic conductivity results taken from Figure 3-8 evaluated with evaporation (circles, triangles and diamonds) and without evaporation (plus signs) taken into account.

## 3.6 Unconfined compression test

### 3.6.1 General

The unconfined compression test is an experimentally simple method where a cylindrical specimen is compressed axially with a constant rate of displacement with no radial confinement or external radial stress. With this test the unconfined compressive strength of the specimen is determined. The strength is commonly determined on specimens having the height equal to double the diameter to allow the failure surface to fully develop. However, to increase the possibility of taking intact samples from the field experiment shorter specimens were used in this study, i.e. the height was equal to the diameter. To minimize the end effect on these short specimens lubrication of the end surfaces was made. Short specimens have previously been used and further commented in the CRT and TBT projects (Dueck et al. 2011 and Åkesson et al. 2012).

### 3.6.2 Test equipment

The saturation or re-saturation was done in specially designed saturation devices for 10 or 6 specimens at a time. For the compression test the specimens were placed in a mechanical press according to Figure 3-10 where a constant rate of displacement was applied. The end surfaces were lubricated to minimize the end effects. During the tests the displacement and the applied force were measured by means of a deformation transducer and a load cell. All transducers were calibrated prior to the shearing of one series and checked afterwards.

### 3.6.3 Preparation of specimen and test procedure

Tests were made on material both from the field experiment and from the LOT reference material. The specimens were prepared in three different ways:

- trimmed to fit the sample holder,
- ground to a grain size less than 1.5 mm and then re-compacted,
- compacted from powder samples.

The material from the field experiment was prepared by the two first methods and the target dry density of the re-compacted specimens was 1 540 kg/m<sup>3</sup>. The reference material was prepared by the third method aiming at different dry densities between 1 350 and 1 600 kg/m<sup>3</sup>. The specimens from parcels S2 and A3 were taken from equal positions.

Both the diameter and height of the specimens were 20 mm. All specimens were prepared in a saturation device before the tests. Two different types of preparation were used for the specimens; they were either saturated with LOT-water (see Section 3.3) or ion-exchanged with 1M CaCl<sub>2</sub>.

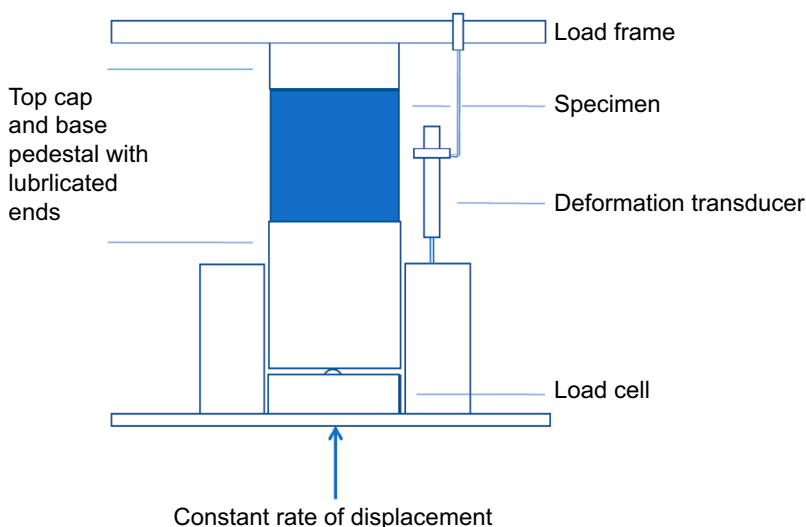


**Figure 3-10.** Set-up for the unconfined compression test.

The specimens saturated with LOT-water were exposed to circulating LOT-water above and under the specimens over a short time period but as stagnant water during the main part of the saturation time. The time used for the saturation was more than two weeks. The specimens ion-exchanged with 1M CaCl<sub>2</sub> were handled in a similar way as the specimens prepared for measurement of swelling pressure and hydraulic conductivity (Section 3.5.3), in the following steps:

1. Saturation by stagnant LOT-water.
2. Circulation of LOT-water, more or less continuously, to remove air trapped in the filters.
3. Ion-exchange to be Ca-dominated by continuous circulation of 1M CaCl<sub>2</sub> for approximately 50 days.
4. Removing excess salt by continuous circulating of DI-water (de-ionized water) for 22–36 days.
5. End of test and dismantling.

The time used for the ion-exchange was calculated to correspond to approximately 80 % ion-exchange in the central part of the specimens. The time used for the circulation of DI-water in the filters, to remove excess salt, was chosen to get low electrical conductivity, lower than 0.1 mS/cm. After preparation the specimens were removed from the saturation device at least 12h before shearing in order to homogenize, but still protected from evaporation.

The specimens were placed in a mechanical press and the compression was run at a constant deformation rate of 0.16 mm/min which corresponds to a strain rate of 0.8 %/min. The specimens were placed between lubricated end plates and were surrounded by a thin plastic film to minimize evaporation during shearing. After failure the water content and density were determined on all specimens according to Section 3.4.

The specimens were undrained during shearing and no volume change was taken into account. The deviator stress  $q$  (kPa) and the axial strain  $e$  (%) were derived according to:

$$q = \frac{F}{A_0} \cdot \left( \frac{l_0 - \Delta l}{l_0} \right) \quad (\text{Equation 3-4})$$

$$\varepsilon = \frac{\Delta l}{l_0} \quad (\text{Equation 3-5})$$

where  $F$  is the applied vertical load (kN),  $A_0$  is the original cross section area (m<sup>2</sup>),  $l_0$  is the original length (m) and  $\Delta l$  is the axial displacement (m). The results were corrected for initial problems with the contact surface by decreasing the strain with the intercept on the x-axis of the tangent to the stress-strain curve taken at a stress of 500 kPa.

### 3.6.4 Results

Below the results are presented for specimens from test parcels S2 and A3 separately. Additional results can be found in Appendix 3. The Sample ID is given according to Section 3.2.

#### **Specimens from Test Parcel S2**

The results from tests on specimens from S2 are given in Table 3-7 where maximum deviator stress and the corresponding strain for each specimen are presented with the dry density, water content and degree of saturation.

**Table 3-7. Maximum deviator stress and corresponding strain resulting from unconfined compression tests on specimens from test parcel S2. All specimens had a height equal to the diameter. For each specimen the Test ID is given together with the dry density and water content after dismantling. The positions of the specimens from the field experiment are given with block number and radial distance.**

Test ID	Material	Block	Radial distance mm	Preparation	Test solution <sup>2</sup>	Dry density kg/m <sup>3</sup>	Water content %	Degree of saturation %	Max deviator stress kPa	Corresponding strain %
UC1 1	LS2-09-20	9	20	drilled	LOT-water	1505	29.8	99	2123	5.4
UC1 2	LS2-09-40	9	40	drilled	LOT-water	1450	32.1	98	1515	6.4
UC1 3	LS2-09-80	9	80	drilled	LOT-water	1424	33.8	100	1489	6.3
UC1 4	LS2-11-20	11	20	drilled	LOT-water	1418	33.7	99	1323	7.6
UC1 5	LS2-11-40	11	40	drilled	LOT-water	1428	33.3	99	1377	8.4
UC1 6	LS2-11-80	11	80	drilled	LOT-water	1360	36.8	99	874	9.1
UC1 7	LS2-09-20cr	9	20	crushed + comp.	LOT-water	1555	27.6	99	2718	8.1
UC1 8	LS2-09-40cr	9	40	crushed + comp.	LOT-water	1552	27.7	99	2522	8.3
UC1 9	LS2-11-20cr	11	20	crushed + comp.	LOT-water	1534	28.3	98	2350	9.7
UC1 10	LS2-11-40cr	11	40	crushed + comp.	LOT-water	1519	29.0	98	2049	11.2
UC3 1	LOT Ref			compacted	LOT water	1395	34.6	98	1358	8.3
UC3 2	LOT Ref			compacted	LOT water	1441	32.3	98	1738	8.0
UC3 3	LOT Ref			compacted	LOT water	1464	31.1	97	2063	8.0
UC3 4	LOT Ref			compacted	LOT water	1512	28.6	96	2631	7.3
UC3 5	LOT Ref			compacted	LOT water	1550	26.6	95	3229	7.0
UC3 6	LOT Ref			compacted	LOT water	1596	24.9	95	3846	6.7
UC4 1	LOT Ref			compacted	LOT water	1380	35.2	97	1153	7.9
UC4 2	LOT Ref			compacted	LOT water	1474	30.7	97	1991	6.9
UC4 3	LOT Ref			compacted	LOT water	1578	25.9	96	3474	6.1
UC4 4	LOT Ref			compacted	DI-water	1370	36.2	99	1147	6.6
UC4 5	LOT Ref			compacted	DI water	1453	31.7	98	1913	7.1
UC4 6	LOT Ref			compacted	DI water	1443	32.4	98	1733	7.3
UC5 1	LS2-09-20	9	20	drilled	LOT, CaCl <sub>2</sub> , DI <sup>1</sup>	148 <sup>63</sup>	30.6	99	1949	6.1
UC5 2	LS2-09-40	9	40	drilled	LOT, CaCl <sub>2</sub> , DI <sup>1</sup>	146 <sup>43</sup>	31.6	99	1762	5.6
UC5 3	LS2-09-80	9	80	drilled	LOT, CaCl <sub>2</sub> , DI <sup>1</sup>	140 <sup>83</sup>	33.9	98	1541	8.1
UC5 4	LS2-11-20	11	20	drilled	LOT, CaCl <sub>2</sub> , DI <sup>1</sup>	143 <sup>83</sup>	32.6	98	1820	8.5
UC5 5	LS2-11-40	11	40	drilled	LOT, CaCl <sub>2</sub> , DI <sup>1</sup>	138 <sup>63</sup>	35.4	99	1265	8.7
UC5 6	LS2-11-80	11	60	drilled	LOT, CaCl <sub>2</sub> , DI <sup>1</sup>	142 <sup>13</sup>	33.8	99	1171	3.9
UC5 7	LS2-09-20cr	9	20	crushed + comp.	LOT, CaCl <sub>2</sub> , DI <sup>1</sup>	152 <sup>43</sup>	28.9	99	2219	12.9
UC5 8	LS2-09-40cr	9	40	crushed + comp.	LOT, CaCl <sub>2</sub> , DI <sup>1</sup>	153 <sup>53</sup>	28.5	99	2291	12.2
UC5 9	LS2-11-20cr	11	20	crushed + comp.	LOT, CaCl <sub>2</sub> , DI <sup>1</sup>	154 <sup>03</sup>	28.6	100	2355	10.8
UC5 10	LS2-11-40cr	11	40	crushed + comp.	LOT, CaCl <sub>2</sub> , DI <sup>1</sup>	155 <sup>23</sup>	27.6	98	2544	12.5
UC7 1	LOT Ref			compacted	LOT, CaCl <sub>2</sub> , DI <sup>1</sup>	1374	35.6	98	1283	8.5
UC7 2	LOT Ref			compacted	LOT, CaCl <sub>2</sub> , DI <sup>1</sup>	1433	33.0	99	1768	8.5
UC7 3	LOT Ref			compacted	LOT, CaCl <sub>2</sub> , DI <sup>1</sup>	1458	31.9	99	1873	8.8
UC7 4	LOT Ref			compacted	LOT, CaCl <sub>2</sub> , DI <sup>1</sup>	1499	29.8	98	2459	8.5
UC7 5	LOT Ref			compacted	LOT, CaCl <sub>2</sub> , DI <sup>1</sup>	1540	28.2	99	2955	7.6
UC7 6	LOT Ref			compacted	LOT, CaCl <sub>2</sub> , DI <sup>1</sup>	1572	26.6	98	3309	6.9

<sup>1</sup> Three solutions were used subsequently; LOT-water, 1M CaCl<sub>2</sub> and DI water (Section 3.6.3).

<sup>2</sup> LOT water is defined in Section 3.3.

<sup>3</sup> Some uncertainty in the results which might be 8 % less than given.

Results from test parcel S2 are shown in Figure 3-11 and Figure 3-12. The colours (yellow, light blue, dark blue) denote the distances (20 mm, 40 mm, 80 mm) from the heater. The different markers, circles and diamonds, denote drilled specimens and crushed and re-compacted specimens, respectively. The references are shown with black markers together with a best fit line (marked Eq in the legends).

In Figure 3-11 test results from specimens saturated with LOT-water are shown together with results from reference material prepared in the same way. Compared to the references, the maximum deviator stress is lower in the results from the field experiment, i.e. from both the drilled specimens and from the crushed and re-compacted specimen. The corresponding strain at failure of the drilled specimens is equal to or lower than the references while the crushed and re-compacted specimens yield larger strain at failure compared to the references. No influence of position is seen.

In Figure 3-12 the results of specimens ion-exchanged with 1M CaCl<sub>2</sub>, according to Section 3.6.3, are shown together with results from reference material prepared in the same way. Results of the ion-exchanged specimens are marked with (2) in the diagrams. In this series, UC5, the load cell showed larger deviation, between the check before and after the tests, than was seen in the other test series. This gives that the results in this series is somewhat uncertain and could be 8 % less than given in the diagrams and tables.

In spite of this, the behaviour of specimens ion-exchanged with 1M CaCl<sub>2</sub> are similar compared to those saturated with LOT-water, see above, compared to their respective reference lines. No influence of position is seen.

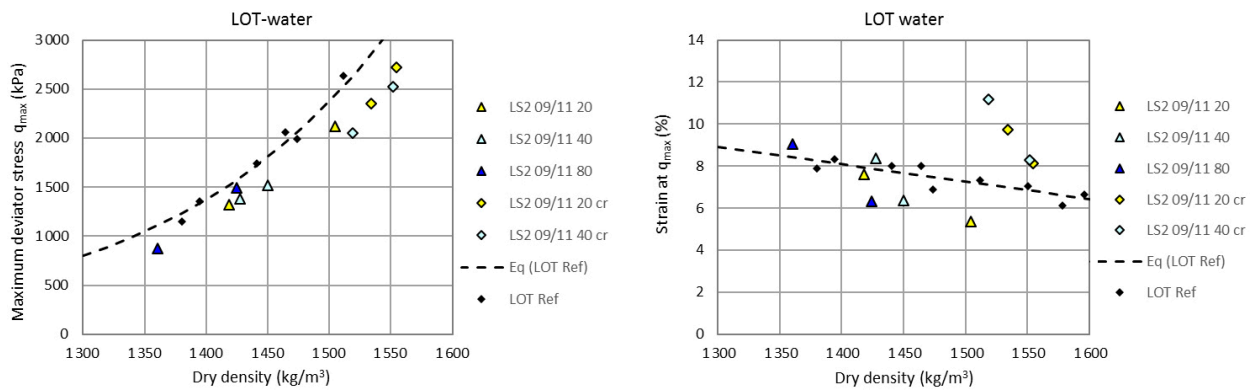


**Figure 3-11.** Maximum deviator stress (left) and corresponding strain (right) as a function of dry density of specimens from test parcel S2 at different distances from the heater. The specimens were saturated with LOT-water. Results of drilled specimens (triangles) and crushed/compacted specimens (diamonds) are shown together with reference results (black markers). The labels contain information about parcel, block and distance in mm (e.g. S2 9/11 40) and cr means crushed/compacted specimen.

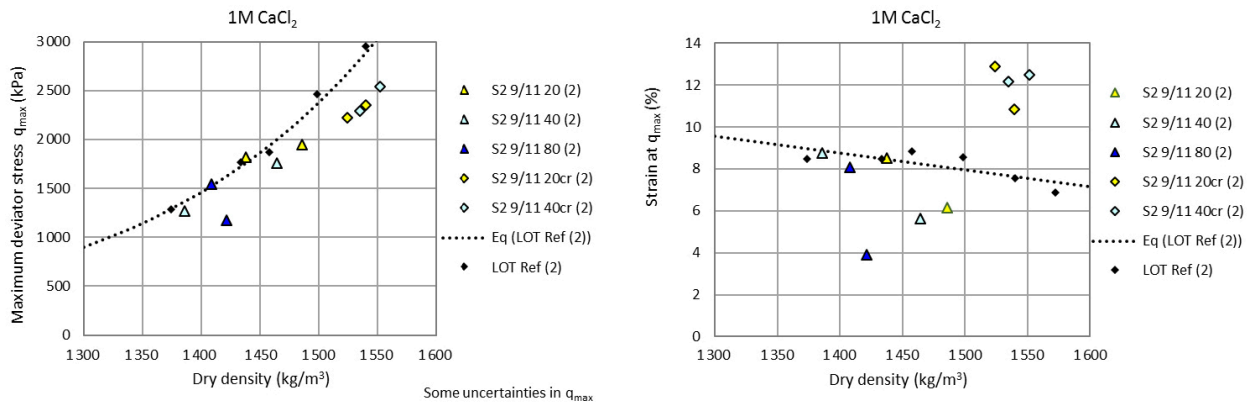


**Figure 3-12.** Maximum deviator stress (left) and corresponding strain (right) as a function of dry density of specimens from test parcel S2. The specimens were ion-exchanged with CaCl<sub>2</sub>, marked with (2), otherwise the markers and labels are the same as in Figure 3-11.

Deviator stress as a function of strain of the drilled specimens saturated with LOT-water and ion-exchanged with 1M CaCl<sub>2</sub>, (2), are shown in Figure 3-13 and Figure 3-14, respectively. Applicable references are also shown. Failure occurs at reduced strain for some of the specimens, which was also seen in Figure 3-11 and Figure 3-12.

### Results from Test Parcel A3

The results from tests on specimens from test parcel A3 are given in Table 3-8 where maximum deviator stress and the corresponding strain for each specimen are presented with the dry density, water content and degree of saturation.

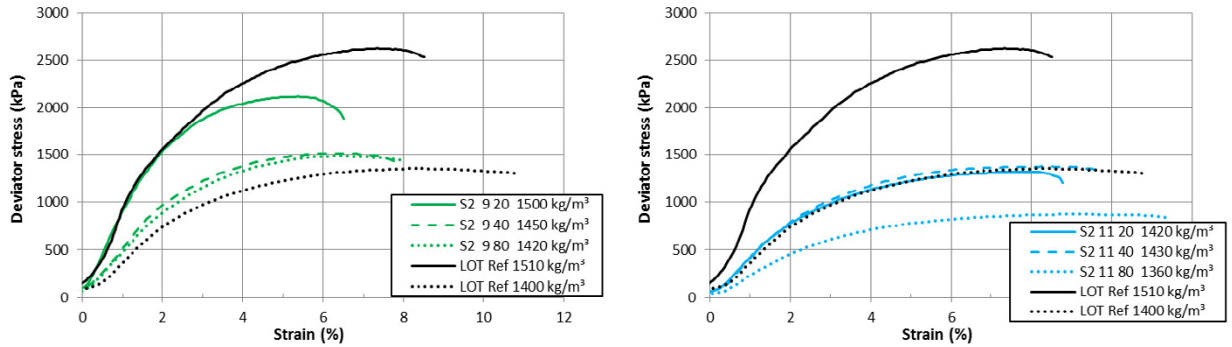


**Figure 3-13.** Deviator stress as a function of strain of drilled specimens from test parcel S2 at different positions of block 09 (left) and 11 (right). The specimens were saturated with LOT water. Two references are used for comparison. The legend contains information about the parcel, block, position and dry density.

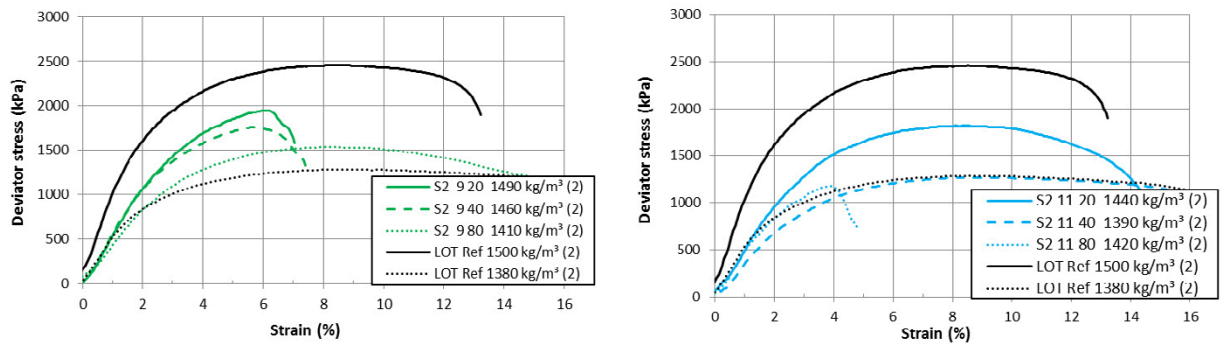


**Figure 3-14.** Deviator stress as a function of strain of drilled specimens from test parcel S2 at different positions of block 09 (left) and 11 (right). The specimens were ion-exchanged with 1M CaCl<sub>2</sub> (2). Two references are used for comparison. The legend contains information about the parcel, block, position and dry density.

**Table 3-8. Maximum deviator stress and corresponding strain resulting from unconfined compression tests on specimens from test parcel A3. All specimens had a height equal to the diameter. For each specimen the Test ID is given together with the dry density and water content after dismantling. The positions of the specimens from the field experiment are given with block number and radial distance.**

Test ID	Material	Block	Radial distance mm	Preparation	Test solution <sup>2</sup>	Dry density kg/m <sup>3</sup>	Water content %	Degree of saturation %	Max deviator stress kPa	Corresponding strain %
UC2 1	LA3-09-20	9	20	drilled	LOT-water	1500	30.1	99	2253	4.1
UC2 2	LA3-09-40	9	40	drilled	LOT-water	1468	30.9	97	1480	2.9
UC2 3	LA3-09-80	9	80	drilled	LOT-water	1382	34.9	97	1229	3.6
UC2 4	LA3-11-20	11	20	drilled	LOT-water	1459	32.1	100	1561	2.7
UC2 5	LA3-11-40	11	40	drilled	LOT-water	1425	33.5	99	1563	5.1
UC2 6	LA3-10-80	10	80	drilled	LOT-water	1361	36.5	98	1034	4.0
UC2 7	LA3-09-20cr	9	20	crushed + comp.	LOT-water	1531	28.9	100	2366	9.4
UC2 8	LA3-09-40cr	9	40	crushed + comp.	LOT-water	1523	28.6	98	2266	9.0
UC2 9	LA3-11-20cr	11	20	crushed + comp.	LOT-water	1533	27.8	96	2470	8.7
UC2 10	LA3-11-40cr	11	40	crushed + comp.	LOT-water	1538	28.2	98	2492	9.1
UC6 1	LA3-09-20	9	20	drilled	LOT, CaCl <sub>2</sub> , DI <sup>1</sup>	1482	30.6	98	1963	4.9
UC6 2	LA3-09-40	9	40	drilled	LOT, CaCl <sub>2</sub> , DI <sup>1</sup>	1458	32.1	100	1791	6.2
UC6 3	LA3-09-80	9	60 <sup>3</sup>	drilled	LOT, CaCl <sub>2</sub> , DI <sup>1</sup>	1441	32.6	99	1560	6.6
UC6 4	LA3-11-20	11	20	drilled	LOT, CaCl <sub>2</sub> , DI <sup>1</sup>	1423	33.4	98	1468	6.4
UC6 5	LA3-11-40	11	40	drilled	LOT, CaCl <sub>2</sub> , DI <sup>1</sup>	1408	34.1	98	1365	6.7
UC6 6	LA3-11-80	11	60 <sup>3</sup>	drilled	LOT, CaCl <sub>2</sub> , DI <sup>1</sup>	1424	33.5	99	1477	6.9
UC6 7	LA3-09-20cr	9	20	crushed + comp.	LOT, CaCl <sub>2</sub> , DI <sup>1</sup>	1505	30.2	100	2166	11.3
UC6 8	LA3-09-40cr	9	40	crushed + comp.	LOT, CaCl <sub>2</sub> , DI <sup>1</sup>	1510	29.8	100	2130	12.2
UC6 9	LA3-11-20cr	11	20	crushed + comp.	LOT, CaCl <sub>2</sub> , DI <sup>1</sup>	1526	29.0	99	2438	10.8
UC6 10	LA3-11-40cr	11	40	crushed + comp.	LOT, CaCl <sub>2</sub> , DI <sup>1</sup>	1529	28.6	98	2416	11.2

<sup>1</sup> Three solutions were used subsequently; LOT-water, 1M CaCl<sub>2</sub> and DI water (Section 3.6.3).

<sup>2</sup> LOT water is defined in Section 3.3.

<sup>3</sup> Deviating distance from the heater compared to the test plan.

Results from test parcel A3 are shown in Figure 3-15 and Figure 3-16. The colours (red, orange, yellow) denote the distances (20 mm, 40 mm, 80 mm) from the heater. The markers circles and diamonds show drilled specimens and crushed and re-compacted specimens, respectively. The references are shown with black markers together with a best fit line (marked Eq in the legends).

In Figure 3-15 test results from specimens saturated with LOT-water are shown together with results from reference material prepared in the same way. Compared to the references, the maximum deviator stress is equal or lower in the results from the field experiment, i.e. from both the drilled and the crushed and re-compacted specimen. The corresponding strain at failure of the drilled specimens is markedly lower than the references while the crushed and re-compacted specimens yield larger strain at failure compared to the references. No influence of position is seen.

In Figure 3-16 the results of specimens ion-exchanged with 1M CaCl<sub>2</sub>, according to Section 3.6.3, are shown together with results from reference material prepared in the same way. Results of the ion-exchanged specimens are marked with (2) in the diagrams. The maximum deviator stress of all the specimens is lower than the references. The corresponding strains show similar behaviour as the specimens saturated with LOT-water in relation to the respective references. No influence of position is seen.

Deviator stress as a function of strain of the drilled specimens saturated with LOT water and ion-exchanged with 1M CaCl<sub>2</sub>, marked with (2), are shown in Figure 3-17 and Figure 3-18, respectively. Applicable references are shown. Failure occurs at reduced strain in all results. Rapid decrease in stress at low strain is seen in some of the tests both among the specimens saturated with LOT-water and those ion-exchanged.

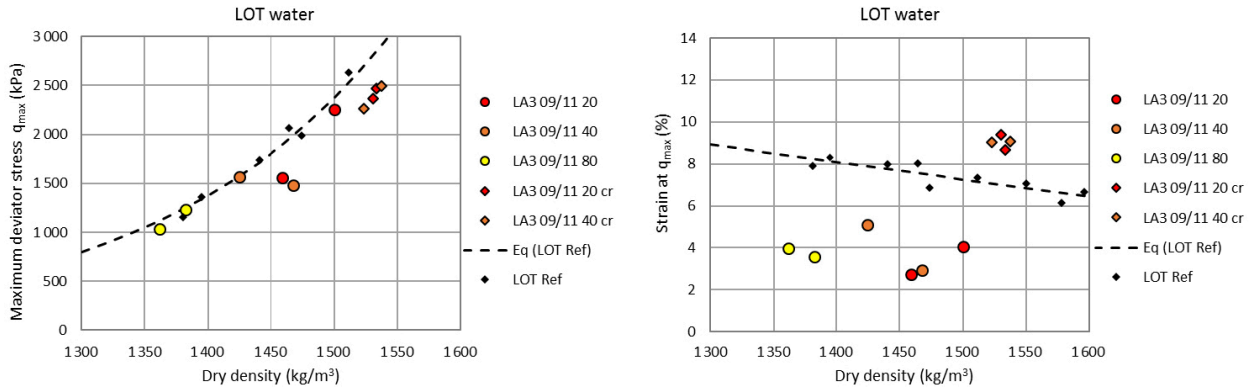


**Figure 3-15.** Maximum deviator stress (left) and corresponding strain (right) as a function of dry density of specimens from test parcel A3 at different distances from the heater. The specimens were saturated with LOT-water. Results of drilled specimens (circles) and crushed/compacted specimens (diamonds) are shown together with reference results (black markers). The labels contain information about parcel, block and distance in mm (e.g. A3 9/11 40) and cr means crushed/compacted specimens.

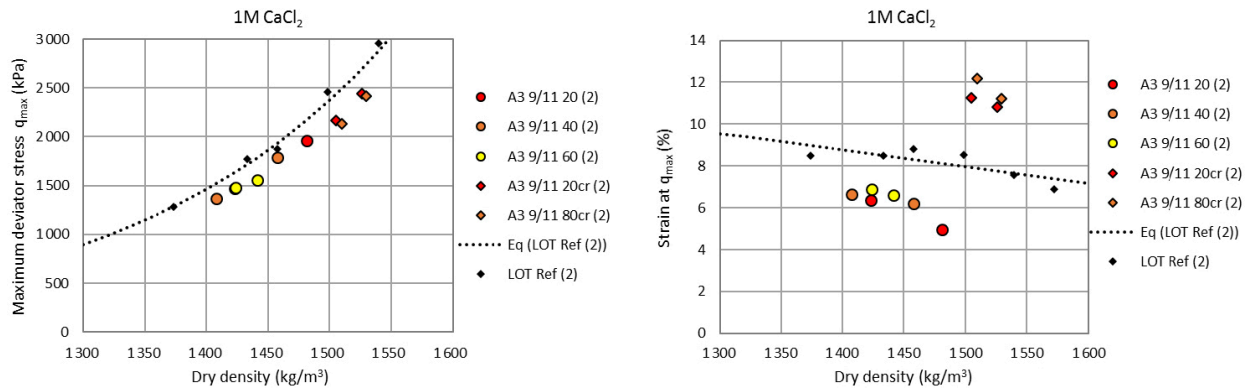


**Figure 3-16.** Maximum deviator stress (left) and corresponding strain (right) as a function of dry density of specimens from test parcel A3. The specimens were ion-exchanged with  $\text{CaCl}_2$ , marked with (2), and otherwise the markers and labels are the same as in Figure 3-15.

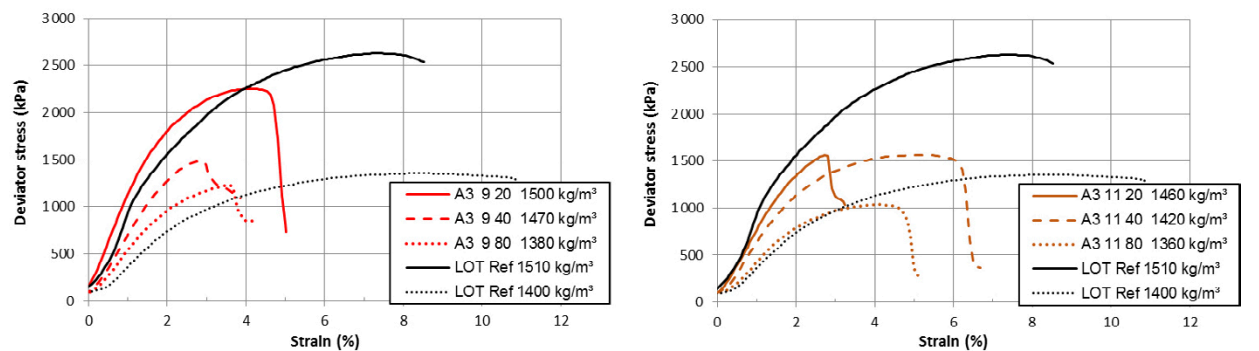


**Figure 3-17.** Deviator stress as a function of strain of specimens from test parcel A3 at different positions of block 09 (left) and 11 (right). The specimens were saturated with LOT water. Two references are used for comparison. The legend contains information about the parcel, block, position and dry density.

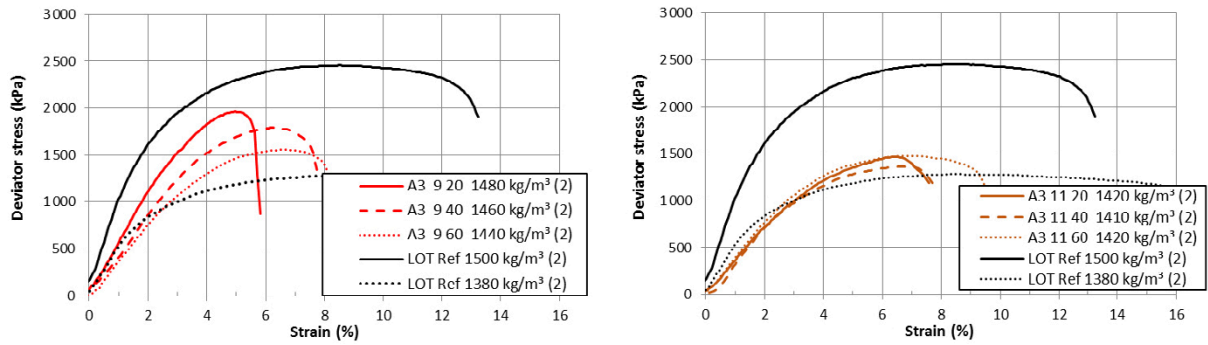


**Figure 3-18.** Deviator stress as a function of strain of specimens from test parcel A3 at different positions of block 09 (left) and 11 (right). The specimens were ion-exchanged with 1M CaCl<sub>2</sub> (2). Two references are used for comparison. The legend contains information about the parcel, block, position and dry density.

### 3.6.5 Discussion

The results in Figure 3-11 and Figure 3-15 are compiled in Figure 3-19. The results of drilled specimens from test parcel S2 (triangles) and A3 (circles) are shown together with results from crushed and re-compacted specimens (diamonds). The results from reference tests are also shown (black markers and dashed line).

Specimens at a specific distance from the heater in test parcel S2 and A3 were exposed to a specific temperature, according to Section 1.2. In Figure 3-19 the colours (red, orange, yellow, light blue, dark blue) denote the different temperatures (100 °C, 90 °C, 80 °C, 70 °C, 60 °C). No influence of position or temperature on the deviator stress at failure can be seen, but the corresponding strain is in general lower for the specimens from A3 compared to those from S2.

In Figure 3-19 the maximum deviator stress of specimens from the field experiment are equal to or lower than the references as commented above. There may be slight uncertainties regarding the results of the reference tests at dry density higher than 1 500 kg/m<sup>3</sup>, since they had a relatively low degree of saturation, although larger than 95 %. Since the degree of saturation was higher in all ion-exchanged specimens, including the references at high dry density, these results can be used to confirm the tendency that the maximum deviator stress of the crushed and re-compacted specimens are lower than the references.

The final dry density of the drilled specimens was slightly lower than the densities determined from the field experiment due to the technique used for the installation in the test equipment.

In all diagrams the references are shown with test results and best fit lines, marked Eq. In Figure 3-20 the results of the reference tests and the best fit lines are shown, both for the specimens saturated with LOT-water and the specimens ion-exchanged with CaCl<sub>2</sub>. No large difference can be seen between the two types of preparation.

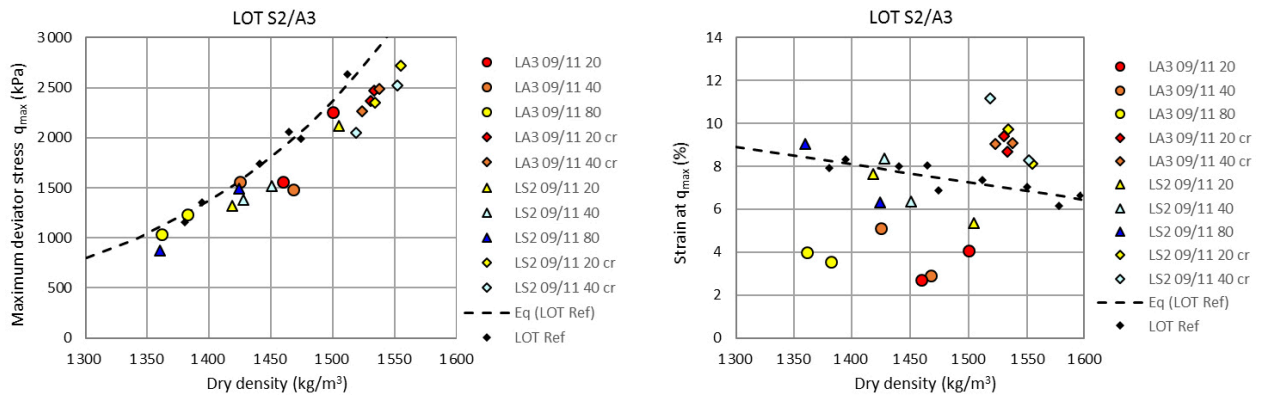


**Figure 3-19.** Maximum deviator stress and corresponding strain versus dry density after dismantling for all specimens saturated with LOT-water. The circles and triangles denote specimens drilled from the test parcels A3 and S2, respectively. The diamonds represent crushed/ compacted specimens from both A3 and S2 (labels ending with cr). References are shown with black markers and dashed lines. The labels show the parcel (A3 or S2) the block (09 or 11) and the distance from the heater in mm.

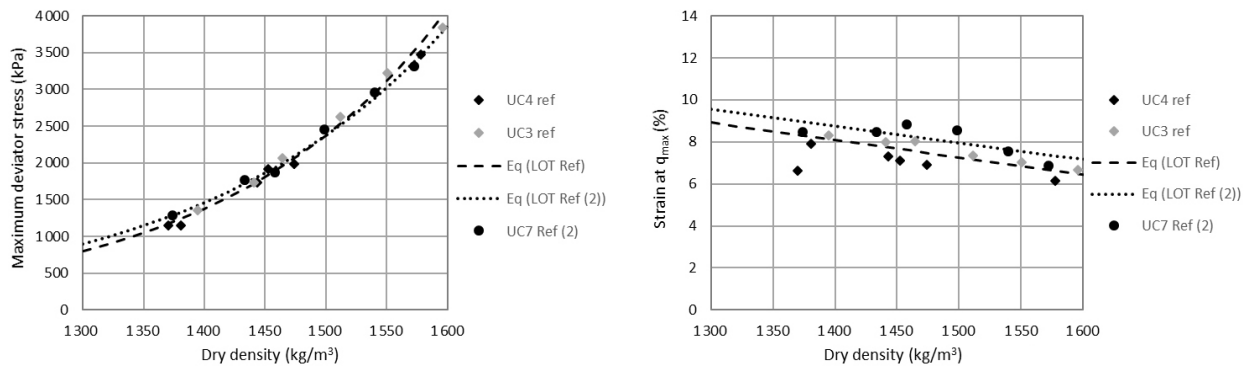


**Figure 3-20.** Results from tests on reference material in series UC3, UC4 and UC7. The dashed and dotted lines are best fit lines of specimens saturated with LOT-water and ion-exchanged with  $CaCl_2$ , respectively.

### 3.6.6 Comparison with LOT A2

In the previous tests on material from LOT parcel A2 (Karnland et al. 2009) a significantly reduced strain at failure was measured for specimens from the warm part and a pronounced failure was observed. In the actual tests this behaviour was seen for specimens from test parcel A3. In addition, indications of reduced deviator stress at failure was also observed.

In the previous LOT A2 the unconfined compression tests showed that the failure at reduced strain disappeared when the material was crushed and re-compacted which, is also seen in the tests on specimens from both test parcels S2 and A3. However, in contrast to the crushed and re-compacted specimens from LOT A2, which showed a maximum deviator stress and corresponding strain in agreement with or slightly higher than the references, the corresponding results from parcels S2 and A3 indicate reduced deviator stress and higher strain at failure compared to the actual references.



## 4 Mössbauer spectroscopy, Åbo Akademi

### 4.1 Experimental

For this project ten bentonite samples were measured using  $^{57}\text{Fe}$  Mössbauer spectroscopy. These ten samples belong to two batches of five samples each, with one group being marked as LOT S2, block 21s and the other group LOT A3, block 23. Each group of five samples consists of one sample at 0–10 mm, one sample at 10–20 mm, one sample at 20–50 mm, one sample at 50–100 mm and one reference sample (referenslera, lacking the block notion). The samples were sent to our laboratory in a vacuum-sealed bag containing the samples packed in individual sealed ziplock bags. After having arrived at our laboratory the samples were stored, while still in the ziplock bags, in a glove box with a nitrogen atmosphere, containing less than 1 ppm  $\text{O}_2$  and  $\text{H}_2\text{O}$ .

Absorbers for the Mössbauer spectroscopy measurements were made in the glove box by mixing dry sample powder with epoxy glue (Casco Strong Epoxy). The powder-glue mixture was evenly spread over a circular area with a diameter of 1.9 cm on an aluminum foil. The absorbers were stored in the glove box until the measurements began. When possible, the small amount of sample needed for the measurements were taken from the middle of the bentonite pieces. The samples used for the measurements were carved out of the larger sample pieces and ground into a powder using a pestle and a mortar. During the absorber-preparation process some moisture evaporated from the sample causing the dark-grey samples to turn into dry light-grey powders. The evaporation of the moisture caused the  $\text{H}_2\text{O}$  level in the glove box to momentarily rise to 25–35 ppm but no change in the oxygen level was noticed.

The Mössbauer spectroscopy measurements were done using a fresh 50 mCi  $^{57}\text{Co}$  Ritverc source in a rhodium matrix (activated early June 2020). A Fast ComTec MA-250 velocity transducer was used for moving the source. It was equipped with a Halder MR-351 Drive unite. The Mössbauer transducer was driven using a triangular velocity profile. The  $\gamma$  quanta were detected using a LND45431 proportional counter with a beryllium window. The data were collected using a Fast ComTec MCA-3 multichannel-analyzer PCI card in an ordinary desktop PC. The MCA card was set in a multiscaling mode. Each of the 512 channels was sequentially opened and collecting data during an equal amount of time. Owing to the linear velocity scale each channel corresponds to the same velocity width  $\Delta v$ . Although measurements were performed at 300 K an Oxford ITC4 continuous flow cryostat was used as a “sample chamber” kept under vacuum to ensure non-oxidative and constant-temperature conditions. The sample temperature was set to 300 K to ensure that only minute resistive heating sufficed for maintaining an even temperature. Simultaneously with the main measurement an older 25 mCi source placed at the other side of the velocity transducer was used for recording a velocity-calibration spectrum from an  $\alpha$ -Fe foil using another LND45431 proportional counter.

For the measurements the absorbers were quickly transferred from the glove box to the sample chamber of the measurement setup. This means that the sample powders, embedded in epoxy glue, only were exposed to air for a couple of minutes during the transfer. Two measurements of about 48 h were done for each sample; the first with a maximum Doppler velocity of 10.25 mm/s and the second with a maximum Doppler velocity of 4.50 mm/s. The high-velocity spectra were measured to detect possible magnetic components with a wider split of the lines. The low-velocity spectra were intended to better resolve the low-velocity paramagnetic components. The 48 h measurements gave a folded background level of about  $4.5 \times 10^6$  counts.

The Mössbauer spectrum of one component with no hyperfine interactions would consist of a single absorption line with the line width  $\Gamma$  and intensity  $I$ . Due to the chemical isomer shift  $\delta$ , expressed in relation to  $\alpha$ -Fe, the center of the absorption line shifts along the velocity axis. The shift is a rather direct measure of the iron valence, assuming we are dealing with only high-spin divalent and trivalent iron. A magnetic interaction splits the single line into 6 evenly spaced lines with intensity ratios of 3:2:1:1:2:3, in a powder sample. The quadrupole splitting splits the singlet into two absorption lines of equal intensity, separated by the quadrupole splitting  $\Delta$ . In a typical spectrum all or some of these hyperfine interactions will be simultaneously acting on various Fe species, giving rise to a more complicated pattern of lines.

The spectra were fitted using a home-written Fortran program utilizing the full Hamiltonian of combined electric and magnetic hyperfine interactions. One component pertaining to trace amounts of iron in the beryllium detector window is added to each spectrum in addition to the components originating from the samples. This component is usually minute, but become clearly visible in these samples due to the low iron content. The background of the folded spectra were corrected for a small incline of the background using a velocity dependent linear equation, with the parameters fitted to the background of the high-velocity spectra also used to correct the low-velocity spectra of the same sample. The following parameters were used when fitting the spectra:  $I$ ,  $\delta$  and  $\Delta$ , having unique values for each component, representing a specific Fe species. Additionally, the line width parameter  $\Gamma$  was fitted, but set equal of Fe species of similar valence. As no magnetic sextets were observed, the internal magnetic field was fixed to zero for each component. The parameters of the component pertaining to the Fe impurity in Be are previously known and were not released in the fits

By assuming the same recoil-free fraction for all components the relative portion of the components can be obtained from the areas of the components, given by

$$A_i = \frac{\pi}{2} I_i \Gamma_i. \quad (4-1)$$

The relative portion of  $\text{Fe}^{3+}$  and  $\text{Fe}^{2+}$  is obtained by adding all components with the same valence and comparing to the total area, excluding the area of the component pertaining to the detector window.

## 4.2 Results

The intensity of a Mössbauer spectrum *i.e.* sample absorption is directly proportional to the amount of  $^{57}\text{Fe}$  in the absorber. By using thicker absorbers absorption increases, but at the same time the signal-to-noise ratio and the count rate of the gamma spectrum decreases. By testing using absorbers of 50, 75, 100, 150, 200, 250, 300 and 350 mg we were able to find an optimal sample amount of 300 mg, which was used throughout the measurements. The optimum depends also on the sample matrix, which in the present case probably is dominated by silicates, which fortunately are not very strongly absorbing. To test the chemical stability of the absorbers the first absorber to be measured was measured again 37 days later, exhibiting no change exceeding the detection limit.

The high velocity spectra show no traces of any magnetic lines exceeding the detection limit of a single-line absorption of  $\sim 0.05\%$ . In the current spectra that rules out the existence of magnetically split components constituting more than 2.4 % of the total area, *i.e.* total amount of Fe. The paramagnetic spectra, best studied from the low velocity spectra, contain two major components. One (component  $\text{Fe}_1^{3+}$ ) has  $\delta \approx 0.34$  mm/s and  $\Delta \approx \pm 0.55$  mm/s, which are typical hyperfine parameters for high-spin  $\text{Fe}^{3+}$ . The other (component  $\text{Fe}_1^{2+}$ ) has  $\delta \approx 1.14$  mm/s and  $\Delta \approx \pm 2.8$  mm/s, which are typical hyperfine parameters for high-spin  $\text{Fe}^{2+}$ . The sign of  $\Delta$  cannot be determined for paramagnetic spectra and hence a positive sign is assumed. Both these components were fitted with their own values for  $\Gamma$ , giving a significantly larger value for the  $\text{Fe}^{3+}$  component than the  $\text{Fe}^{2+}$  one. From a pure nuclear point of view practically identical values would be expected. However, line broadening can appear e.g. due to lattice strain or various distributions in the electric hyperfine parameters, caused by variation in next-neighboring elements. These hyperfine parameter-values corresponds well to those reported in Ref. (1), although the isomer shift values are lower here due to the higher sample temperature. In addition to the major components the spectra contain two smaller components ( $\text{Fe}_2^{3+}$  and  $\text{Fe}_2^{2+}$ ). These minor components have hyperfine parameters close to one of the major components, but shifted slightly towards the other component. Because of the small area of these minor components their line widths are hard to fit and they were, consequently, shared with that of the corresponding major component. These minor components could pertain to iron sites with some small variation in the chemical surrounding compared to that of the major components.

The fitted spectra are displayed in the Appendix in Figure A4-1 to Figure A4-10. The five components used for the analysis, all corresponding to various Fe species, are also shown. In Table A4-1 and A4-2 the hyperfine parameters and the valence ratios for all samples are presented. Table 4-1 summarizes the valence data. Visual inspection reveals that the two reference samples are rather similar to each other and all the other samples are similar to each other. The reference samples contain a significantly lower relative portion of  $\text{Fe}^{2+}$  compared to the rest of the samples. A quick comparison shows that

the  $\text{Fe}^{3+}:\text{Fe}^{2+}$  ratio is close to 2:1 in the reference samples, while it is close to 1:1 in the other samples. The two batches of samples show different behavior as a function of the depth. Samples from LOT S2, block 21S have an almost exact 1:1 ratio of  $\text{Fe}^{2+}$  vs  $\text{Fe}^{3+}$  in the 0–10 mm sample while the relative amount of  $\text{Fe}^{2+}$  increases for higher mm values. However, the values are somewhat scattered. Samples from LOT A3, block 23 show the opposite trend, but an even evolution with the depth scale. The  $\text{Fe}^{3+}:\text{Fe}^{2+}$  ratio is closest to 1:1 in the 50–100 mm sample and the relative amount of  $\text{Fe}^{2+}$  increases when the depth value decreases.

Ten bentonite samples were measured by  $^{57}\text{Fe}$  Mössbauer spectroscopy at 300 K. The ratio of paramagnetic Fe(II) to Fe(III) was readily obtained. No traces of magnetically-ordered Fe were observed. Fe(II) occurred as two distinct components, one with a huge quadrupole splitting of  $\sim 2.8$  mm/s, typical of bentonite samples (1) and the other in much smaller concentrations and slightly smaller quadrupole splitting and isomer shift, indicating a slight shift towards trivalency. Fe(III) also occurred as two components with similar hyperfine parameter values. The minor component was slightly shifted towards divalency judging by the isomer shift value. Nevertheless, the trivalent components might originate from similar chemical surroundings, as the differences between them are rather small.

**Table 4-1. Concentration of Fe(II) and Fe(III).**

Sample	Fe(II) (%)	Fe(III) (%)
A3, bl. 23, 0–10 mm	52.63(5)	47.4(1)
A3, bl. 23, 10–20 mm	50.7(3)	49.32(4)
A3, bl. 23, 20–50 mm	49.6(1)	50.4(1)
A3, bl. 23, 50–100 mm	49.6(3)	50.4(1)
A3 Reference	27.8(3)	72.16(7)
S2, bl. 21s, 0–10 mm	50.0(2)	49.95(7)
S2, bl. 21s, 10–20 mm	50.76(4)	49.2(2)
S2, bl. 21s, 20–50 mm	50(4)	50.0(1)
S2, bl. 21s, 50–100 mm	52.01(5)	48(3)
S2 Reference	30.14(3)	69.9(2)



## 5 Mineralogy at James Hutton Limited Analytical Laboratory Services

### 5.1 Samples

Two samples were submitted to James Hutton Limited Analytical Laboratory Services. Both samples were from the swelling pressure – hydraulic conductivity investigations at Äspö. Hence, they were Ca-exchanged and washed free from salts.

SPHC LOT A3 block 33 sample (d5c7b0) was a combined sample from the different samples from the swelling pressure measurements done on this profile. The combination of samples was done in order to achieve enough of sample needed for the analysis. So, this sample was from the LOT A3 experiment and represents approximately an average of block 33.

SPHC LOT Reference A3 (d5c7b1) was also a combined sample from several samples used for the SPHC measurements. This is a reference sample and was not from the LOT A3 experiment but was the same batch of clay used for the installation of the experiment.

### 5.2 Method description

XRPD bulk quantitative analysis samples were wet ground for 12 minutes in a McCrone mill and spray dried to produce random powder specimens (Hillier, 1999; Hillier, 2003). X-ray powder diffraction (XRD) patterns were recorded using Cu radiation. Quantitative analysis was made by a normalised full pattern reference intensity ratio (RIR) method as described in Omotoso et al. (2006) and Butler and Hillier (2021).

### 5.3 Statistics and error estimates

Unless stated otherwise, expanded uncertainty using a coverage factor of 2, i.e. 95 % confidence, is given by  $\pm X^{0.35}$ , where X = concentration in wt.%, e.g. 30 wt.%  $\pm 3.3$  (Hillier 2003). Note also, that for phases present at the trace level (10 wt.% uncertainty is estimated as better than  $\pm 5$ wt.% at the 95 % confidence level.

### 5.4 Results

The samples were dominated by dioctahedral smectite, with quartz, K-feldspar, and opal-C/cristobalite (Table 5-1). Trace amounts of calcite and pyrite were also present. A trace amount of clinoptilolite may also be present. The duplicate analyses of the bulk samples are essentially identical, well within analytical uncertainties. Clay fraction analysis indicates that the samples are dominated by dioctahedral smectite, no other clay minerals were detected.

Table 5-1. Mineralogy based on XRD.

Sample	Quartz	K-feldspar	Calcite	Pyrite	Clinoptilolite	Cristobalite	Smectite	Clay fraction
SPHC LOT A3 #33 sample d5c7b0	4.7	2.3	0.3	0.2	0.4	5.6	86.5	100 % smectite
	4.5	2.2	0.3	0.3	0.4	5.6	86.7	100 % smectite
SPHC LOT Reference A3 d5c7b1	4.7	2.1	0.2	0.3	0.3	5.9	86.5	100 % smectite
	4.9	2.2	0.2	0.3	0.3	5.7	86.4	100 % smectite



## 6 Assessment of the evolution of the bentonite in the LOT S2 and A3 parcels

The LOT S2 and A3 experiments were running for 20 years, and were among the longest running field experiments at Äspö with bentonite. They were analysed with regards to important central properties, as well as chemical and mineralogical content, including Fe redox chemistry.

### 6.1 Hydromechanical properties

#### *Swelling pressure*

No change was observed for the crushed and re-compacted specimens of either LOT A3 or S2. A minor reduction of the swelling pressure for specimens drilled from the warmer position, at 40 mm from heater from LOT A3 was however observed.

#### *Hydraulic conductivity*

At the Äspö laboratory small increase in the hydraulic conductivity were observed in both experiments on crushed and re-compacted specimens. The impact seems to be of the same magnitude in both experiments so there seems to be no impact from the temperature on the parameter. At Clay Technology no significant deviations were observed on either crushed and recompact specimens or drilled specimens.

#### *Unconfined compression tests*

In LOT S2 there were indications of reduced maximum deviator stress for the main part of the drilled specimens and for all crushed and re-compacted specimens. Significantly reduced strain of the drilled specimens, significantly higher strain after crushing and re-compaction, no significant influence of position and thus temperature.

In LOT A3 there were indications of reduced maximum deviator stress for all drilled and all crushed and re-compacted specimens. Significantly reduced strain for all drilled specimens and significantly higher strain after crushing and re-compaction. Failure at reduced strain and rapidly decreasing stress for some of the drilled specimens, i.e. a tendency towards more brittle material. No significant influence of position and thus temperature.

### 6.2 Chemistry and mineralogy

Cation exchange capacity (CEC): Generally in both S2 and A3 no significant changes were observed. However, in the warmer mid section of the LOT A3 there seems to be a small increase in the CEC (block 9 and 11). The average of the 3 innermost samples in A3 block 9 was 83.2 cmol(+)/kg and the reference was 80.5 cmol(+)/kg, making the average value 3.3 % higher than the reference value.

Chemical composition (XRF): a minor increase in MgO was observed in towards the heater in LOT A3 block 9, 11, 15, and 16, but not in the rest of the samples.

The XRD data of the A3 and S2 samples were visually indistinguishable from the reference samples after cation exchange and washing out the salts (on the samples from the swelling pressure – hydraulic conductivity measurements). Quantification using Siroquant 5 showed an average of the reference samples of 83.1 wt% montmorillonite (6 measurements) and the average of the LOT A3 samples was 85.3 wt% montmorillonite (6 measurements).

In average the A3 samples were 2.6 % higher than the reference in montmorillonite, and had a relative increase in Mg content of 3 %, and the Mg/Al ratio of the warmest sample increased with 5 % in relation to the reference.

The CEC of the clay fractions in LOT S2 are very close to the LOT clay fraction reference value. While the clay fractions of the LOT A3 mid section (block 9 and 11) show a small but significant increase in the CEC. The reference clay fraction was 87.3 and the LOT A3 clay fractions were 93–94 cmol(+)/kg. The scattering between clay fractions are higher compared to bulk samples due to the more compact nature of them (more difficult to disperse), and the smaller sample size available.

XRD of the clay fractions show a decrease in quartz and possibly also in cristobalite in the LOT A3 #11N 0–10 mm sample, and no change in the S2 9E sample. This is an observation, but more data is needed to draw strong conclusions. Some oriented samples were saturated with ethylene glycol (EG) before XRD measurement in order to investigate differences in swelling behaviour or forming of interstratified phases. No significant change could be observed.

In the chemical composition of the clay fractions both Al and Mg increased, and Si decreased. Al had a relative increase of 2.2 %, while Mg had a relative increase of 17 %. Hence, the increase in Mg was larger compared to the increase in Al. The relative increase in Al/Si ratio was 6.1 %, which was very close to the relative increase in CEC of 6.5 %.

Closer to the rock, the Ca values were close to or lower than the reference values in most cases, indicating very limited cation exchange with the ground water that typically is very rich in Ca. Some exceptions were LOT A3 block 33 and 35, where some Ca entered into the bentonite from the ground-water. This was observed also in the XRD patterns where two water layer 001 reflection was observed, confirming that some Ca<sup>2+</sup> had replaced Na<sup>+</sup> in the montmorillonite interlayer.

No significant change in the potassium content was observed. Chloride (Cl) was 0.02 wt% in the reference material and roughly 0.1–0.3 wt% in the samples from the experiments (being very homogeneously distributed), the slight increase due to the interaction with the Äspö ground water.

A sample from the LOT A3 block 33 profile and a reference sample was sent to the James Hutton Limited Analytical Laboratory Services for evaluation of the quantitative mineralogy using XRD for comparison. No difference could be observed between the LOT A3 sample and the reference, and dioctahedral smectite was the only clay mineral observed in both samples.

### ***Calcium sulfate phases (gypsum/anhydrite)***

In both LOT A3 and S2 heterogeneous accumulation of calcium sulfate was observed towards the heater, very similar to previous field experiments. This is explained by the solubility maximum of gypsum at 43 °C and the decreasing solubility of anhydrite as a function of temperature, hence the point of lowest solubility of calcium sulfates in the experiment is at the heater interface, hence that is where it will accumulate and precipitate. The highest measured value of sulfur, as SO<sub>3</sub>, is 10 wt%. This was found in the heater/bentonite interface in block 15 in the S2 package (Table 2-2b). The highest measured value in the A3 package was 5 wt% (Table 2-2c). The reference material contained on average 0.75 wt% SO<sub>3</sub>, which means that the accumulation can be rather significant. Intuitively, the accumulation should have been higher in A3 than in S2, since the solubility is lower and the diffusivity is higher at higher temperatures. However, other factors may also impact the results, such as hydration history, distribution of sulfur in the original material and the rather limited data set. The colder blocks in both S2 and A3 are, on average, depleted in sulfur, which means that sulfur is either lost to the groundwater or transported in the axial direction in the test.

### ***Iron redox chemistry (Mössbauer spectroscopy)***

The reference clays were between 28–30 % in Fe(II) and the samples from the LOT S2 and A3 experiments were all around 50 % Fe(II). Hence, a minor but still significant part of the Fe(III) in the bentonite was reduced to Fe(II).

### ***Scraping samples***

The scraping samples had elevated levels of Cu, however no specific copper phases were identified.

## 6.2.1 Comparison with other similar field experiments

### **LOT A2 Experiment (Karnland et al. 2009)**

In the LOT A2 experiment, accumulation of  $\text{CaSO}_4$ , was observed towards the heater. No formation of illite or other typical montmorillonite alteration minerals occurred. There was a decrease in strain at failure for bentonite exposed to high temperatures. Overall, the mineralogical alterations resulting from the water saturation process and high temperature exposure were relatively minor. These alterations did not significantly change the properties of the bentonite to have an impact on its buffer function.

There was a small increase in the cation exchange capacity (CEC) of the bentonite in areas exposed to high temperatures. The LOT A2 reference bentonite had a CEC of 81 cmol(+)/kg (SD=0.64; n=5). The samples from the colder part of parcel A2 (block 33) had a CEC of 80 cmol(+)/kg (SD=0.34), while the warmer samples had CEC in the range of 82–83 cmol(+)/kg (relative increase =  $82.5/81 = 2\%$ ).

Clay fractions (Table 6-1) from the warmer part were 89 cmol(+)/kg (block 9) and 90 (block 11), while in the colder part 86 (block 33) and 87 (block 34). The relative increase in CEC of the clay fractions in the warmer part of the experiment was in average  $86.5/81 = 6.8\%$ .

Higher contents of non-exchangeable Mg in the and higher Mg-concentrations in the pore water was observed.

### **ABM2 and ABM5 Experiments (Svensson et al. 2023)**

In the ABM2 and ABM5 experiments, no significant alteration of smectite in the bentonite was observed. Minor changes were detected in the CEC, with bulk clays showing a slight decrease and clay fractions exhibiting a slight increase in CEC (Table 6-1). Crucially, the properties of swelling pressure and hydraulic conductivity remained largely unaffected by the extremely high temperatures in the ABM5 experiment. A very minor formation of trioctahedral smectite, likely ferrosaponite, was noted in the “Febex bentonite” in ABM2 (Svensson, 2015). However, this formation was minimal and is not expected to impact the performance of the bentonite. Furthermore, this reaction has not been observed in experiments using copper heaters, which are the actual canister material in the SKB KBS-3 design.

## 6.2.2 Increase of CEC in hot sections

In Table 6-1, it is evident that the clay fractions from the warmer parts of the hottest experiments exhibit increased CEC compared to the reference clays. The chemical data suggest that this correlates with a change in the (Mg+Al)/Si ratio, indicating a relative decrease in silicon. Due to the heterogeneous composition of the clay fraction, it is challenging to determine whether this change is due to alterations in montmorillonite or accessory minerals. Both the dissolution of quartz and the dissolution of Si from the montmorillonite tetrahedral sheet can increase CEC. Karnland and Birgersson (2006) suggested that an increasing layer charge due to the release of silicon from the tetrahedral sheet might signal the onset of montmorillonite alteration.

Based on SEM-EDX studies on ABM5 samples, Sudheer Kumar et al. (2021) reported that bentonites near the heater showed smectite alterations, including tetrahedral substitution of  $\text{Si}^{4+}$  by  $\text{Al}^{3+}$  and some octahedral metal substitutions, leading to decreased CEC values. Since montmorillonite is closely associated with quartz and cristobalite even on the microscale, such interpretations should be approached with caution, it is however an interesting observation.

Kanik et al. 2025 measured the layer charge on several ABM5 samples using a vibrational spectroscopic method. In ABM2, a slight increase of the layer charge was observed, typically within measurement error, that seemed to correlate with CEC increase. However, the increase was too small to be definitively quantified and might result from  $\text{Fe}^{3+}$  reduction in the smectite structure. In ABM5, both CEC and layer charge data showed a general decreasing trend towards the heater. The decrease in smectitic layer charge was concluded to cause the CEC decrease in both ABM packages, attributed to partial cation fixation within the smectite interlayers, e.g.  $\text{Mg}^{2+}$ . This decrease in CEC is similar to what was found by Svensson et al. (2023) that observed that ABM5 bulk samples had lower CEC, while the clay fraction exhibited higher CEC, indicating that probably several different processes are involved.

The CEC increase observed by Karnland et al. (2009) in LOT A2 was of similar magnitude to that in LOT A3 in the current study. Block 11 in LOT A2 showed a 7.4 % higher CEC compared to the reference, while the same block in LOT A3 had a 6.5 % higher CEC. The longer duration of the A3 experiment did not seem to impact this. The CEC increase in ABM5 block 20 MX80 was also similar at 6 %.

One explanation could be that the solubility of quartz increases with temperature, and the dissolution rate increases with decreasing particle size. Thus, the quartz particles most susceptible to dissolution are the very fine ones in the clay fraction. This was observed in LOT A3 through XRD of the clay fractions, which showed decreased intensity of the quartz main reflection. Dissolution of quartz and/or cristobalite has also been sporadically observed in other field experiments at elevated temperatures, such as TBT and ABM1 (Svensson and Hansen, 2013; Åkesson et al. 2012) and ABM5 (Kaufhold et al. 2021).

This hypothesis is further supported by the small increase in montmorillonite content of the A3 samples (2.6 % higher than the reference in montmorillonite), which aligns with the increase in CEC in some bulk samples of the mid LOT A3 (3.3 % higher). All these changes are very small and close to the detection limit.

**Table 6-1 Summary of CEC of clay fractions from LOT A2 (Karnland et al. 2009), S2, A3 and ABM5 (Svensson et al. 2023).**

Sample	CEC (cmol(+)/kg)	Relative increase	Type of sample
LOT A3 CF Reference block 15 c65fe0	87.3	1.000	Reference
LOT S2 CF block 33 0–10 mm d5c793	89.5	1.025	Cold
LOT A3 CF block 9 0–10 mm d5c791	94.5	1.082	Hot
LOT A3 CF block 11 0–10 mm d5c797	93	1.065	Hot
LOT A2 Reference	87.5	1.000	Reference
A2 block 9 BW1b CF	91	1.040	Hot
A2 block 11 BW1b CF	94	1.074	Hot
A2 block 33 BW1b CF	86	0.983	Cold
MX80 ABM Reference CF	92.7	1.000	Reference
ABM5 MX80 # 20 0–10 mm CF	98.3	1.060	Hot

### 6.2.3 Accumulation of Mg towards the heater

In the LOT A2 experiment, an increase was observed in both exchangeable and non-exchangeable Mg (Karnland et al. 2009). Several examples of Mg accumulation towards the heaters were identified in the ABM1, ABM2, and ABM5 experiments (Svensson et al. 2011; Svensson and Hansen, 2013; Kaufhold et al. 2013; Kaufhold et al. 2017; Kaufhold et al. 2021).

In the LOT A3 experiment, an increase in MgO was observed in the hot sections of blocks 9, 11, 15, and 16, but not in the colder samples, indicating that the Mg increase is temperature-related. Reference samples contained 2.38 wt% MgO, while LOT S2 samples ranged from 2.14 to 2.38 wt% MgO near the heater.

Specific observations from LOT A3 include:

- Hot section: block 9 (3.38 wt%), block 11 (3.24 wt%), block 15 (3.19 wt%), block 16 (2.96 wt%) near the heater.
- Cold section: block 35 (2.31 wt%), block 33 (2.24 wt%) near the heater.

For the clay fraction, the reference was 2.5 wt% MgO. Observations from LOT A3 include:

- Block 33 (2.57 wt%), block 9 (2.93 wt%), and block 11 (2.92 wt%) MgO.

SP-HC samples had a reference of 1.98 wt% MgO, with block 11 showing 2.09 wt% at 10–20 mm and 2.04 wt% at 20–50 mm.

The data indicate that Mg accumulation occurs predominantly in the hot sections, with the colder sections showing some depletion. The SP-HC samples, which were Ca-exchanged and washed with water, exhibited the smallest increase in MgO. This suggests that a significant portion of Mg is dissolvable/exchangeable, consistent with the conclusions by Karnland et al. (2009).

The phase of non-exchangeable Mg remains unclear; however, the quantity is very small, shows minimal increase over time, and does not appear to impact the bentonite buffer properties significantly. It is possible that Mg is partly fixated in montmorillonite, causing a temporary decrease in CEC, which is restored after prolonged exposure to a strong salt solution, such as Na or Ca solution. This is supported by the observation that SP-HC samples that were exposed to prolonged periods of 1 M CaCl<sub>2</sub> solutions in this study showed the lowest increase in Mg relative to Al (Table 6-2).

In the ABM2 experiment using Febex bentonite, an Mg-rich ferrosaponite was identified at the heater contact (Svensson, 2015), demonstrating that Mg accumulation in field experiments can, in some cases, lead to the formation of new distinct phases.

**Table 6-2 Summary of Mg content of different kind of samples from LOT A3 and S2.**

Sample	MgO (wt%)	Relative increase	Type of sample
LOT A3 Reference	2.38	1.00	Reference
LOT S2	2.14–2.38	0.9–1.0	Cold
LOT A3 block 9	3.38	1.42	Hot
LOT A3 block 11	3.24	1.36	Hot
LOT A3 block 15	3.19	1.34	Hot
LOT A3 block 16	2.96	1.24	Hot
LOT A3 block 35	2.31	0.97	Cold
LOT A3 block 33	2.24	0.94	Cold
Clay fraction reference	2.5	1.00	Reference
Clay fraction LOT A3 block 33	2.57	1.03	Cold
Clay fraction LOT A3 block 9	2.93	1.17	Hot
Clay fraction LOT A3 block 11	2.92	1.17	Hot
SP-HC sample reference	1.98	1.00	Reference
SP-HC LOT A3 block 11, 10–20 mm	2.09	1.06	Hot
SP-HC LOT A3 block 11, 20–50 mm	2.04	1.03	Hot

#### 6.2.4 Reduction of trivalent to divalent iron

One potential mechanism could be oxidation of pyrite that potentially reduce the Fe(III) in the montmorillonite to Fe(II). Pyrite FeS<sub>2</sub> is composed of a ferrous (Fe<sup>2+</sup>) cation and an S<sub>2</sub><sup>2-</sup> anion with an ideal Fe:S ratio of 1:2. In oxic conditions pyrite may oxidize and form products such as hematite (Fe<sub>2</sub>O<sub>3</sub>), magnetite (Fe<sub>3</sub>O<sub>4</sub>), ferric or ferrous sulfate (Fe<sub>2</sub>(SO<sub>4</sub>)<sub>3</sub>, FeSO<sub>4</sub>) and sulfur dioxide (SO<sub>2</sub>).

When sulfide S(-I)<sub>2</sub><sup>2-</sup> oxidise to sulfate S(VI)O<sub>4</sub><sup>2-</sup>, sulfur goes from -I to + VI, hence releasing 7 electrons per sulfur atom oxidised. Hence oxidising 1 molar of pyrite (FeS<sub>2</sub>) can reduce 14 molar of Fe(III) to Fe(II).

Molar mass of pyrite is 120 gram per mol, and montmorillonite is approximately 360 g/moles.

In 1 kg bentonite with 80 wt% montmorillonite, there is 800 grams of montmorillonite or approximately 2.2 moles.

In MX80 there is about 0.5–0.9 wt% pyrite and about 0.37 atoms of Fe per unit cell of montmorillonite (Karnland et al. 2006). Let's assume 0.5 wt% pyrite, that is 5 grams of pyrite, or 0.042 mol. This pyrite may reduce 0.042 × 14 = 0.588 mol of iron, or 0.588/0.37 = 1.59 mol of montmorillonite. Hence, there is by far more than enough of pyrite in MX80 to explain the minor reduction of ferric to ferrous iron observed.

Similar reduction of ferric to ferrous iron was observed in the outer section of the Prototype experiment (Olsson et al. 2013).



## 7 Summary and conclusions

Minor changes in the chemistry and mineralogy of the bentonite were observed, particularly in the warmer sections of the LOT A3 experiment. It's important to note that most of these changes were minimal, often close to the detection limit. All observations were consistent with expectations and closely aligned with previous field experiments conducted at the Äspö laboratory using bentonite clay. No signs of montmorillonite alteration were observed.

A slight accumulation of magnesium (Mg) was detected near the heater, possibly due to the adsorption of ionic Mg onto the montmorillonite. Additionally, a very minor decrease in silicon (Si) content was noted closer to the heater, possibly resulting from the dissolution of silica phases, such as quartz, cristobalite and/or amorphous silica, which reprecipitate nearer to the cooler rock. This minor change in silica content was interpreted as a possible cause of the minor increase in montmorillonite content observed close to the heater (based on quantitative XRD and CEC measurements). The magnitude of the changes are in the vicinity of the detection limits of the methods.

A slight increase in the Fe(II)/Fe(III) ratio was also observed, most likely due to the chemical reduction of iron within the montmorillonite's octahedral sheet through reaction with pyrite.

These changes were too minor to impact the swelling pressure performance, which remained unaffected throughout the experiments. A minor increase in hydraulic conductivity was observed, along with indications of reduced maximum deviator stress in unconfined compression tests.

The minor changes observed in the unconfined compression tests and hydraulic conductivity may be linked to the dissolution and reprecipitation of silica phases, potentially altering particle sizes and causing slight cementation. However, the extent of these changes is too small to significantly affect the overall performance of the repository.

Sulfate accumulation was observed towards the heater in LOT A3/S2 and the amount was rather substantial. The results are snap shots in time and even higher accumulations cannot be excluded. An increase in sulfates close to canister will result in a decrease in montmorillonite content. The process is expected to be reversible and that the sulfates are expected to dissolve when the temperature decreases. It is however difficult to predict if this sulfate accumulation have any impact on the properties of the bentonite close to the canister. A lower sulfate content in the original bentonite material could therefore be an advantage.



## References

SKB's (Svensk Kärnbränslehantering AB) publications can be found at [www.skb.com/publications](http://www.skb.com/publications).

- Ammann L, Bergaya F, Lagaly G, 2005.** Determination of the cation exchange capacity of clays with copper complexes revisited. *Clay Minerals* 40, 441–453.
- Arlinger J, Bengtsson A, Edlund J, Eriksson L, Johansson J, Lydmark S, Rabe L, Pedersen K, 2013.** Prototype repository – Microbes in the retrieved outer section. SKB P-13-16, Svensk Kärnbränslehantering AB.
- Butler B M, Hillier S, 2021.** Automated full-pattern summation of x-ray powder diffraction data for high-throughput quantification of clay-bearing mixtures. *Clays Clay Miner.* 69, p. 38–51.
- Dueck A, Johannesson L-E, Kristensson O, Olsson S, 2011.** Report on hydro-mechanical and chemical-mineralogical analyses of the bentonite buffer in Canister Retrieval Test. SKB TR-11-07, Svensk Kärnbränslehantering AB.
- Hillier S, 1999.** Use of an air brush to spray dry samples for X-ray powder diffraction: *Clay Minerals*, v. 34, no. 1, p. 127–135.
- Hillier S, 2003.** Quantitative analysis of clay and other minerals in sandstones by X-ray powder diffraction (XRPD), in RH Worden and S Morad eds., *Clay Mineral Cements in Sandstones: International Association of Sedimentologists, Special Publication 34*, p. 213–251.
- Huang W L, Longo J M, Pevear D R, 1993.** An Experimentally Derived Kinetic Model for Smectite-to-Illite Conversion and Its Use as a Geothermometer. *Clays Clay Miner.* 41, 162–177.
- Kanik N J, Derkowski A, Kaufhold S, Dohrmann R, 2025.** Probing subtle alterations of smectite layer charge by the spectroscopic O-D method in bentonite from the Alternative Buffer Materials tests in Äspö, Sweden. *Applied Clay Science* 263, 107641.
- Karnland O, Birgersson M, 2006.** Montmorillonite stability. With special respect to KBS-3 conditions. SKB TR-06-11, Svensk Kärnbränslehantering AB.
- Karnland O, Sandén T, Johannesson L-E, Eriksen T E, Jansson M, Wold S, Pedersen K, Motamedi M, Rosborg B, 2000.** Long term test of buffer material. Final report on the pilot parcels. SKB TR 00-22, Svensk Kärnbränslehantering AB.
- Karnland O, Olsson S, Nilsson U, 2006.** Mineralogy and sealing properties of various bentonites and smectite-rich clay materials. SKB TR-06-30, Svensk Kärnbränslehantering AB.
- Karnland O, Olsson S, Dueck A, Birgersson M, Nilsson U, Hernan-Håkansson T, Pedersen K, Nilsson S, Eriksen T E, Rosborg B, 2009.** Long term test of buffer material at the Äspö Hard Rock Laboratory, LOT project. Final report on the A2 test parcel, SKB TR 09-29, Svensk Kärnbränslehantering AB.
- Karnland O, Olsson S, Sandén T, Fälth B, Jansson M, Eriksen T E, Svärdström K, Rosborg B, Muurinen A, 2011.** Long term test of buffer material at the Äspö HRL, LOT project. Final report on the A0 test parcel. SKB TR 09-31, Svensk Kärnbränslehantering AB.
- Kaufhold S, Dohrmann R, Sandén T, Sellin P, Svensson D, 2013.** Mineralogical investigations of the alternative buffer material test – I. Alteration of bentonites. *Clay Minerals* 48, 199–213.
- Kaufhold S, Dohrmann R, Götze N, Svensson D, 2017.** Characterization of the second parcel of the alternative buffer material (ABM) Experiment—I mineralogical reactions. *Clays Clay Miner* 65, 27–41.
- Kaufhold S, Dohrmann R, Ufer K, Svensson D, Sellin P, 2021.** Mineralogical Analysis of Bentonite from the ABM5 Heater Experiment at Äspö Hard Rock Laboratory, Sweden. *Minerals* 11, 669.
- Meier L P, Kahr G, 1999.** Determination of the cation exchange capacity (CEC) of clay minerals using the complexes of copper(II) ion with triethylenetetramine and tetraethylenepentamine. *Clays and Clay Minerals* 47, 386–388.

**Omotoso O, McCarty D K, Hillier S, Kleeberg R, 2006.** Some successful approaches to quantitative mineral analysis as revealed by the 3rd Reynolds Cup contest: *Clays and Clay Minerals*, v. 54, no. 6, p. 748–760.

**Olsson S, Jensen V, Johansson L E, Hansen E, Karnland O, Kumpulainen S, Kirivanta L, Svensson D, Hansen S, Lindén J, 2013.** Prototype Repository. Hydromechanical, chemical and mineralogical characterization of the buffer and backfill material from the outer section of the Prototype Repository. SKB TR-13-21, Svensk Kärnbränslehantering AB.

**Sandén T, Nilsson U, 2020.** Installation, monitoring, dismantling and initial analyses of material from LOT test parcel S2 and A3. Results from field test. SKB TR-20-11, Svensk Kärnbränslehantering AB.

**Sudheer Kumar R, Podlech C, Grathoff G, Warr L N, Svensson D, 2021.** Thermally Induced Bentonite Alterations in the SKB ABM5 Hot Bentonite Experiment. *Minerals* 11:1017.

**Svensson D, 2015.** The bentonite barrier: swelling properties, redox chemistry and mineral evolution. PhD thesis. Lund University, Sweden.

**Svensson D, Hansen S, 2013.** Redox chemistry in two iron-bentonite field experiments at Äspö Hard Rock Laboratory, Sweden: An XRD and Fe K-edge XANES study. *Clays and Clay Minerals* 61, 566–579.

**Svensson D, Dueck A, Nilsson U, Olsson S, Sandén T, Lydmark S, Jägerwall S, Pedersen K, Hansen S, 2011.** Alternative buffer material. Status of ongoing laboratory investigation of reference material and test package 1. SKB TR-11-06, Svensk Kärnbränslehantering AB.

**Svensson D, Eriksson P, Johansson L-E, Lundgren C, Bladström T, 2019.** Development and testing of methods suitable for quality control of bentonite as KBS-3 buffer and backfill. SKB TR-19-25, Svensk Kärnbränslehantering AB.

**Åkesson M, Olsson S, Dueck A, Nilsson S, Karnland O, Kiviranta L, Kumpulainen S, Lindén J, 2012.** Temperature buffer test, Hydro-mechanical and chemical/mineralogical characterizations. SKB Report P-12-06, Svensk Kärnbränslehantering AB.

**Svensson D, Bladström T, Sandén T, Dueck A, Nilsson U, Jensen V, 2023.** Alternative Buffer Material (ABM) experiment. Investigations of test packages ABM2 and ABM5. SKB technical report TR-23-25.

## Photos from the sampling for the hydro-mechanical analyses

Photos from the sampling to HM-analyses of material from LOT parcels S2 and A3.



*Figure A1-1. Bags with samples from LOT S2 and A3 arrived at Clay Technology.*



*Figure A1-2. Sampling from LOT S2 block 9 (2019-11-25).*



*Figure A1-3. Sampling from LOT S2 block 9 (2020-11-09).*

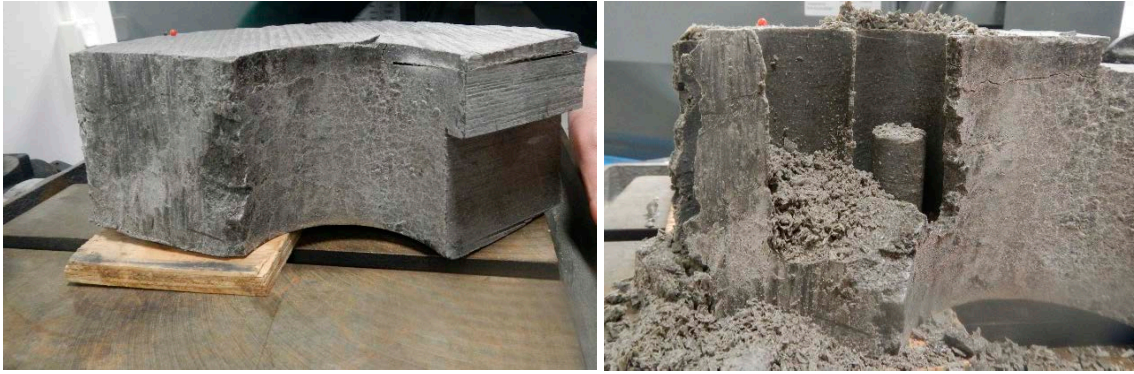


*Figure A1-4. Sampling from LOT S2 block 11 (2019-11-25).*



*Figure A1-5. Sampling from LOT S2 block 11 (2020-11-05).*



*Figure A1-6. Sampling from A3 block 9 (2020-02-12)*



*Figure A1-7. Sampling from A3 block 09 (2020-11-05).*



*Figure A1-8. Sampling from LOT A3 block 11 (2020-02-12, left) (2020-11-05, right).*



### Swelling pressure tests – time evolution

In Figure A2-1 to Figure A2-4 the time evolution of the swelling pressure is given for the series PC1–PC4. Table A2-1 and Table A2-2 show the results from Section 3.5.4.

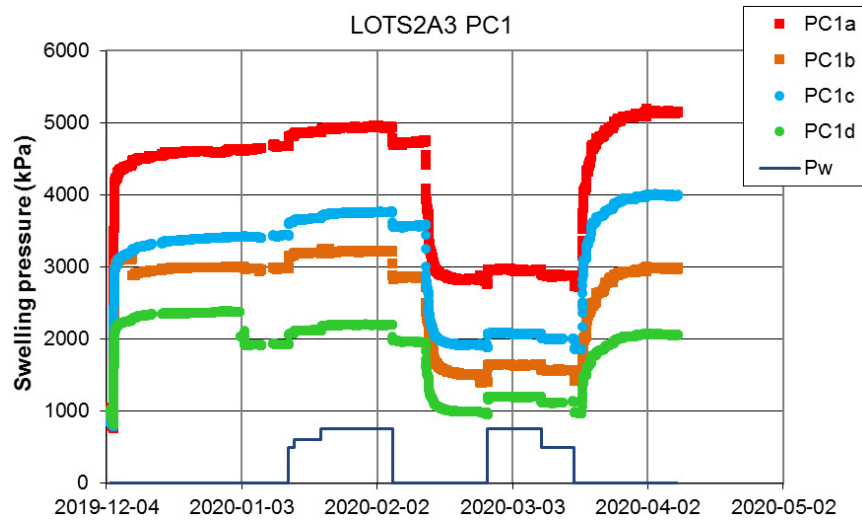


**Figure A2-1.** Time evolution of the swelling pressure of Test PC1 with specimens from test parcel S2. The applied water pressure used for the determination of hydraulic conductivity is also shown.

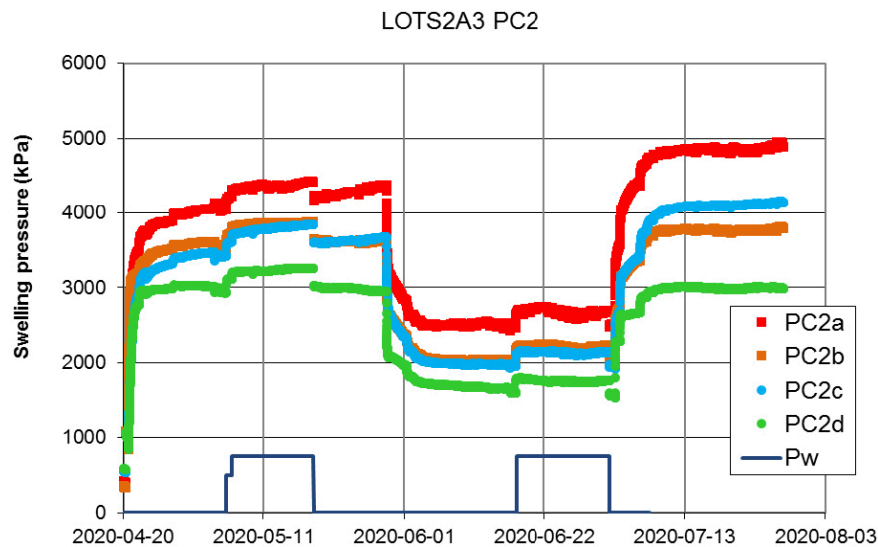


**Figure A2-2.** Time evolution of the swelling pressure of Test PC2 with specimens from test parcel A3. The applied water pressure used for the determination of hydraulic conductivity is also shown.

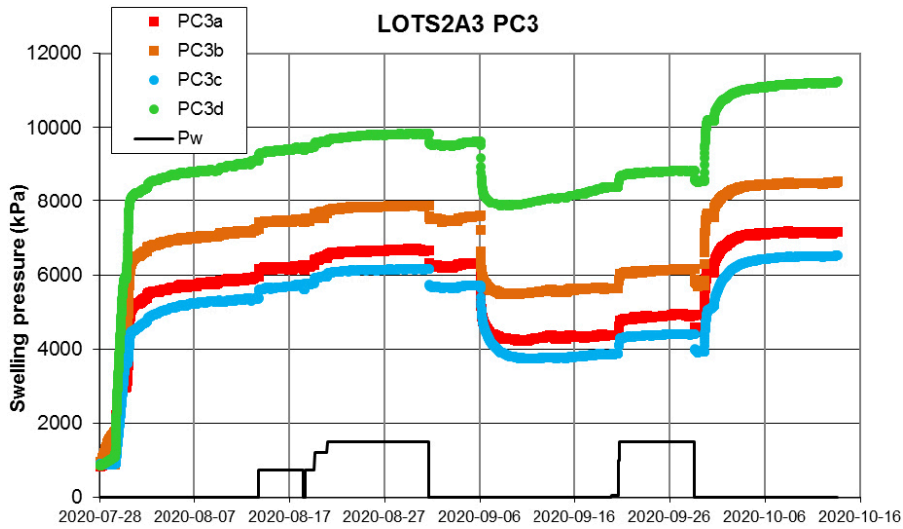


**Figure A2-3.** Time evolution of the swelling pressure of Test PC3 with crushed/compacted specimens from test parcels S2 and A3. The applied water pressure used for the determination of hydraulic conductivity is also shown.

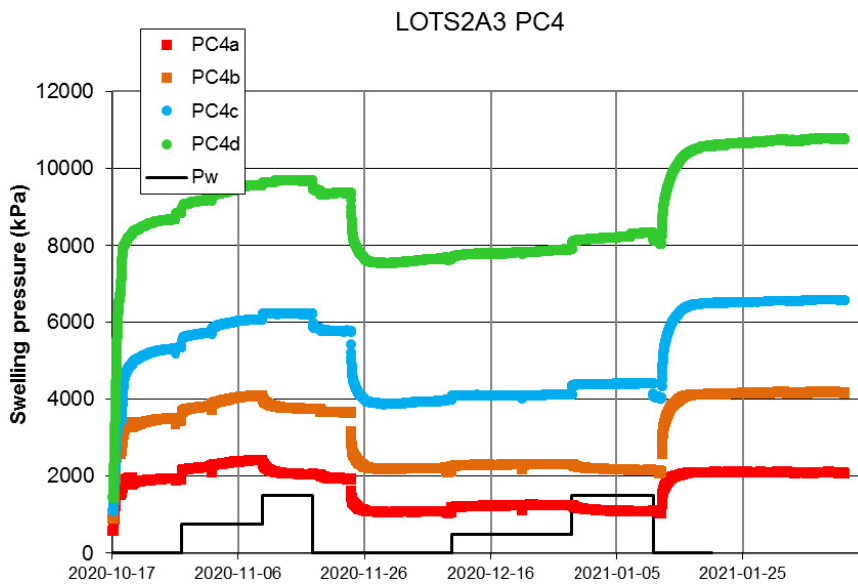


**Figure A2-4.** Time evolution of the swelling pressure of Test PC4 with reference specimens. The applied water pressure used for the determination of hydraulic conductivity is also shown.

**Table A2-1. Results from measurements of swelling pressure and hydraulic conductivity at equilibrium with LOT-water from Table 3-3 and Table 3-5.**

Test ID	Material	Test parcel	Block	Radial distance mm	Preparation	Test solution <sup>1</sup>	Dry density kg/m <sup>3</sup>	Degree of saturation %	Swelling pressure kPa	Hydraulic conductivity m/s
PC1a	LS2-09-40	LOT S2	9	40	drilled	LOT water	1474	101	4706	1.2E-13
PC1b	LS2-09-80	LOT S2	9	80	drilled	LOT water	1395	101	2856	1.6E-13
PC1c	LS2-11-40	LOT S2	11	40	drilled	LOT water	1437	100	3557	1.3E-13
PC1d	LS2-11-80	LOT S2	11	80	drilled	LOT water	1360	100	1976	2.3E-13
PC2a	LA3-09-40	LOT A3	9	40	drilled	LOT water	1482	99	4203	1.0E-13
PC2b	LA3-09-80	LOT A3	9	80	drilled	LOT water	1417	98	3628	1.1E-13
PC2c	LA3-11-40	LOT A3	11	40	drilled	LOT water	1450	99	3595	1.5E-13
PC2d	LA3-11-80	LOT A3	11	80	drilled	LOT water	1396	98	3012	1.5E-13
PC3a	LS2-09-40cr	LOT S2	9	40	crushed + comp	LOT water	1530	100	6238	7.2E-14
PC3b	LS2-11-40cr	LOT S2	11	40	crushed + comp	LOT water	1537	99	7474	5.5E-14
PC3c	LA3-09-40cr	LOT A3	9	40	crushed + comp	LOT water	1514	99	5660	1.1E-13
PC3d	LA3-11-40cr	LOT A3	11	40	crushed + comp	LOT water	1576	98	9522	7.0E-14
PC4a	LOT Ref				compacted	LOT water	1346	101	2029	3.0E-13
PC4b	LOT Ref				compacted	LOT water	1428	101	3717	1.9E-13
PC4c	LOT Ref				compacted	LOT water	1508	100	5813	8.3E-14
PC4d	LOT Ref				compacted	LOT water	1579	99	9391	6.4E-14

<sup>1</sup> LOT water is defined in Section 3.3.

**Table A2-2. Results from measurements of swelling pressure and hydraulic conductivity at equilibrium with LOT-water from Table 3-4 and Table 3-6.**

Test ID	Dry density kg/m <sup>3</sup>	Ps1 (LOTs) kPa	Ps1 (LOTc) kPa	Ps2 (1M CaCl <sub>2</sub> ) kPa	Ps3 (DI) kPa	Gradient 1 m/m	kw1 (LOT) m/s	Gradient 2 m/m	kw2 (1M CaCl <sub>2</sub> ) m/s
PC1a	1474	4706	4741	2740	5135	6923	1.2E-13	6923	1.1E-13
PC1b	1395	2856	2862	1422	2970	6923	1.6E-13	6923	1.5E-13
PC1c	1437	3557	3576	1857	3986	6923	1.3E-13	6923	1.4E-13
PC1d	1360	1976	1953	971	2053	6923	2.3E-13	4606	2.3E-13
PC2a	1482	4203	4363	2507	4918	6932	1.0E-13	6923	1.2E-13
PC2b	1417	3628	3625	2019	3803	6932	1.1E-13	6923	1.1E-13
PC2c	1450	3595	3675	1951	4150	6932	1.5E-13	6923	1.5E-13
PC2d	1396	3012	2949	1564	2992	6932	1.5E-13	6923	1.5E-13
PC3a	1530	2029	1925	4508	7153	11093	7.2E-14	13873	6.3E-14
PC3b	1537	3717	3654	5783	8516	11093	5.5E-14	13873	4.9E-14
PC3c	1514	5813	5773	3964	6518	11093	1.1E-13	13873	9.4E-14
PC3d	1576	9391	9374	8559	11220	11093	7.0E-14	13873	4.9E-14
PC4a	1346	2029	1925	1050	2098	6932	3.0E-13	4606	3.6E-13
PC4b	1428	3717	3654	2104	4177	6932	1.9E-13	4606	1.7E-13
PC4c	1508	5813	5773	4027	6589	13882	8.3E-14	13873	8.9E-14
PC4d	1579	9391	9374	8058	10785	13882	6.4E-14	13873	5.3E-14



### Unconfined compression tests – deviator stress as a function of strain

Figure A3-1 and Figure A3-2 show deviator stress as a function of strain of corresponding specimens from parcels S2 and A3 and in Figure A3-3 the corresponding references are shown. Evolution of deviator stress with strain for all test series are shown in Figure A3-4 to Figure A3-10. Tabulated test results from all tests from Section 3.6.4 are shown in Table A3-1.

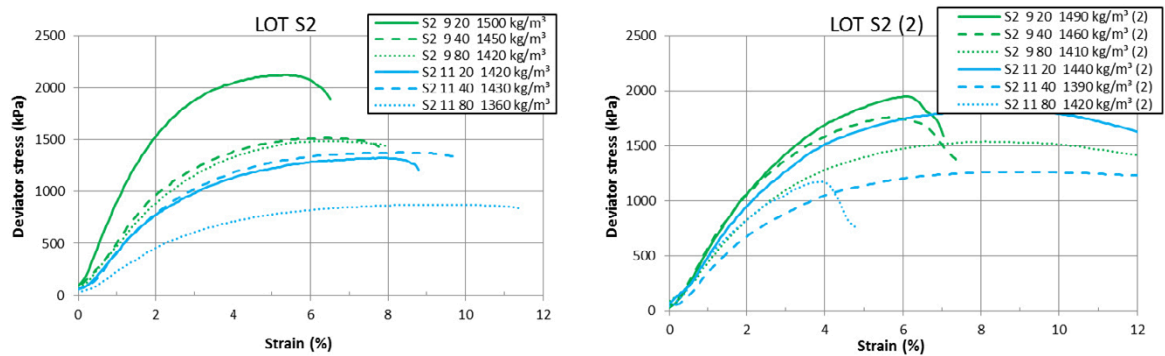


**Figure A3-1.** Evolution of deviator stress as a function of strain. Specimens drilled from parcel S2 and saturated with LOT water and ion-exchanged with CaCl<sub>2</sub> (2). The label contains information according to Section 3.6.4.

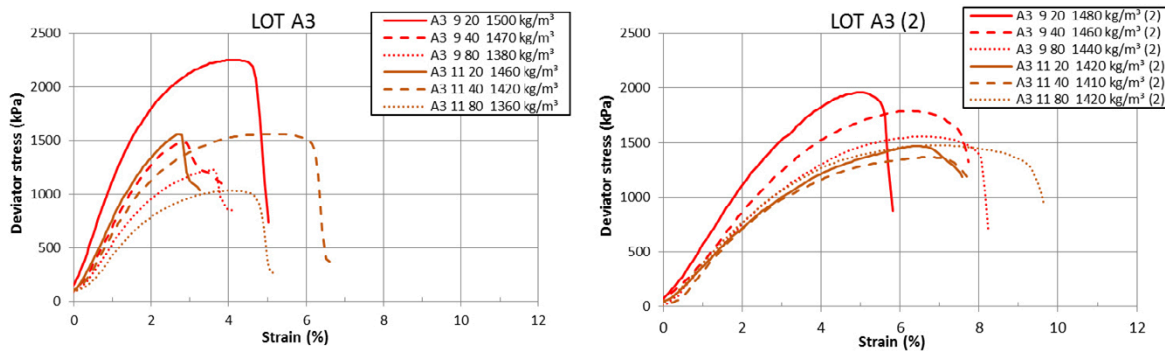


**Figure A3-2.** Evolution of deviator stress as a function of strain. Specimens drilled from parcel A3 and saturated with LOT water and ion-exchanged with CaCl<sub>2</sub> (2). The label contains information according to Section 3.6.4.

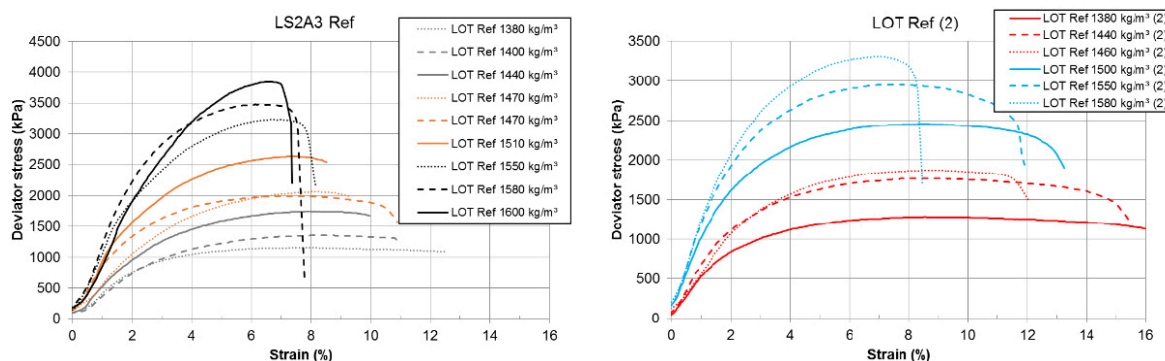


**Figure A3-3.** Evolution of deviator stress as a function of strain of reference specimens saturated with LOT water and ion-exchanged with CaCl<sub>2</sub> (2). The label contains information according to Section 3.6.4.

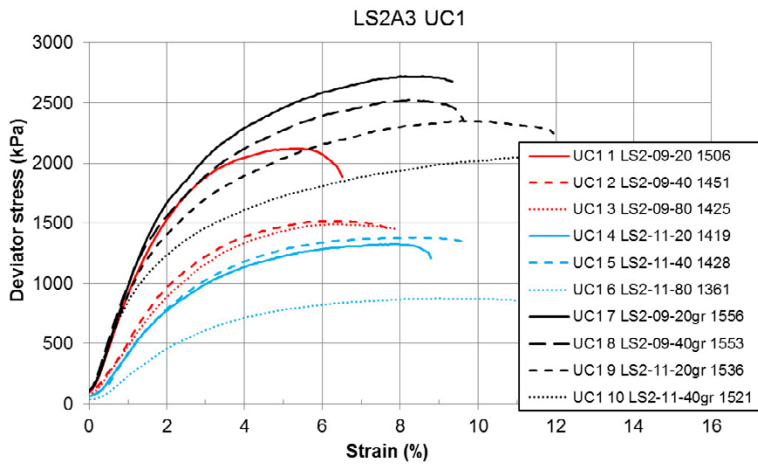


**Figure A3-4.** Evolution of deviator stress as a function of strain from test series UC1 with specimens from test parcel S2 saturated with LOT-water. The labels give information about the dry density of the specimens.

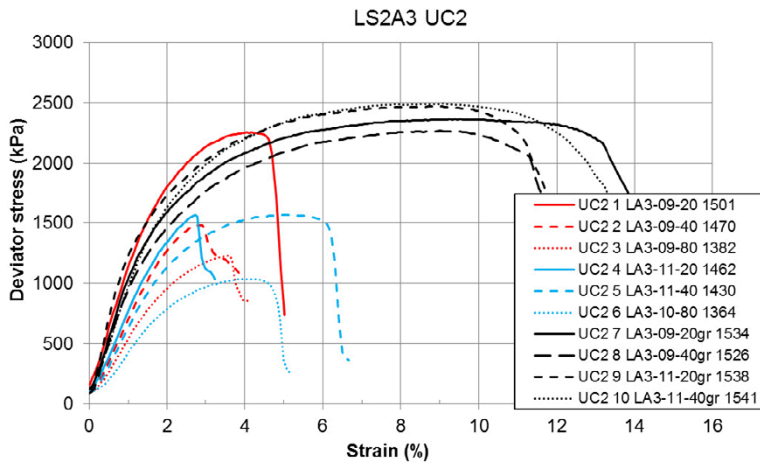


**Figure A3-5.** Evolution of deviator stress as a function of strain from test series UC2 with specimens from test parcel A3 saturated with LOT-water. The labels give information about the dry density of the specimens.

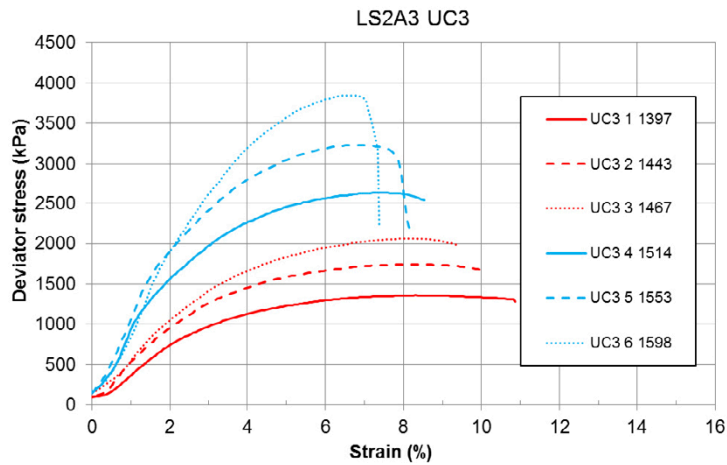


**Figure A3-6.** Evolution of deviator stress as a function of strain from test series UC3 with reference specimens saturated with LOT-water. The labels give information about the dry density of the specimens.

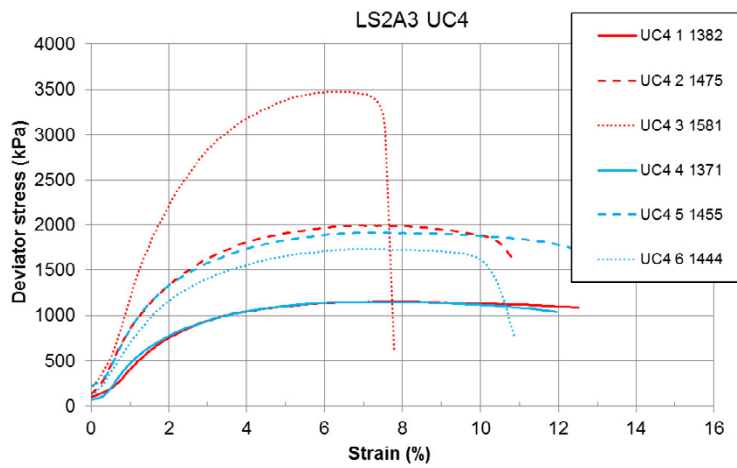


**Figure A3-7.** Evolution of deviator stress as a function of strain from test series UC4 with reference specimens saturated with either LOT-water or DI-water. The labels give information about the dry density of the specimens.

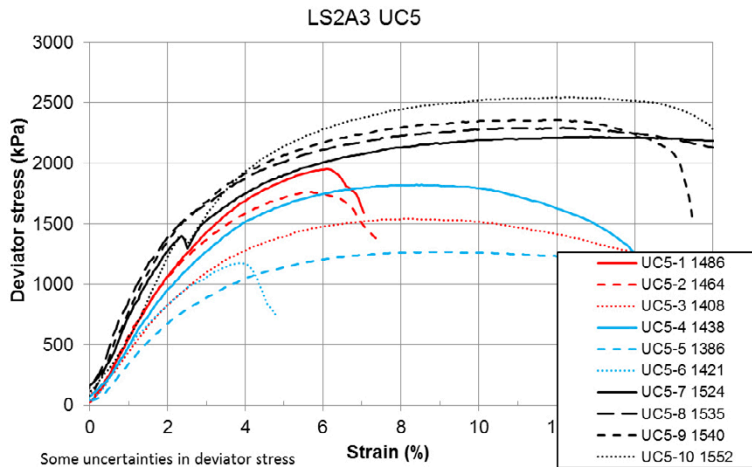


**Figure A3-8.** Evolution of deviator stress as a function of strain from test series UC5 with specimens from test parcel S2 ion-exchanged with  $\text{CaCl}_2$ . The labels give information about the dry density of the specimens.

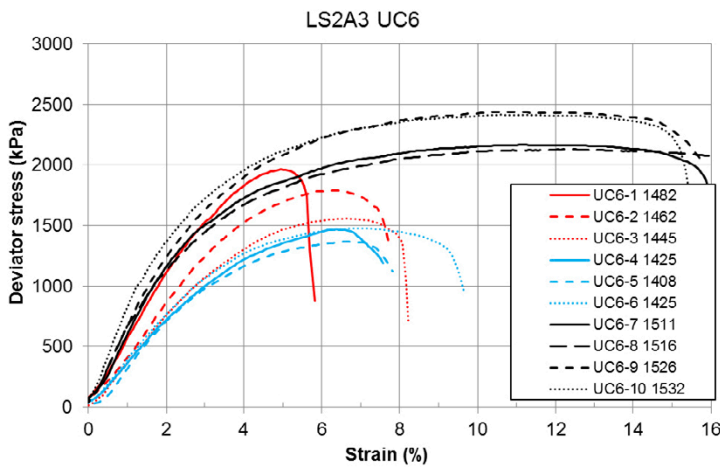


**Figure A3-9.** Evolution of deviator stress as a function of strain from test series UC6 with specimens from test parcel A3 ion-exchanged with  $\text{CaCl}_2$ . The labels give information about the dry density of the specimens.

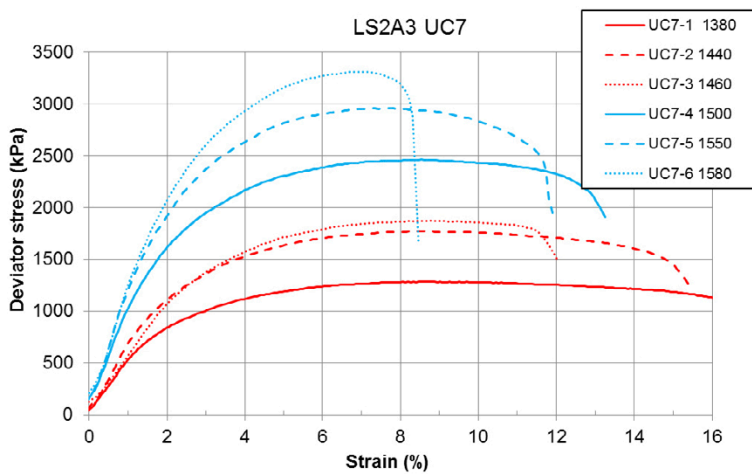


**Figure A3-10.** Evolution of deviator stress as a function of strain from test series UC7 with reference specimens ion-exchanged with  $\text{CaCl}_2$ . The labels give information about the dry density of the specimens.

**Table A3-1. Maximum deviator stress and corresponding strain resulting from unconfined compression tests on all specimens from test parcels S2 and A3 from Table 3-7 and Table 3-8.**

Test ID	Material	Test parcel	Block	Radial distance mm	Preparation	Saturation fluid <sup>2</sup>	Dry density kg/m <sup>3</sup>	Water content %	Deg of saturation %	Max deviator stress kPa	Corresponding strain, %
UC1 1	LS2-09-20	LOT S2	9	20	drilled	LOT-water	1505	29.8	99	2123	5.4
UC1 2	LS2-09-40	LOT S2	9	40	drilled	LOT-water	1450	32.1	98	1515	6.4
UC1 3	LS2-09-80	LOT S2	9	80	drilled	LOT-water	1424	33.8	100	1489	6.3
UC1 4	LS2-11-20	LOT S2	11	20	drilled	LOT-water	1418	33.7	99	1323	7.6
UC1 5	LS2-11-40	LOT S2	11	40	drilled	LOT-water	1428	33.3	99	1377	8.4
UC1 6	LS2-11-80	LOT S2	11	80	drilled	LOT-water	1360	36.8	99	874	9.1
UC1 7	LS2-09-20cr	LOT S2	9	20	crushed + comp.	LOT-water	1555	27.6	99	2718	8.1
UC1 8	LS2-09-40cr	LOT S2	9	40	crushed + comp.	LOT-water	1552	27.7	99	2522	8.3
UC1 9	LS2-11-20cr	LOT S2	11	20	crushed + comp.	LOT-water	1534	28.3	98	2350	9.7
UC1 10	LS2-11-40cr	LOT S2	11	40	crushed + comp.	LOT-water	1519	29.0	98	2049	11.2
UC2 1	LA3-09-20	LOT A3	9	20	drilled	LOT-water	1500	30.1	99	2253	4.1
UC2 2	LA3-09-40	LOT A3	9	40	drilled	LOT-water	1468	30.9	97	1480	2.9
UC2 3	LA3-09-80	LOT A3	9	80	drilled	LOT-water	1382	34.9	97	1229	3.6
UC2 4	LA3-11-20	LOT A3	11	20	drilled	LOT-water	1459	32.1	100	1561	2.7
UC2 5	LA3-11-40	LOT A3	11	40	drilled	LOT-water	1425	33.5	99	1563	5.1
UC2 6	LA3-10-80	LOT A3	10	80	drilled	LOT-water	1361	36.5	98	1034	4.0
UC2 7	LA3-09-20cr	LOT A3	9	20	crushed + comp.	LOT-water	1531	28.9	100	2366	9.4
UC2 8	LA3-09-40cr	LOT A3	9	40	crushed + comp.	LOT-water	1523	28.6	98	2266	9.0
UC2 9	LA3-11-20cr	LOT A3	11	20	crushed + comp.	LOT-water	1533	27.8	96	2470	8.7
UC2 10	LA3-11-40cr	LOT A3	11	40	crushed + comp.	LOT-water	1538	28.2	98	2492	9.1
UC3 1	LOT Ref				compacted	LOT water	1395	34.6	98	1358	8.3
UC3 2	LOT Ref				compacted	LOT water	1441	32.3	98	1738	8.0
UC3 3	LOT Ref				compacted	LOT water	1464	31.1	97	2063	8.0
UC3 4	LOT Ref				compacted	LOT water	1512	28.6	96	2631	7.3
UC3 5	LOT Ref				compacted	LOT water	1550	26.6	95	3229	7.0
UC3 6	LOT Ref				compacted	LOT water	1596	24.9	95	3846	6.7
UC4 1	LOT Ref				compacted	LOT water	1380	35.2	97	1153	7.9
UC4 2	LOT Ref				compacted	LOT water	1474	30.7	97	1991	6.9
UC4 3	LOT Ref				compacted	LOT water	1578	25.9	96	3474	6.1

Test ID	Material	Test parcel	Block	Radial distance mm	Preparation	Saturation fluid <sup>2</sup>	Dry density kg/m <sup>3</sup>	Water content %	Deg of saturation %	Max deviator stress kPa	Corresponding strain, %
UC4 4	LOT Ref				compacted	DI-water	1370	36.2	99	1147	6.6
UC4 5	LOT Ref				compacted	DI water	1453	31.7	98	1913	7.1
UC4 6	LOT Ref				compacted	DI water	1443	32.4	98	1733	7.3
UC5 1	LS2-09-20	LOT S2	9	20	drilled	LOT-water, CaCl <sub>2</sub> , DI-water <sup>1</sup>	148 <sup>63</sup>	30.6	99	1949	6.1
UC5 2	LS2-09-40	LOT S2	9	40	drilled	LOT-water, CaCl <sub>2</sub> , DI-water <sup>1</sup>	146 <sup>43</sup>	31.6	99	1762	5.6
UC5 3	LS2-09-80	LOT S2	9	80	drilled	LOT-water, CaCl <sub>2</sub> , DI-water <sup>1</sup>	140 <sup>83</sup>	33.9	98	1541	8.1
UC5 4	LS2-11-20	LOT S2	11	20	drilled	LOT-water, CaCl <sub>2</sub> , DI-water <sup>1</sup>	143 <sup>83</sup>	32.6	98	1820	8.5
UC5 5	LS2-11-40	LOT S2	11	40	drilled	LOT-water, CaCl <sub>2</sub> , DI-water <sup>1</sup>	138 <sup>63</sup>	35.4	99	1265	8.7
UC5 6	LS2-11-80	LOT S2	11	60	drilled	LOT-water, CaCl <sub>2</sub> , DI-water <sup>1</sup>	142 <sup>13</sup>	33.8	99	1171	3.9
UC5 7	LS2-09-20cr	LOT S2	9	20	crushed + comp.	LOT-water, CaCl <sub>2</sub> , DI-water <sup>1</sup>	152 <sup>43</sup>	28.9	99	2219	12.9
UC5 8	LS2-09-40cr	LOT S2	9	40	crushed + comp.	LOT-water, CaCl <sub>2</sub> , DI-water <sup>1</sup>	1535 <sup>3</sup>	28.5	99	2291	12.2
UC5 9	LS2-11-20cr	LOT S2	11	20	crushed + comp.	LOT-water, CaCl <sub>2</sub> , DI-water <sup>1</sup>	1540 <sup>3</sup>	28.6	100	2355	10.8
UC5 10	LS2-11-40cr	LOT S2	11	40	crushed + comp.	LOT-water, CaCl <sub>2</sub> , DI-water <sup>1</sup>	1552 <sup>3</sup>	27.6	98	2544	12.5
UC6 1	LA3-09-20	LOT A3	9	20	drilled	LOT-water, CaCl <sub>2</sub> , DI-water <sup>1</sup>	1482	30.6	98	1963	4.9
UC6 2	LA3-09-40	LOT A3	9	40	drilled	LOT-water, CaCl <sub>2</sub> , DI-water <sup>1</sup>	1458	32.1	100	1791	6.2
UC6 3	LA3-09-80	LOT A3	9	60	drilled	LOT-water, CaCl <sub>2</sub> , DI-water <sup>1</sup>	1441	32.6	99	1560	6.6
UC6 4	LA3-11-20	LOT A3	11	20	drilled	LOT-water, CaCl <sub>2</sub> , DI-water <sup>1</sup>	1423	33.4	98	1468	6.4
UC6 5	LA3-11-40	LOT A3	11	40	drilled	LOT-water, CaCl <sub>2</sub> , DI-water <sup>1</sup>	1408	34.1	98	1365	6.7
UC6 6	LA3-11-80	LOT A3	11	60	drilled	LOT-water, CaCl <sub>2</sub> , DI-water <sup>1</sup>	1424	33.5	99	1477	6.9
UC6 7	LA3-09-20cr	LOT A3	9	20	crushed + comp.	LOT-water, CaCl <sub>2</sub> , DI-water <sup>1</sup>	1505	30.2	100	2166	11.3
UC6 8	LA3-09-40cr	LOT A3	9	40	crushed + comp.	LOT-water, CaCl <sub>2</sub> , DI-water <sup>1</sup>	1510	29.8	100	2130	12.2
UC6 9	LA3-11-20cr	LOT A3	11	20	crushed + comp.	LOT-water, CaCl <sub>2</sub> , DI-water <sup>1</sup>	1526	29.0	99	2438	10.8
UC6 10	LA3-11-40cr	LOT A3	11	40	crushed + comp.	LOT-water, CaCl <sub>2</sub> , DI-water <sup>1</sup>	1529	28.6	98	2416	11.2
UC7 1	LOT Ref				compacted	LOT-water, CaCl <sub>2</sub> , DI-water <sup>1</sup>	1374	35.6	98	1283	8.5
UC7 2	LOT Ref				compacted	LOT-water, CaCl <sub>2</sub> , DI-water <sup>1</sup>	1433	33.0	99	1768	8.5
UC7 3	LOT Ref				compacted	LOT-water, CaCl <sub>2</sub> , DI-water <sup>1</sup>	1458	31.9	99	1873	8.8
UC7 4	LOT Ref				compacted	LOT-water, CaCl <sub>2</sub> , DI-water <sup>1</sup>	1499	29.8	98	2459	8.5
UC7 5	LOT Ref				compacted	LOT-water, CaCl <sub>2</sub> , DI-water <sup>1</sup>	1540	28.2	99	2955	7.6
UC7 6	LOT Ref				compacted	LOT-water, CaCl <sub>2</sub> , DI-water <sup>1</sup>	1572	26.6	98	3309	6.9

<sup>1</sup> Three solutions were used subsequently; LOT-water, 1M CaCl<sub>2</sub> and DI water (Section 3.6.3).

<sup>2</sup> LOT water is defined in Section 3.3.

<sup>3</sup> Some uncertainty in the results which might be 8 % less than given.

## Mössbauer spectroscopy

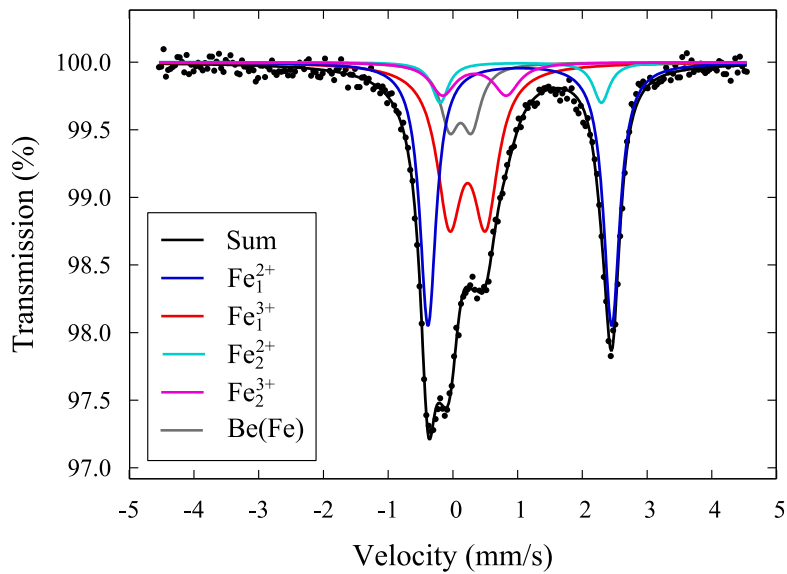


**Figure A4-1.** Mössbauer spectrum recorded from sample LOT A3, block 23, 0–10 mm. The sum of the fit is displayed as a black line, while the components of the fit are displayed in colors: Trivalent Fe (red and purple), divalent Fe (blue and cyan), Fe impurity in Be window of detector (grey).

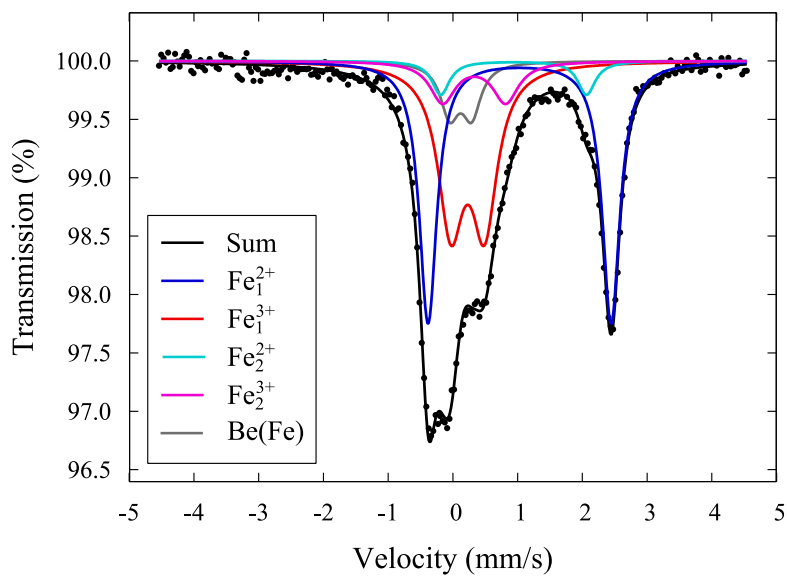


**Figure A4-2.** Mössbauer spectrum recorded from sample LOT A3, block 23, 10–20 mm. The sum of the fit is displayed as a black line, while the components of the fit are displayed in colors: Trivalent Fe (red and purple), divalent Fe (blue and cyan), Fe impurity in Be window of detector (grey).

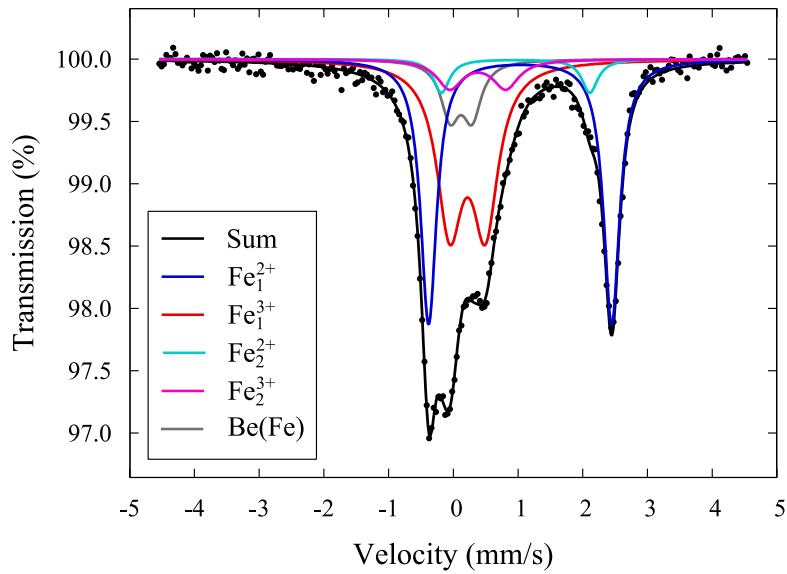


**Figure A4-3.** Mössbauer spectrum recorded from sample LOT A3, block 23, 20–50 mm. The sum of the fit is displayed as a black line, while the components of the fit are displayed in colors: Trivalent Fe (red and purple), divalent Fe (blue and cyan), Fe impurity in Be window of detector (grey).

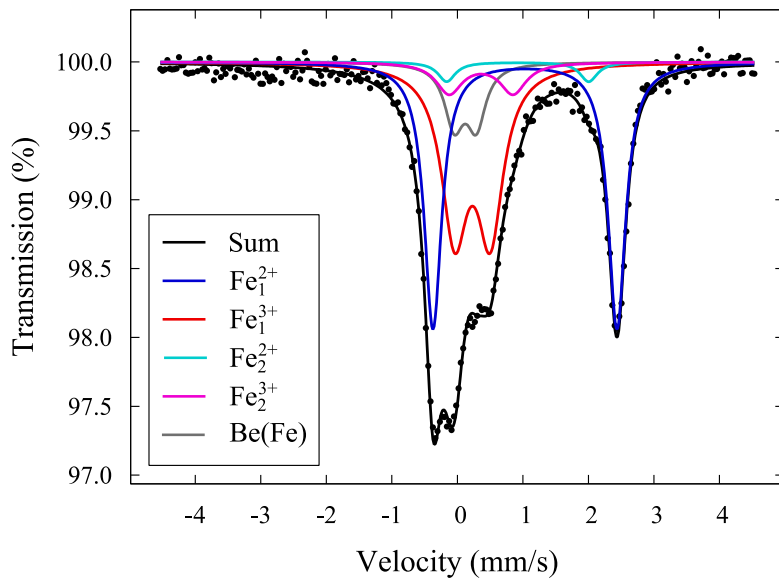


**Figure A4-4.** Mössbauer spectrum recorded from sample LOT A3, block 23, 50–100 mm. The sum of the fit is displayed as a black line, while the components of the fit are displayed in colors: Trivalent Fe (red and purple), divalent Fe (blue and cyan), Fe impurity in Be window of detector (grey).

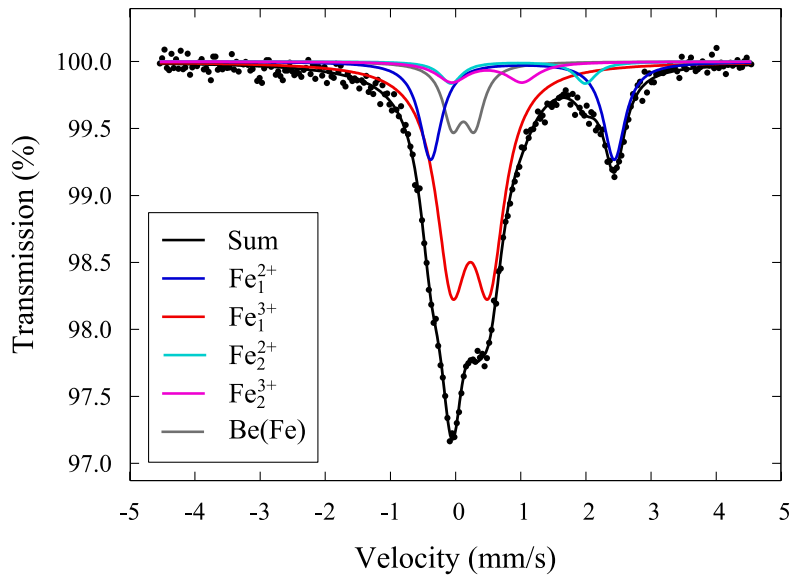


**Figure A4-5.** Mössbauer spectrum recorded from sample LOT A3, referenslera. The sum of the fit is displayed as a black line, while the components of the fit are displayed in colors: Trivalent Fe (red and purple), divalent Fe (blue and cyan), Fe impurity in Be window of detector (grey).

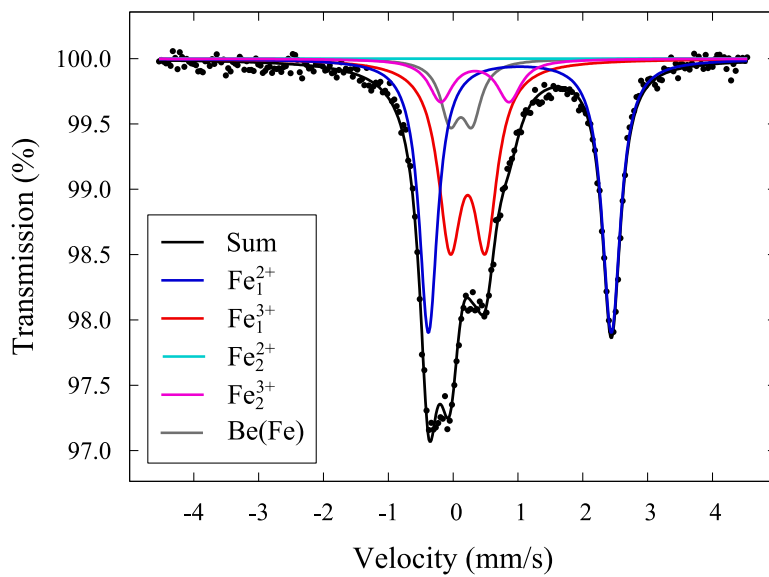


**Figure A4-6.** Mössbauer spectrum recorded from sample LOT S2, block, 21S, 0–10 mm. The sum of the fit is displayed as a black line, while the components of the fit are displayed in colors: Trivalent Fe (red and purple), divalent Fe (blue and cyan), Fe impurity in Be window of detector (grey).

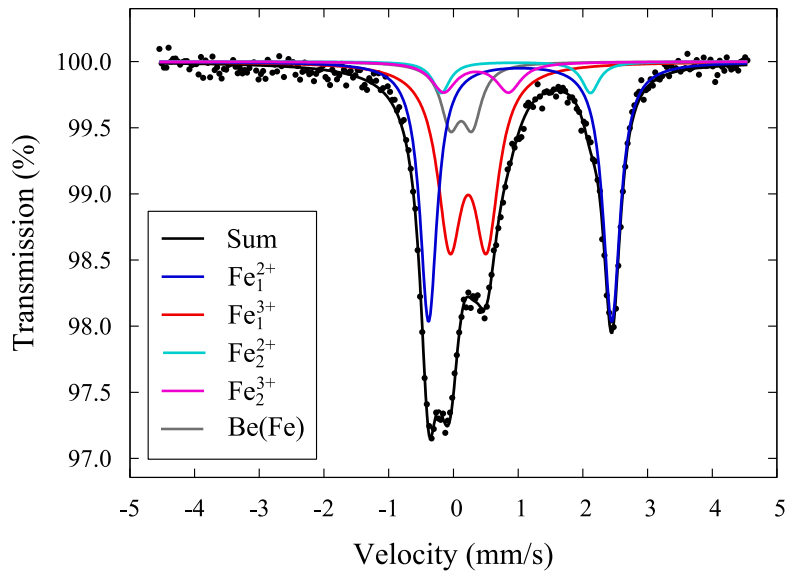


**Figure A4-7.** Mössbauer spectrum recorded from sample LOT S2, block, 21S, 10–20 mm. The sum of the fit is displayed as a black line, while the components of the fit are displayed in colors: Trivalent Fe (red and purple), divalent Fe (blue and cyan), Fe impurity in Be window of detector (grey).

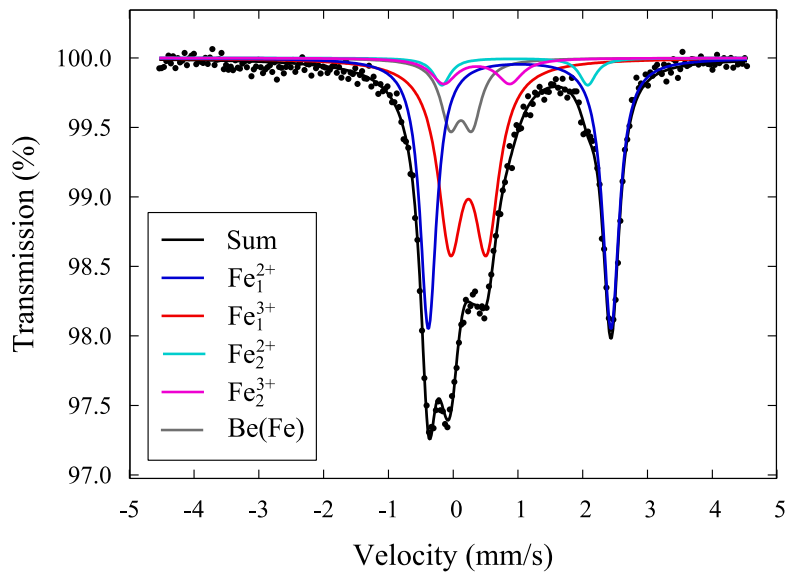


**Figure A4-8.** Mössbauer spectrum recorded from sample LOT S2, block, 21S, 20–50 mm. The sum of the fit is displayed as a black line, while the components of the fit are displayed in colors: Trivalent Fe (red and purple), divalent Fe (blue and cyan), Fe impurity in Be window of detector (grey).

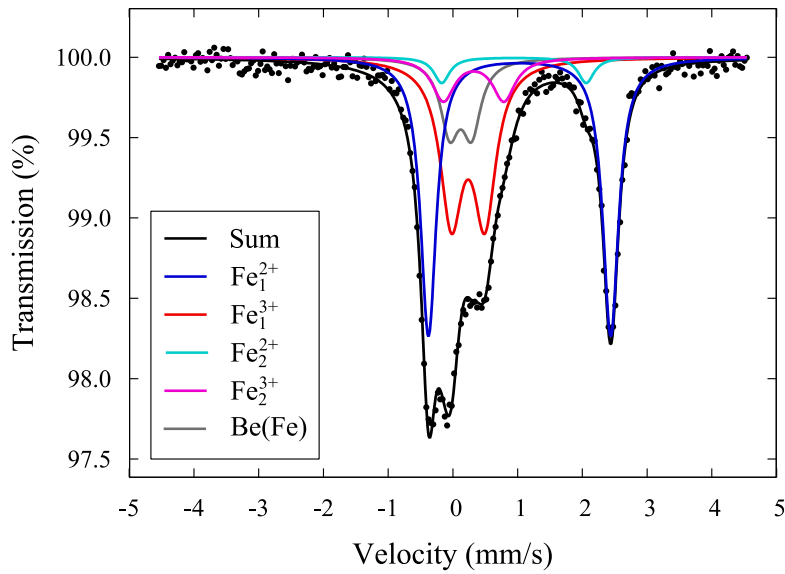


**Figure A4-9.** Mössbauer spectrum recorded from sample LOT S2, block, 21S, 50–100 mm. The sum of the fit is displayed as a black line, while the components of the fit are displayed in colors: Trivalent Fe (red and purple), divalent Fe (blue and cyan), Fe impurity in Be window of detector (grey).

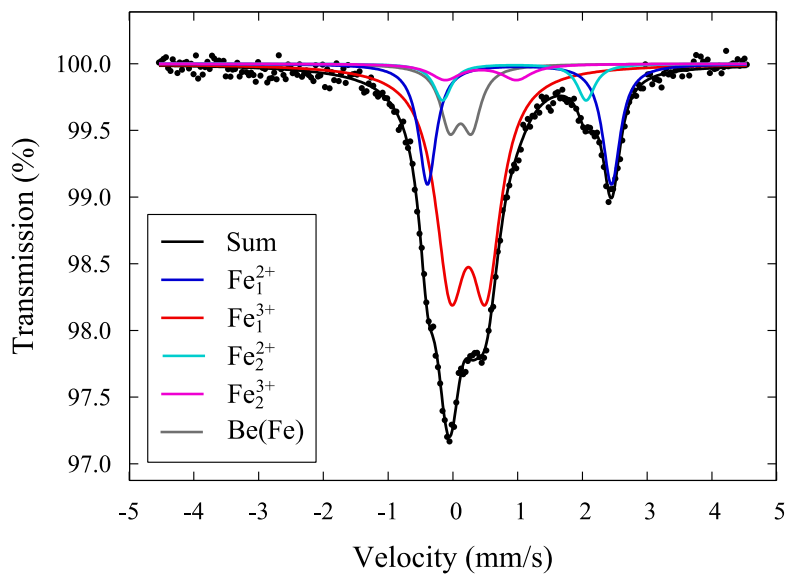


**Figure A4-10.** Mössbauer spectrum recorded from sample LOT S2, referenslera. The sum of the fit is displayed as a black line, while the components of the fit are displayed in colors: Trivalent Fe (red and purple), divalent Fe (blue and cyan), Fe impurity in Be window of detector (grey).

**Table A4-1. Hyperfine parameters of samples from Lot A3, block 23. Intensity of detector impurity is omitted intentionally and the component is presented only once, although it is present in all spectra.**

	<i>I</i> %	$\Delta$ (mm/s)	$\delta$ (mm/s)	$\Gamma$ (mm/s)	$\chi^2$
A3, bl. 23, 0–10 mm					
Fe <sub>1</sub> <sup>3+</sup>	39.0(1)	0.56(10)	0.339(1)	0.466(1)	1.173
Fe <sub>2</sub> <sup>3+</sup>	8.42(6)	0.98(11)	0.445(8)	0.466(1)	
Fe <sub>1</sub> <sup>2+</sup>	45.61(5)	2.838(9)	1.146(2)	0.3052(3)	
Fe <sub>2</sub> <sup>2+</sup>	7.02(fix)	2.49(1)	1.160(4)	0.3052(3)	
A3, bl. 23, 10–20 mm					
Fe <sub>1</sub> <sup>3+</sup>	39.17(4)	0.52(1)	0.340(6)	0.4782(5)	1.433
Fe <sub>2</sub> <sup>3+</sup>	10.16(2)	0.97(2)	0.440(3)	0.4782(5)	
Fe <sub>1</sub> <sup>2+</sup>	44.9(3)	2.827(4)	1.1416(5)	0.3283(5)	
Fe <sub>2</sub> <sup>2+</sup>	5.79(2)	2.25(1)	1.050(3)	0.3283(5)	
A3, bl. 23, 20–50 mm					
Fe <sub>1</sub> <sup>3+</sup>	42.7(1)	0.55(5)	0.331(3)	0.481(1)	1.100
Fe <sub>2</sub> <sup>3+</sup>	7.68(3)	0.87(6)	0.489(8)	0.481(1)	
Fe <sub>1</sub> <sup>2+</sup>	43.99(7)	2.828(6)	1.144(7)	0.2993(3)	
Fe <sub>2</sub> <sup>2+</sup>	5.59(8)	2.29(3)	1.07(2)	0.2993(3)	
A3, bl. 23, 50–100 mm					
Fe <sub>1</sub> <sup>3+</sup>	42.4(1)	0.545(8)	0.34(2)	0.481(1)	1.365
Fe <sub>2</sub> <sup>3+</sup>	8.00(3)	0.97(6)	0.47(1)	0.481(1)	
Fe <sub>1</sub> <sup>2+</sup>	46.2(5)	2.81(7)	1.143(3)	0.323(3)	
Fe <sub>2</sub> <sup>2+</sup>	3.40(4)	2.17(8)	1.03(2)	0.323(3)	
A3, referenslera					
Fe <sub>1</sub> <sup>3+</sup>	65.55(7)	0.568(9)	0.339(3)	0.5822(6)	1.037
Fe <sub>2</sub> <sup>3+</sup>	6.61(1)	1.1(1)	0.59(1)	0.5822(6)	
Fe <sub>1</sub> <sup>2+</sup>	22.8(3)	2.82(5)	1.137(3)	0.405(5)	
Fe <sub>2</sub> <sup>2+</sup>	5.08(7)	2.1(1)	1.07(3)	0.405(5)	
Be(Fe)	-	0.676	0.231	0.3477	

**Table A4-2. Hyperfine parameters of samples from Lot S2 block 21s. Intensity of detector impurity is omitted intentionally and the component is presented only once, although it is present in all spectra.**

	<i>I</i> %	$\Delta$ (mm/s)	$\delta$ (mm/s)	$\Gamma$ (mm/s)	$\chi^2$
S2, bl. 21s, 0–10 mm					1.310
Fe <sub>1</sub> <sup>3+</sup>	40.16(7)	0.54(1)	0.336(7)	0.4418(8)	
Fe <sub>2</sub> <sup>3+</sup>	9.79(2)	1.05(1)	0.448(3)	0.4418(8)	
Fe <sub>1</sub> <sup>2+</sup>	50.0(2)	2.821(3)	1.1407(3)	0.345(1)	
Fe <sub>2</sub> <sup>2+</sup>	-	-	-	-	
S2, bl. 21s, 10–20 mm					1.299
Fe <sub>1</sub> <sup>3+</sup>	41.9(2)	0.568(6)	0.340(6)	0.459(2)	
Fe <sub>2</sub> <sup>3+</sup>	7.34(6)	1.00(6)	0.462(5)	0.459(2)	
Fe <sub>1</sub> <sup>2+</sup>	45.29(4)	2.83(1)	1.1424(7)	0.3220(3)	
Fe <sub>2</sub> <sup>2+</sup>	5.467(4)	2.31(6)	1.077(4)	0.3220(3)	
S2, bl. 21s, 20–50 mm					1.033
Fe <sub>1</sub> <sup>3+</sup>	43.7(1)	0.56(2)	0.3463(9)	0.466(1)	
Fe <sub>2</sub> <sup>3+</sup>	6.31(6)	1.0(1)	0.48(2)	0.466(1)	
Fe <sub>1</sub> <sup>2+</sup>	45(4)	2.820(2)	1.1378(4)	0.31(3)	
Fe <sub>2</sub> <sup>2+</sup>	4.6(4)	2.25(3)	1.063(4)	0.31(3)	
S2, bl. 21s, 50–100 mm					1.169
Fe <sub>1</sub> <sup>3+</sup>	37.63(5)	0.52(9)	0.347(3)	0.4175(6)	
Fe <sub>2</sub> <sup>3+</sup>	10.36(2)	0.93(18)	0.432(6)	0.4175(6)	
Fe <sub>1</sub> <sup>2+</sup>	47.6(1)	2.815(4)	1.1413(3)	0.2935(5)	
Fe <sub>2</sub> <sup>2+</sup>	4.4(3.7)	2.23(16)	1.05(2)	0.2935(5)	
S2, referenslera					1.085
Fe <sub>1</sub> <sup>3+</sup>	64.8(2)	0.55(1)	0.350(3)	0.560(1)	
Fe <sub>2</sub> <sup>3+</sup>	5.06(3)	1.1(9)	0.54(13)	0.560(1)	
Fe <sub>1</sub> <sup>2+</sup>	23.13(3)	2.84(1)	1.14(4)	0.3297(4)	
Fe <sub>2</sub> <sup>2+</sup>	7.02(2)	2.2(2)	1.06(5)	0.3297(4)	
Be(Fe)	-	0.676	0.231	0.3477	

